LASER TREATMENT ON SYNTHETIC FIBRES

WONG CHI KIN, MENDEL

M.PHIL.

THE HONG KONG POLYTECHNIC UNIVERSITY

AUGUST 2001

Abstract

Laser irradiated materials, such as semi-conductors, metals and dielectrics have characteristic morphological features on the surface. Similar features are found on synthetic polymeric materials irradiated by excimer lasers. After laser irradiation, certain synthetic fibers develop characteristic roughness in the form of granular or ripple like structures on the originally smooth surface.

The structures can be generally classified according to the irradiated laser fluence into two streams, namely high-fluence laser treatment (laser power above the ablation threshold of the irradiated materials) and low-fluence laser treatment (laser power below the ablation threshold of the irradiated materials). The structures produced by both kinds of laser treatment also depend on the nature of materials and laser parameters, such as fluence, dosage, wavelength and sometimes the polarization.

In this report, poly (ethylene terepthalate, PET) and polyamide (Nylon) textile fibers and fabrics were used in the investigation. These samples were irradiated by excimer UV lasers of two different wavelengths, 193 nm and 248 nm. After irradiation, the fibers or fabrics were studied with different methods in order to find out the property changes due to laser processing.

Surface morphological change was observed with scanning electron microscopy (SEM) and atomic force microscopy (AFM). Based on the results, the relationship between laser parameters and the surface morphology was obtained in terms of roughness, mean ripple spacing, etc. For high fluence irradiation, the ripple spacing has the order of microns and the pattern is perpendicular to the fiber axis, i.e. the direction

of the fiber frozen-in tension. In low fluence laser treatment, the ripple/granular structures induced on the surface have spacing mainly around 200 nm. Furthermore, there is a narrow window of low energy fluence beyond which no structuring can be formed. These and other differences in characteristics and the underpinning mechanisms were investigated in this project.

In addition to physical measurements, chemical modifications due to laser treatment were also studied in this project. X-ray photoelectron spectroscopy (XPS) and Fourier transform infrared spectroscopy (FTIR) were used to analyze the changes of the chemical composition of the laser irradiated surface. Again, these results reveal some significant difference between high and low fluence laser treated PET. The O/C ratio of the treated surface decreases in high fluence laser treatment, but increases in low fluence treatment. This can provide a simple chemical explanation for some modified properties observed.

Changes in textile properties as a result of surface modification due to the irradiation of excimer lasers were subsequently studied. Surface luster, wettability, dyeability and stability of the treated fabrics were investigated in this project. These investigations give useful information for further study and may lead to some potential applications in textile industry.

Acknowledgement

I am especially grateful to my chief supervisor, Dr. K. S. Lau, for his close supervision and precious advice throughout the course of this research. Moreover, I would like to express my gratitude to his suggestion regarding the content and organization of this thesis. I would like to thank my co-supervisor, Dr. K. Chan, for his enlightening suggestion. Thanks are also due to Prof. F. G. Shin, Dr. K. H. Wong, Dr. Y. W. Wong and Wilson Wong for their discussions and experience sharing. Apart from these, I owe debt of appreciation to many people including technical staffs of our department and Institute of Textiles & Clothing, my companions Shiang, Leong, Aaron, Jan, Fred, Joanne, Vicky, Cindy, Chuen and Mandy for their support in this research period.

I am grateful to thank Mr. Yeung of Material Research Center of The Hong Kong Polytechnic University for his assistance in performing scanning electron microscope, Dr. Geoffery K. H. Pang of the Department of Applied Physics of The Hong Kong Polytechnic University for his assistance in operating the atomic force microscope, Mr. Nick K. C. Ho of the Hong Kong University of Science and Technology for his assistance in performing the XPS analysis and Mr. C. K. Wong for temperature profiles analysis.

This work is supported by a Research Grant Council of The Hong Kong Polytechnic University under the Code No. GV 725. I am grateful for the award of a research studentship from The Hong Kong Polytechnic University.

Table of Contents

List of Figures

Chapter 1 Introduction

1.1 Background

Synthetic polymeric materials irradiated by excimer lasers have characteristic morphological features on the surface. Similar features are found on laser irradiated materials, such as semi-conductors (germanium [Birnbaum M., 1965; Siegman E. Anthony *et al.*, 1986 and Emmony D. C. *et al.*,1973], silicon [Leamy H. J. *et al.*, 1978 and Lu Y. F., 1996], GaAs [Maracas G. N. *et al.*, 1978]), metals (Cu [Simon P. *et al.*, 1997], Ni-P [Isenor N. R., 1977 and Yu J. J. *et al.*, 1999], brass [Young J. F. *et al.*, 1982], Al [Young J. F. *et al.*, 1983], Fe [Dauscher A., 1996], Hg, In, Sn and Pb [Keilmann F., 1983]) and composite [Yi X. S. *et al.*, 1998 and Silvain J. F. *et al.*, 1999]. After laser irradiation, certain synthetic fibers develop characteristic roughness in the form of granular or ripple like structures on the originally smooth surface. The surface morphological modification results in changes of physical and chemical characteristics of the textile fiber, such as dyeability [Lau K. S. *et al.*, 1995, Watanabe H. *et al.*, 1999 and Knittel D. *et al.*, 1998], wettability [Wong Wilson *et al.*, 1997 and Lippert T. *et al.*, 1997], adhesion [Knittel D. *et al.*, 1998 and Laurens P. *et al.*, 1999], luster [Lau K. S. *et al.*, 1995a, 1995b and Wong Wilson *et al.*, 1997], etc. These characteristics can be exploited to design functional fiber with potential future applications [Lau K. S. *et al.*, 1999], especially for high value-added products. However, there is still much controversy in the understanding of the mechanisms and effects of laser treatment on synthetic fiber.

1.2 Literature Reviews

This section aims to provide a comprehensive review on the past and current research works of the Laser Induced Periodic Surface Structures (LIPSS) on polymers. The section is divided into 2 main parts: 1.2.1 discusses the LIPSS formed by low-fluence (below the ablation threshold) laser irradiation, and 1.2.2 discusses the LIPSS formed by high-fluence (above the ablation threshold) laser irradiation. The main difference in appearance between the two kinds of structures is the size of the ripples formed. When the polymer surface is exposed to laser fluence below the ablation threshold, the surface develops sub-micro-meter size ripples, but for high fluence exposure ripples of dimensions several microns will be formed.

1.2.1 LIPSS formed by low-fluence laser radiation

Niino H. and Yabe A., from the *National Institute of Materials and Chemical Research, Japan*, are the most active researchers who study chemical changes in the surface layer of the UV laser radiated polymers. Their research group uses many techniques to investigate the mechanism of the chemical surface modification, including scanning electron microscopy (SEM), tunneling electron microscopy (TEM), x-ray photoelectron spectroscopy (XPS), laser desorption mass spectroscopy (LD-MS), Fourier transform infra-red spectroscopy (FTIR), secondary ion mass spectroscopy (SIMS), etc.

They are interested in polymers that consist of a photolabile –N=N–N< (triazeno) group in the main chain and have an absorption maximum of ultraviolet around 300 nm. The two laser energy ranges, above and below the threshold for laser ablation of the

polymers reveal pronounced differences. For the case of irradiation below ablation threshold, the polymer surface is modified chemically as well as physically. Irradiation with either excimer laser wavelength 248 nm and 308 nm leads to surface oxidation [Lippert T. *et al.*, 1997] that can be indicated by XPS measurements. This will change the surface affinity to water. To study whether chemical modifications did take place, in addition to the physical changes of the surface, contact angle measurements were used. Similar behavior was obtained for both radiation wavelengths. The contact angle decreased from 57.5° to about 20°. The high fluence studies done by Niino will be discussed in Section 1.2.2.

Lazare S. and Bolle M., the French researchers from *Laboratoire de Photochimie et de Photophysique Moleculaire*, have been studying polymer surface modification by laser irradiation for a long time. Their research works mainly concentrate on the low fluence LIPSS of even periodic ripples and dot patterns with spacing smaller than 200 nm. They used polarized beams of ArF and KrF excimer lasers to irradiate the polymer surface of PBT, PET, PS, PC, etc. They found that the period of the structure increases with the wavelength used and with the angle of incidence of the beam, same as suggested by Dyer P. E. in studying on polyimide, PES, and PEEK [Dyer P. E. *et al.*, 1990]. On the other hand, the ripple direction is parallel to the polarization direction of the laser beam.

Lazare's group observed the surface profile by using SEM, TEM and characterized by ellipsometry [Bolle M. *et al.*, 1993a]. They found that a narrow "fluence window" [Bolle M. *et al.*, 1993b], of 2-10 mJ cm^{-2} and 1000 pulses should be chosen to obtain ripples with 0.2 μm spacing. They also believed that the high absorption of radiation by

the polymer was essential to obtain the ripples. For example, PC and PS are 2 orders of magnitude lower in absorption coefficient when compared with PET at a wavelength by 248 nm. Hence treatment of 248 nm laser does not produce surface structuring on PC and PS but on PET [Bolle M. *et al.*, 1993b].

In the studies of crystalline PET film using ellipsometry, they found that an amorphous layer of 80 nm thick was formed by irradiation with fluence between 5 and 10 mJ cm^{-2} [Bolle *et al.*, 1993c]. That layer is formed even at fluence above the ablation threshold and that the depth does not increase with fluence [Lazare S. *et al.*, 1993]. The formation of that layer is mainly due to the absorption of the laser by the PET. A very thin layer on the surface melts and rapidly solidifies within 25 ns. The depth of the amorphous layer is also proportional to the radiation penetration depth in the materials under the laser radiation.

They also studied the chemical modification of PET films after 193 nm and 248 nm laser treatments. XPS showed that the oxygen to carbon (O/C) ratio was reduced upon ablation. This drop of the O/C ratio is due to the photolysis of the polymer that starts even for pulse energy below the ablation threshold, increases rapidly when the fluence is varied around the threshold, and reaches a plateau at high fluence [Lazare S. *et al.*, 1989].

Csete and Bor, *Department of Optics and Quantum Electronics, JATE University, Hungary*, studied the low fluence laser irradiation on PET film recently [Csete M. *et al.*, 1998]. They investigated the LIPSS formation on the surface of the PET film by AFM using a homemade kinematics base plate, which allowed the study of the surface pattern

shot-to-shot. They concluded the main sequential phases of the LIPSS formation were: laser light scattering on the originally exiting granules, formation of elliptical structures around the granules, and the transformation of ellipses into ripple-shape modulation. The LIPSS generating feedback mechanism was due to the interference of the incoming beam and the beams scattered on the granules and already developed LIPSS. This caused spatially modulated melting and crystallization, which resulted in the structure. The LIPSS spacing also depends on the laser wavelength and on the angle of incidence. The experimental results are in good agreement with the theory of the self-organized diffraction gratings. Furthermore LIPSS have been shown experimentally to form by redistribution of the material on the surface, without significant material removal.

1.2.2 LIPSS formed by high-fluence laser irradiation

It is acknowledged that Schollmeyer E., a German researcher from *Deutsches Textilforschungszentrum Nord-West e.V.*, is one of the most important researchers in the field of the surface structuring on synthetic fiber by laser irradiation above ablation threshold. Recently, he, together with Knittel D., Kesting W. summarized their work in a series of reports [Knittel D. *et al.*, 1997a, 1997b, 1998a and 1998b], which included the phenomenology, mechanisms, chemical changes and the applications.

Since early 1980's, Schollmeyer have carried out a systematic series of researches on the LIPSS of polymer materials. He used many modern techniques; such as scanning electron microscopy, x-ray photoelectron spectroscopy, laser desorption mass spectroscopy (LD-MS), Fourier transform infra-red spectroscopy, etc., to investigate the structure formation. Results showed that the polymer surface developed a certain amount of granular and ripple liked structures after laser exposure. He explained the

mechanism by using a synergetic model [Knittel D. *et al.*, 1997b and Bahners T. *et al.*, 1993]. The model suggests that the structuring effect is purely due to thermal behavior of the outermost layer of the fiber during the influence of a laser pulse. The release of frozen-in tensions within fibers is coupled with high temperature gradients, thus leading to cooperative behavior for the movement of polymer chains. A computer modeling based on a synergistic algorithm of the stress release model supports the idea. Other than the synergetic model, another logarithmic model function was also suggested to describe the surface structure [Knittel D. *et al.*, 1997a]. A relationship between the mean ripple distance <D> and the number of laser pulses (N_p) has been established, namely $<D>=K_1 \log N_p+K_2$, where K_1 and K_2 are constants in a given condition. K_1 is weakly dependent on laser fluence, but sensitive to the given absorption depth and specific fiber properties (e.g. crystallinity, internal tension fields, draw ratio). K_2 describes the morphological dimension after the very first laser shot.

Many physical parameters, such as the wavelength [Kesting W. *et al.*, 1993], fluence, number of pulses, material absorption coefficient and the stress field can affect the structuring [Knittel D. *et al.*, 1997a]. Other influences, such as fiber crystallinity and polymer chain alignment, determine whether or not a fiber can be structured by UV lasers. Actually, in 1993, Schollmeyer already studied the surface morphology by using a combined arrangement of an UV laser and an atomic force microscope (AFM). AFM allows for the first time a highly sensitive surface characterization of the very same area of the irradiated sample between different laser pulses [Wefers L. *et al.*, 1993]. Based on the results obtained, the structure-forming mechanism was developed after several years [Knittel D. *et al.*, 1997a].

In chemical modification, Schollmeyer mentioned that carboxylic group was formed on the surface of PET and C=O bonds was formed on the surface of polypropylene after laser irradiation [Knittel D. *et al.*, 1998a]. Many more data supported the formation of yellow layers on the high fluence laser-treated samples, consisting of debris derived from the ablation process. Analysis by LD-MS [Bahners T. *et al.*, 1990] and XPS confirmed the composition of those layers as highly carbonaceous. The studies of XPS indicated that a reduction in O/C ratio appeared in the laser treated PET foil.

In textile application, the UV laser irradiation was used to change the optical appearance of fabrics and improve dust filtration properties of non-woven [Knittel D. *et al.*, 1998b]. The luster and glossiness studies of the fabrics were also studied by a Hong Kong research group [Lau K. S. *et al.*, 1995b]. The adhesion of pigment dyes and particles on PET and nylon fibers can also be greatly improved.

Recently, Schollmeyer tried to use excimer lamp (222 nm) as the radiation source instead of excimer laser [Praschak D. *et al.*, 1998]. Irradiation of PET with UV lamps causes the generation of radicals at the surface. Due to the lower power density of broadband UV source (UV lamps), with regard to heat generation, long irradiation times are necessary for yielding chemical changes. Only photochemical reaction acts on the material but no morphological modifications appear in the processing. After irradiation, a new layer of the materials was formed, protecting the bulk materials in critical atmospheres or a rise in the hydrophilic behavior to increase the adhesion to certain coating. One of the advantages of using UV lamp is the large irradiated area. This may become an important means for developing an industrial scale application.

Dyer P. E., from the *Department of Applied Physics, University of Hull*, is another very active researcher in the area of LIPSS. His research work mainly concentrates on effects related to polarization, wavelength, angle of incidence, surface scattering, ablation threshold of the polymer materials, etc. He found that LIPSS were most clearly developed on un-oriented polymers (e.g., polyimide, PES, and PEEK) and with fluences ranging between the threshold for ablation E_T and about 3 E_T. The amplitude of the ripple spacing is around 1 μm, depending on the wavelength and angle of incidence of laser. He used a relationship $X_s = \lambda (1\text{-}\sin\theta)^{-1}$ for the TE-polarized laser beam irradiation and $X_c = \lambda (\cos\theta)^{-1}$ for the TM-polarized laser beam irradiation [Sipe J. E. *et al.*, 1982], where X_s and X_c are the ripple spacing, λ is the wavelength of the incident laser and θ is the angle of incidence, to describe the phenomenology of the LIPSS formation [Dyer P. E. *et al.*, 1990]. The idea of surface scattering effect was also introduced to explain the mechanism of the LIPSS formation above the ablation threshold.

Since 1983, Dyer has begun his research work on ablated polymers using excimer lasers. At the beginning [Dyer P. E. *et al.*, 1985, 1986 and 1988], he tried to find the ablation thresholds of some common polymers, e.g. PET, PA, PI etc. After that, [Dyer P. E., 1996] the techniques of High Speed Shadow Photography (HSSP), Probe Beam Deflection (PBD) and Time Resolved Interferometry (TRI) were employed to provide information of the ablation process. He concluded that HSSP and TRI were effective for measuring for the formation and development of the shock-front. PBD could provide information on ablation over a large range of conditions.

Srinivasan R., a researcher from *IBM T. J. Waston Research Center, Yorktown, New*

York, began to study laser ablation of organic materials in 1980s [Srinviasan R. 1983]. He studied the ablation and the etching effect on the polymer materials for many years. Based on the results, he suggested that the etch depth vs pulse was a linear function of the number of pulses at constant laser fluence [Srinivasan R. *et al.*, 1984]. However, although the depth etched on the polymer was a linear function of the number of pulses, there was a very long extrapolation between the origin (zero pulse) and the first data point. He then suggested a very important idea in explaining the starting mechanism of the ablation process. At the first few laser pulses, the uniformity of the etching depth does not exist because the first pulse sees a virgin material whereas each subsequent pulse sees a sample that has already been modified in part by the preceding pulse [Srinivasan R. *et al.*, 1989].

Niino H. and Yabe A. also studied the high fluence laser treatment on surface modification of the polymers which consist of a photolabile –N=N–N< (triazeno) group in the main chain. For 248 nm laser irradiation, a 'nap' like structure was detected, which was black in color and carbonized, suggesting that a thermal or a different photochemical mechanism was involved. In the case of 308 nm irradiation, the chemical composition remained unchanged after several pulses of laser, suggesting that the laser just removed the polymer materials layer by layer without any chemical change [Lippert T. *et al.*, 1997].

On the other hand, they also tried to investigate the formation mechanism by using the time-resolved light scattering technique with pulsed light of a XeF (350 nm) excimer laser [Niino H. *et al.*, 1990] on polyethersulfone (PES) film. They concluded that thermal processes on an ablated surface played a significant role in microstructure

formation, and that the orientation of the micro-pattern depended on the polarization of the ablating beam. Because the XeCl (308) laser beam can deeply penetrate the bulk of the PES film, the temperature on the subsurface in the irradiated region may be raised rapidly and a pool of fluidized material may be formed. The fluidized layer plays an important role in the mechanism of microstructure formation. This dependence is also very similar to the models suggested by Farley-Dyer (surface scattering) [Dyer P. E. *et al.*, 1990] and Bahners-Schollmeyer (Stress field) [Bahners T. *et al.*, 1989].

Niino H. and Yabe A. also studied the chemical change of PEN2,6 polymer by using transmission electron microscopy (TEM) [Niino H. *et al.*, 1989] after 248 nm KrF laser radiation in air at high fluences (40 mJ cm^{-2} and 10 pulses; 500 mJ cm^{-2} and 100 pulses). The results of TEM analysis revealed that the debris of the microstructures were composed of a polymer with a higher density. It can be concluded that cross-linking took place on the polymer surface in the process of laser irradiation.

1.3 Scope of Thesis

The propose of this study is to investigate further the characteristics and formation mechanisms of the ripple liked structure induced by excimer laser irradiation on synthetic textile fibers. In comparison with conventional textile surface treatment, laser irradiation is essentially a dry process, which is much more environmentally friendly than the wet chemical processes. Furthermore, the laser process is easily controllable and can be readily adapted to suit different manufacturing requirements.

In this project, poly (ethylene terepthalate, PET) was used in the investigation, sometime nylon was also used as comparison. Laser treatments on polymeric materials were classified into two classes based on power density, including high fluence laser treatment (fluence used above the ablation threshold) and low fluence laser treatment (fluence used below the ablation threshold of the materials). Samples involved and the experimental setups for different laser treatments in forming "Laser Induced Periodic Surface Structure" (LIPSS) will be described in details in the following section of this chapter.

Scanning electron microscopy and atomic force microscopy were employed to studying the morphological modifications. The relationship between the structural periodicity and different laser parameters is investigated in Chapter 2. Mechanism of LIPSS formation is also discussed in details based on literatures and the results obtained. Other than the physical modification formation, chemical mutation is also an important change. Therefore x-ray photoelectron spectroscopy, infrared and ultraviolet absorption spectroscopy were used to study the composition and bonding of the treated surface.

The experimental techniques and results will be given in Chapter 3.

The laser irradiated synthetic textile materials have special properties for their lustre, wettability, dyeability, etc. that can be utilized for producing higher value-added fabrics. Therefore, some conventional textile property tests conduced in this study are detailed in Chapter 4. The results obtained are explained and analyzed in conjunction with the physical and / or chemical modifications.

1.4 General Experimental Setup

1.4.1 Sample Preparation

Commercially available Poly (ethylene terephthalate) (PET) fiber (drawn to 1.6 under 200 °C with 14 μm diameters), micro-fabrics (Figure 1.1a and 1.1b), thick-fabrics (Figure 1.1c and 1.1d) and films (100 μm thick) were used in the study to investigate the effects of laser treatments. Nylon 6/6 fibers were also used for comparison. All the samples were cut into a suitable size, washed before laser treatment to eliminate oil and other contamination on the surface, and kept under BS 1051 standard condition (20 ± 2 °C and 65% relative humidity) for 24 hours before each experiment. In the study, two kinds of white and plain weave PET fabrics were used.

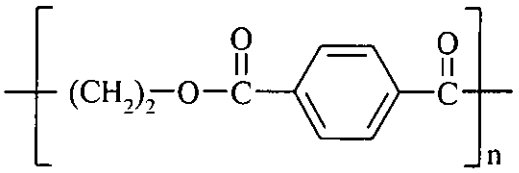

Chemical formula of PET

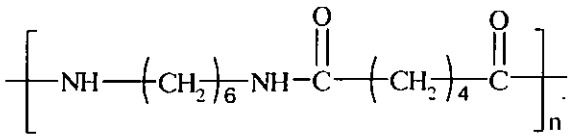

Chemical formula of Nylon 6/6

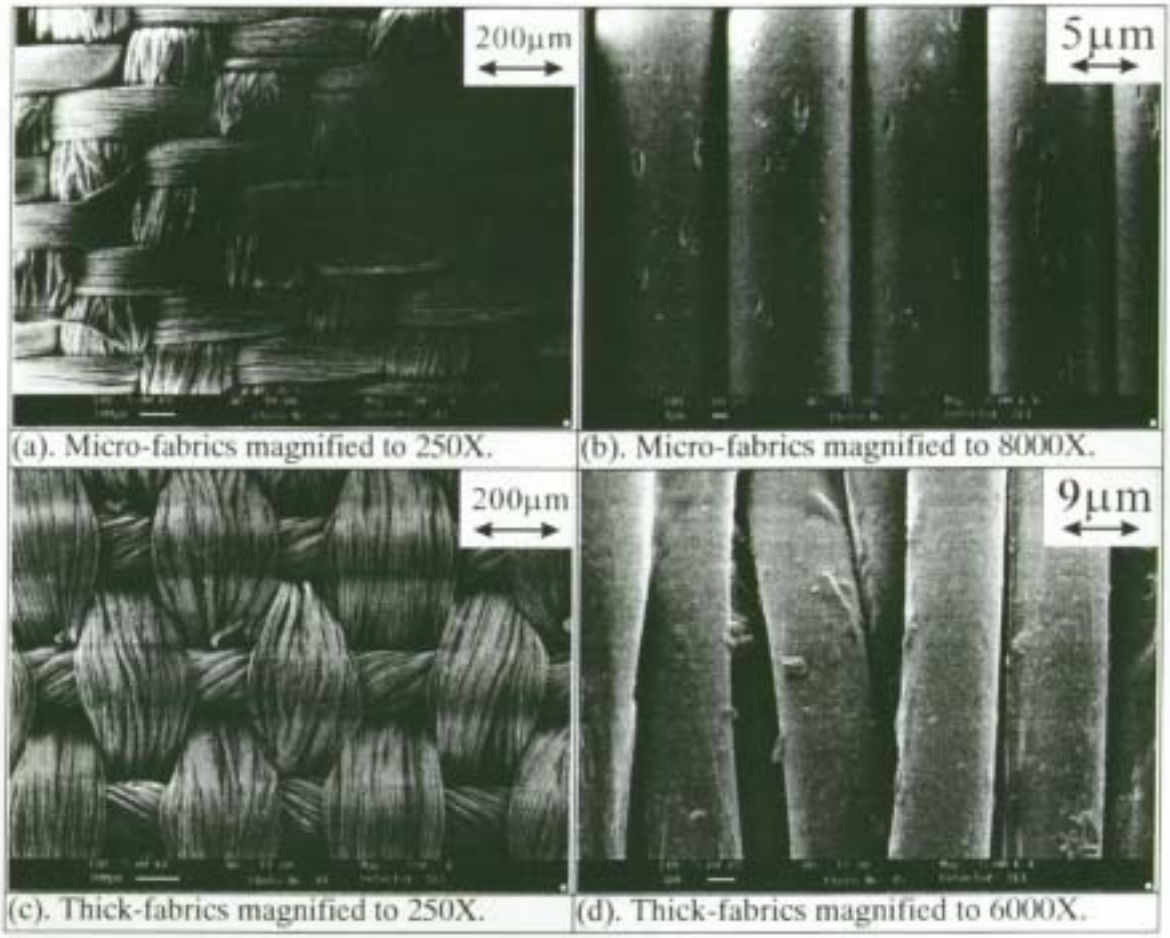

(a). Micro-fabrics magnified to 250X. (b). Micro-fabrics magnified to 8000X.

(c). Thick-fabrics magnified to 250X. (d). Thick-fabrics magnified to 6000X.

Figure 1.1: SEM images of the untreated PET thick-fabric and PET micro-fabric.

1.4.2 Laser Treatments

Samples were irradiated with two different pulsed UV excimer lasers (Lambda Physik COMP EX 205) under atmospheric condition. One laser operates with KrF gas and produces laser of wavelength of 248 nm, and the other with ArF gas and wavelength 193 nm. The laser fluence and the number of pulses are varied in each case in order to study their effects upon surface morphology.

As mentioned before, laser treatment on materials can be cataloged into two streams depending on the laser fluence used. Irradiation at fluence above the ablation

threshold is defined as high fluence laser treatment, and that below the threshold is defined as low fluence laser treatment.

1.4.2.1 Experimental setup of high fluence laser treatment

Figure 1.2 shows a typical setup, which is used to study the high fluence laser treatment on materials. Samples are irradiated directly from the laser beam without using any special photomask nor a focusing lens. An iris is used to define the irradiating position. A convergent lens however may be inserted before the iris in order to obtain a higher laser fluence.

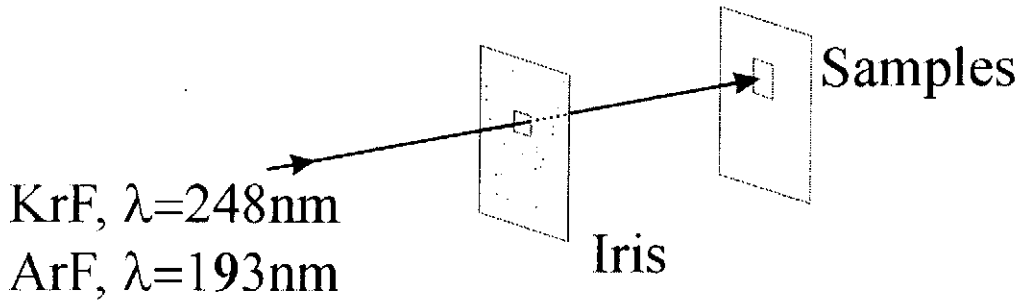

Figure 1.2: High fluence laser treatment

1.4.2.2 Experimental setup of low fluence laser treatment

For low fluence laser treatment, the experimental setup becomes more complicated due to the involvement of more components and their alignment. Figure 1.3 shows an experimental setup of low fluence laser treatment. The laser beam is attenuated by reflection from a silica plate. Laser energy received at the sample surface is monitored by a joulemeter (Molectron JD 2000).

Because of reflection, the attenuated beam is inevitably polarized. By applying the Fresnel equations, intensity of the two electric field components ($E_{r\perp}$ *and* $E_{r//}$

perpendicular and parallel to the plane of incidence respectively) depends on the angle of incidence (Figure 1.4). The degree of polarization of the reflected laser beam ($E_{r\perp}/E_{r//}$) at angle of incidence θ_i =30° is about 2 and that at 58° (approximately Brewster's angle) is about 1700. Therefore the beam with 30° angle of incidence is defined as partially polarized and that of 60° angle of incidence as highly polarized laser beam (shown in Figure 1.5).

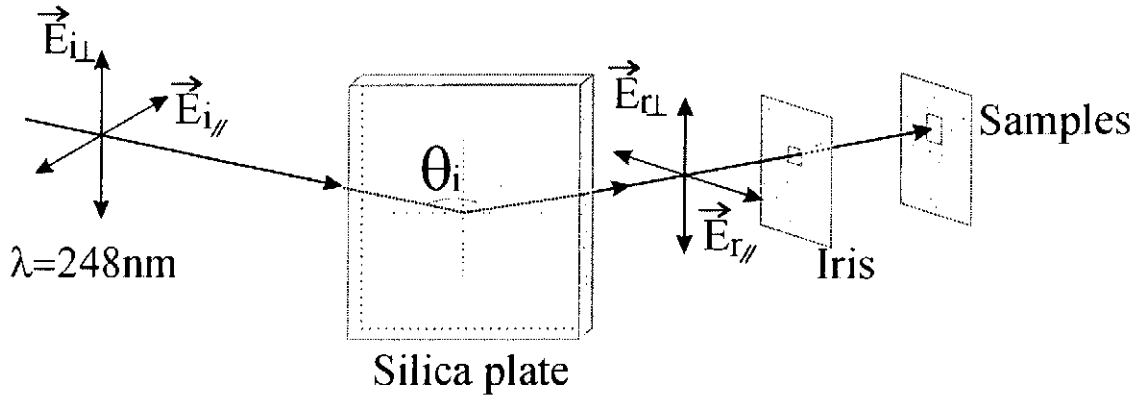

Figure 1.3: Low fluence laser treatment

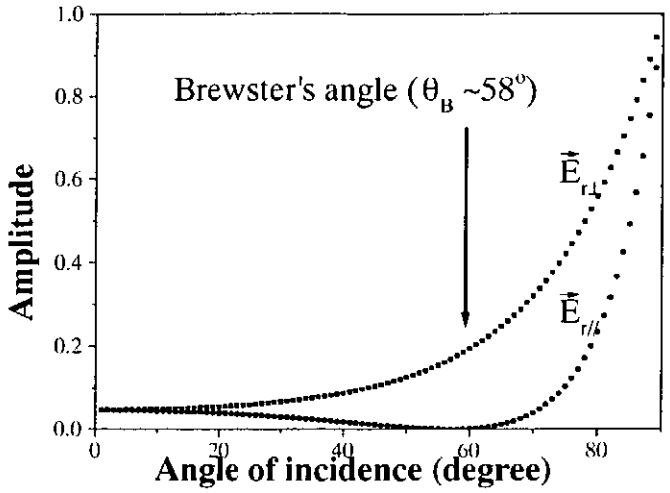

Figure 1.4: The dependency of the two electric field components ($E_{r\perp}$ and $E_{r//}$) at different angle of incidence.

The direction of polarization is defined as the direction where the electric field component is the greatest, and is along $Er_\perp$ in the present setup. Sometimes a divergent

lens may be also inserted between the silica plate and the iris in order to obtain a lower laser fluence by increasing the irradiated area. The degree of polarization, the direction of polarization relative to the sample, the laser fluence and the number of laser pulses are used as variable parameters in order to study their effects upon surface morphology and finding the optimum conditions for the successful formation of a LIPSS. The details will be discussed in Chapter 2.

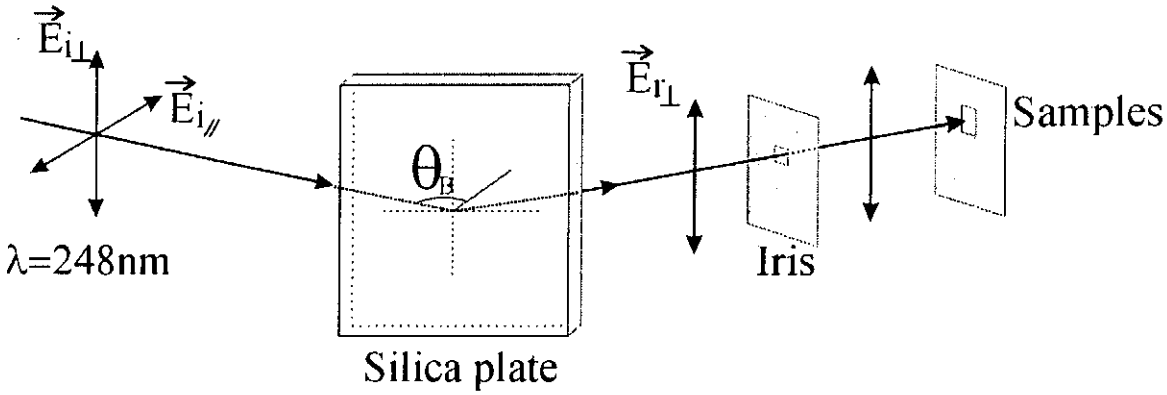

Figure 1.5: Highly polarized (angle of incidence at silica plate is set near Brewster's angle θ_B ~58°) low fluence laser treatment.

Chapter 2 Morphological Modification and Mechanism Study

Of utmost importance for laser induced surface structuring, the modification should be almost restricted to a very thin layer of the surface, (several microns for high fluence laser treatment and below 100 nm for low fluence laser treatment) so that the bulk properties of the fibrous materials are not influenced. A characteristic of LIPSS on fibrous materials is a regular geometry within a thin layer of the irradiated region. Therefore surface morphological information is necessary in understanding the behavior of surfaces. Atomic force microscopy and scanning electron microscopy are employed in the study.

2.1 Experimental Techniques

2.1.1 Atomic Force Microscopy (AFM)

The atomic force microscope, which was invented in 1986, permits resolution of individual atoms on both conducting and insulating surfaces. During measurement, a flexible force-sensing cantilever stylus is scanned in a raster pattern over the surface of the sample. The force acting between the cantilever and the sample surface causes minute cantilever deflections, which are detected by optical means.

In this study, Metrus-2000 (Burleigh) AFM with statistical software was used in the study of the laser induced surface structures on a PET fiber in three-dimension (different from the 2-dimensional images provided by SEM, AFM can given the information of the height of the structures). Other than providing images, the software

can also deduce the cross sectional profile and roughness information of the scanned surfaces. Figure 2.1 shows the schematic side view of experimental setup of AFM in studying the fiber samples.

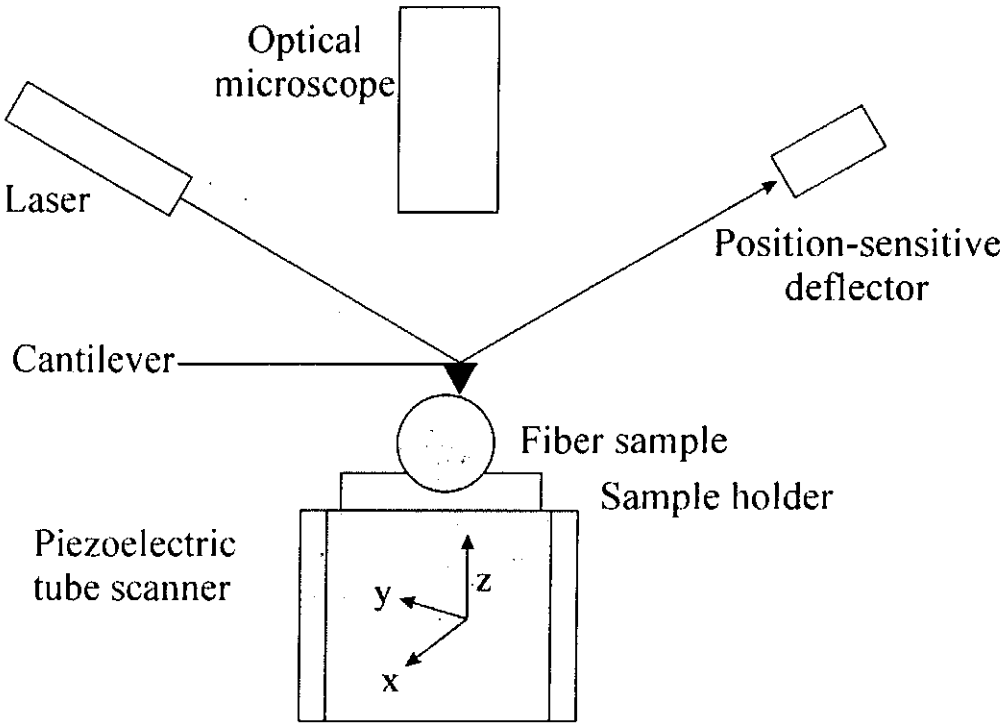

Figure 2.1: Schematic diagram of the AFM

In order to hold the fiber stably, a long horizontal groove was carved on a silicon substrate and the PET fiber with 30 μm diameter was secured inside as shown in Figure 2.1. In order to maximize the position reproducibility of the head to the irradiated area, a high-resolution optical microscope together with a special marking were used.

All the fibers were irradiated by 248 nm excimer laser with fluence of 50 mJ cm^{-2} and various pulse number of 0, 1, 2, 4, 16 and 32 pulses. The scanning area was 10 μm x 14 μm and the scanning direction was along the fiber axis. The details of scanning are shown in Figure 2.2.

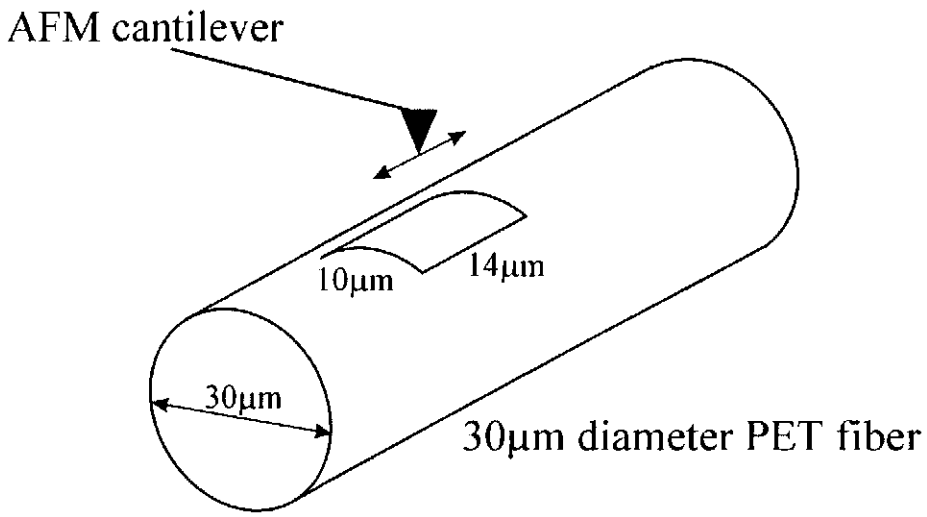

Figure 2.2: The scanning direction of the AFM cantilever on the fiber surface.

2.1.2 Scanning Electron Microscopy (SEM)

The scanning electron microscope is one of the important and commonly used instruments in microscopic imaging. It can provide a detailed image of the samples in various magnifications up to 50,000X.

In this study, Stereoscan 440 SEM operating in the secondary electrons mode was used. Better image quality can be obtained if no extra electrons are accumulated on samples. Therefore gold was coated on the surface in order to have a better conduction between the sample and the chamber of SEM. At the same time, the acceleration potential was kept at 5 kV instead of the normal 20 kV. This could prevent any structuring or etching effect induced by the high-energetic electrons.

2.2 Results and Discussions

2.2.1 Morphological study of high fluence laser treated PET fibers

2.2.1.1 Atomic Force Microscopy

Figure 2.3 depicts a set of AFM images of the laser treated PET fibers. As can be seen, surface of the untreated PET fiber shows only minor irregularities (within 60 nm) but no recognizable damages. These irregularities are believed to be connected with manufacturing defects. With only one shot of laser pulse in fluence of 50 mJ cm^{-2}, the surface topography changed dramatically from the original smooth surface to a fibrous surface characterized by hills and grooves.

The second laser pulses of the same fluence has transformed these hills and grooves to a more uniform ones, which are usually known as ripple-like structures. With four laser pulses, the surface becomes coarser and the z-average (the average height of the scanned surface) has increased from 260 nm of the second pulse to 650 nm. After 16 pulses, a transition of small ripples into a well-developed one is obvious. The topography has not been changed too much with further laser pulses since it is believed the evolution and development of this structure depends mainly on the structure after the first pulse. However, a change in surface roughness was detected by the AFM statistical software in terms of *Rq* (the root mean square of the surface).

$$Rq = \sqrt{\frac{1}{N}\sum_{i}^{N}(Z_i - Z_{avg})^2}$$

Where Z_i is the height of the surface at the ith point, N is the total number of the scanned points and Z_{avg} is the average height of the scanned surface.

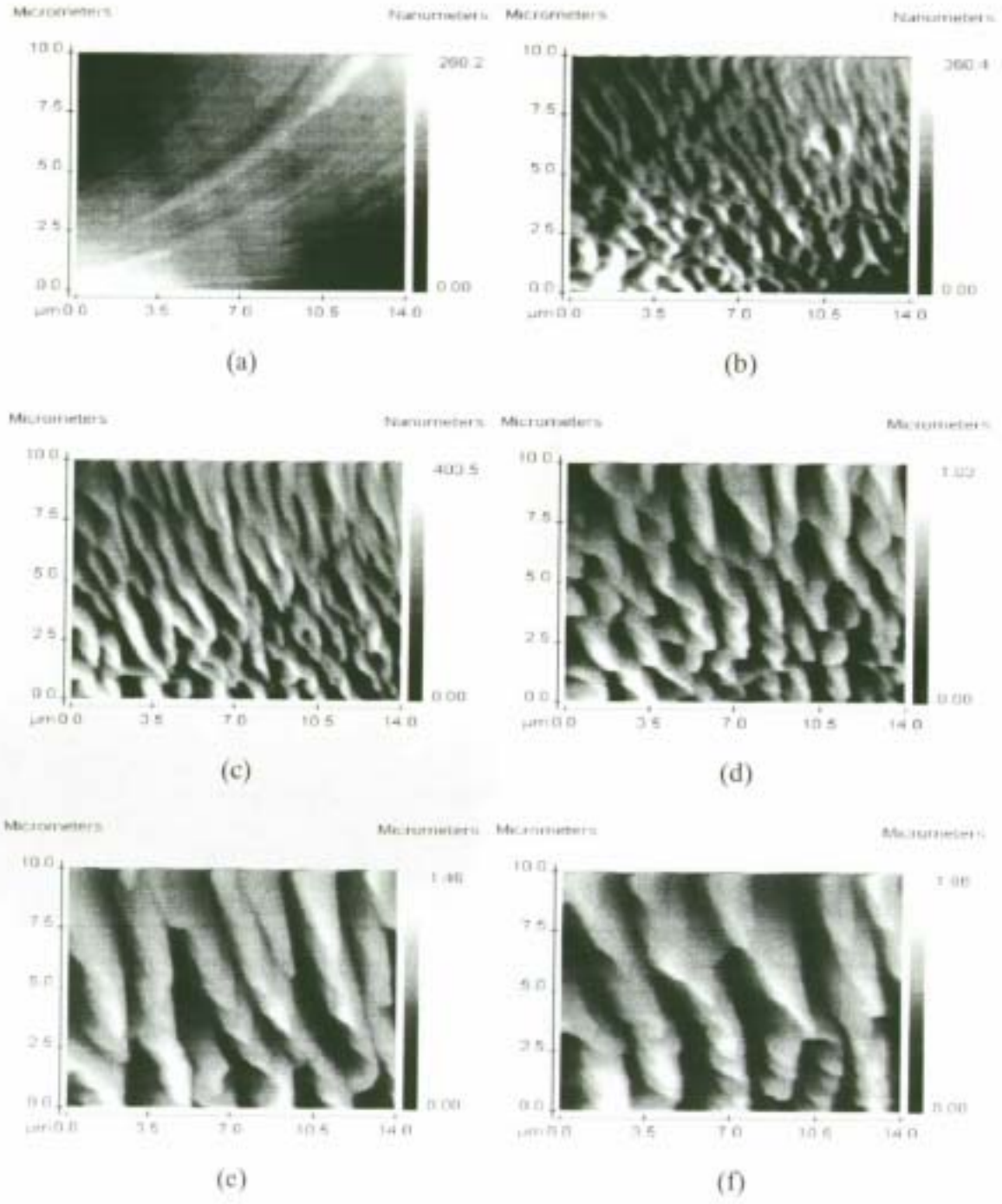

Figure 2.3: A series of AFM images of PET fiber treated with 248 nm excimer laser with fluence of 50 mJ cm^{-2} at different laser pulses. (a) Untreated, (b) 1 pulse, (c) 2 pulses, (d) 4 pulses, (e) 16 pulses and (f) 32 pulses.

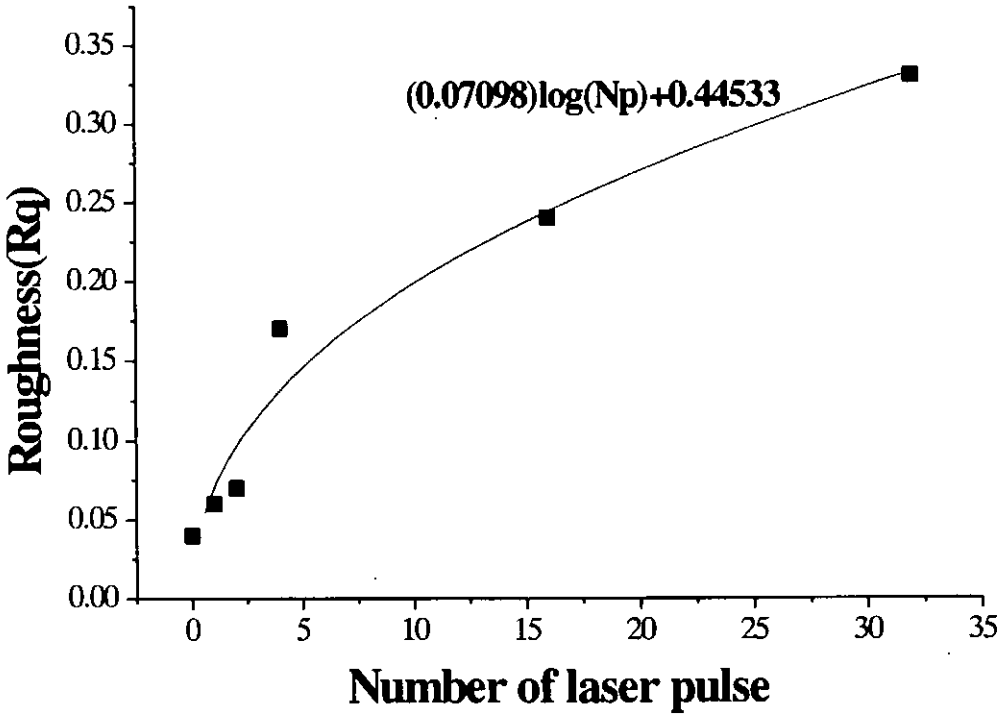

Figure 2.4: Roughness (Rq) of the laser treated PET fiber determined by AFM.

The dependence of the roughness (*Rq*) on the number of laser pulse provided by the software of AFM is shown in Figure 2.4 (0.07098 log (Np) + 0.44533). It can be seen that the roughness increases monotonically with the number of laser shots. The *Rq* value increases dramatically after the second pulse and slows down therefore. The reason of the increase is due to the formation of LIPSS. Actually, 35 pulses of laser irradiation may not be enough to indicate the whole picture of the variation of roughness. At the same time, some minor effects, such as the curvature of the sample fiber, the orientation of the fiber, etc, can also affect the accuracy of the results. However it is believed that the roughness obtained from the AFM experiments is mainly produced by the surface structures. The details will be discussed in the following section with the results of the SEM images.

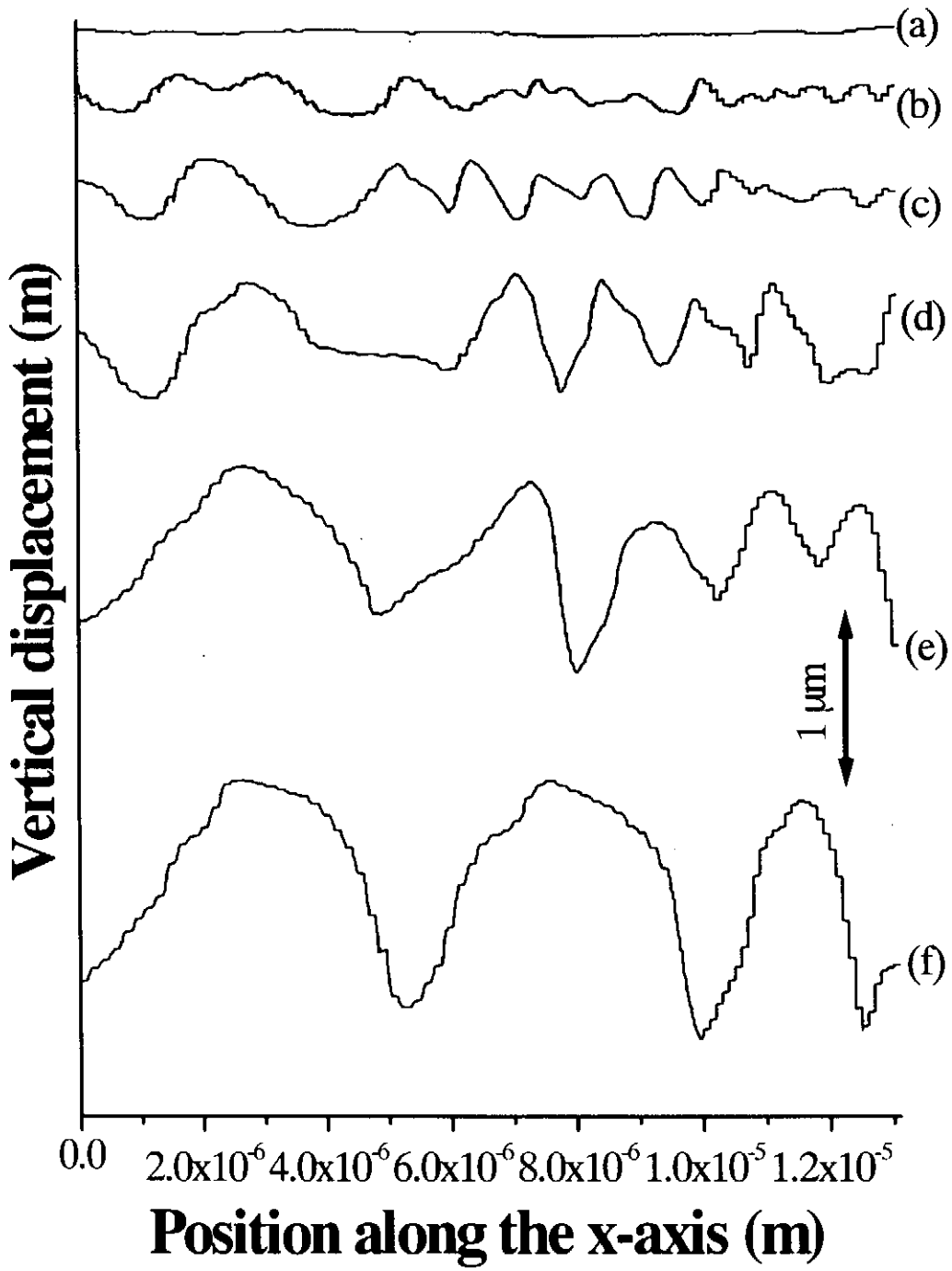

Figure 2.5: Cross sectional profiles of PET fiber treated with 248 nm excimer laser with fluence of 50 mJ cm^{-2} at different laser pulses by using AFM software. (a) Untreated, (b) 1 pulse, (c) 2 pulses, (d) 4 pulses, (e) 16 pulses and (f) 32 pulses.

Other than the images and the values of roughness, the cross sectional profile of the ripple-like structure at different number of pulses can also provide valuable information to study the formation mechanism. Figure 2.5 shows the profiles obtained by AFM plotted in a common scale for better comparison.

As shown above, the structure evolves from nano-meter sized to microns sized as the number of laser pulse increases. The hills represent the tops of ripples, therefore the number of hills decreases with the number of laser irradiation and the reason is believed to be the merging of the ripples during the laser heating and cooling process. Since the enhancement of ripple is from self-movement of the materials, therefore more laser dosage should give larger distance between hills and deeper structures. More morphological information will be given in the SEM section.

2.2.1.2 Scanning Electron Microscopy

For high fluence laser treatment, the surface modification is almost restricted to a very thin layer of the surface due to high absorption of the materials. Bulk properties of the fibrous materials are not influenced. A characteristic of laser induced surface structures on fibrous materials is a regular geometry within the whole irradiated areas. The mean distance of the ripple like structures obtained is between 1-5 μm (for PET fiber irradiated by 248 nm laser at fluence above the ablation threshold). In addition, a preferential orientation of the ripples is observed, being almost perpendicular to the fiber axis. Smaller structures can be obtained on the irradiated fibers with the low fluence laser treatment and the details of their structures will be discussed in the low fluence treatment section.

Existing excimer lasers offer many experimental parameters (wavelength, fluence pulse rate and number of laser pulses) for different laser treatments. Therefore, the dependence of such kind of parameters was studied in the experiment and the optimum parameters in forming successful periodic structures on the irradiated PET fibers were found.

One shoot effect

For the one shoot effect on PET fibers, Schollmeyer [Knittel D. *et al*, 1997] suggested that 20-30 mJ cm^{-2} was the threshold for ablation. Since the LIPSS formation have a close relation with the materials ablation threshold, therefore the threshold for LIPSS formation was tried to obtain by studying the one shoot effect. It is, however, very difficult to define and identify the threshold of the formation of LIPSS accurately. Figure 2.6 shows a series of SEM images of PET fibers irradiated by a single pulse of

248 nm excimer laser at fluence of 30 mJ cm^{-2} to 1200 mJ cm^{-2}. As the fluence increases the structures become more conspicuous. Following one laser pulse with 30 mJ cm^{-2} only small uneven areas are created, but no periodic ripple-like structure is detected. As the fluence increases, the unevenness becomes denser. For one pulse with fluence above 1000 mJ cm^{-2}, distinct ripple-like structures can be seen with periodicity about 1-2 μm.

These results indicated the formation of surface structures starts at very beginning of the laser pulse, even a single shot. It also coincided with the findings of Srinivasan & Braren [Srinivasan R. *et al*, 1984]. They based on the time-dependent photoacoustic measurements, a pressure up to 10^8 Pa may be created on the surface during the laser irradiation. (at fluences of about 1 J cm^{-2}). The detail mechanism will be discussed in the mechanism section.

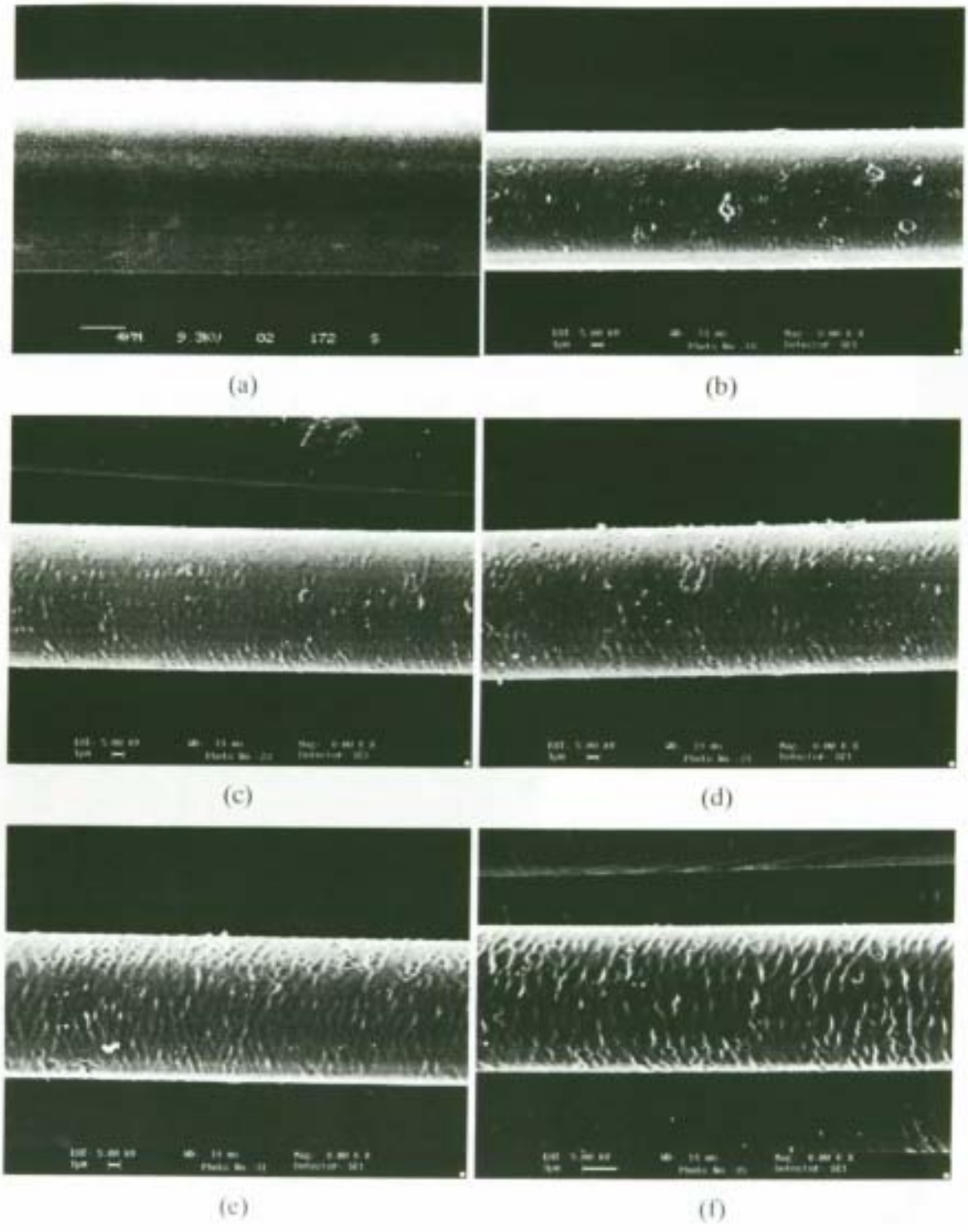

Figure 2.6: A series of SEM images of PET fiber treated with 248 nm excimer laser for a single laser pulse at different fluences. (a)Untreated, (b) 30 mJ cm^{-2}, (c) 80 mJ cm^{-2}, (d) 100 mJ cm^{-2}, (e) 1000 mJ cm^{-2} and (f) 1500 mJ cm^{-2}.

Laser wavelength dependence

In order to form the micron sized LIPSS on the materials, high UV absorption and sufficient stress field of the material are necessary. Therefore the selection of the laser wavelength becomes very important in creating LIPSS. Figure 2.7 shows the absorption spectrum of PET and Nylon materials in the UV range from 200 nm to 350 nm. From the experimental results (Figure 2.7), it can be concluded why 248 nm laser cannot induce any LIPSS on nylon due to its low absorption ability at 248 nm. In fact, nylon forms ripples only for 193 nm laser irradiation. Similar properties also found by Kesting *et al.* [Kesting W. *et al.*, 1993]. The SEM images shown in Figure 2.8 are nylon 66 fibers irradiated by lasers of different wavelengths. LIPSS are only seen for 193 nm laser irradiation, but no structure is found after 248 nm laser exposure.

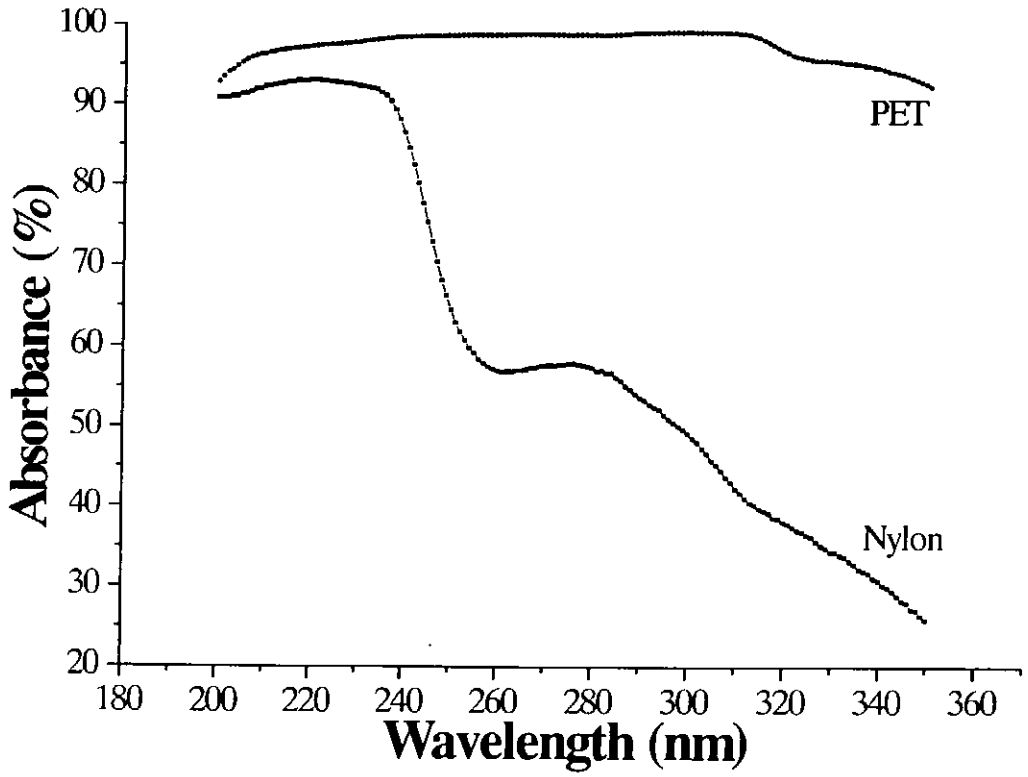

Figure 2.7: The UV absorption spectra of PET and Nylon.

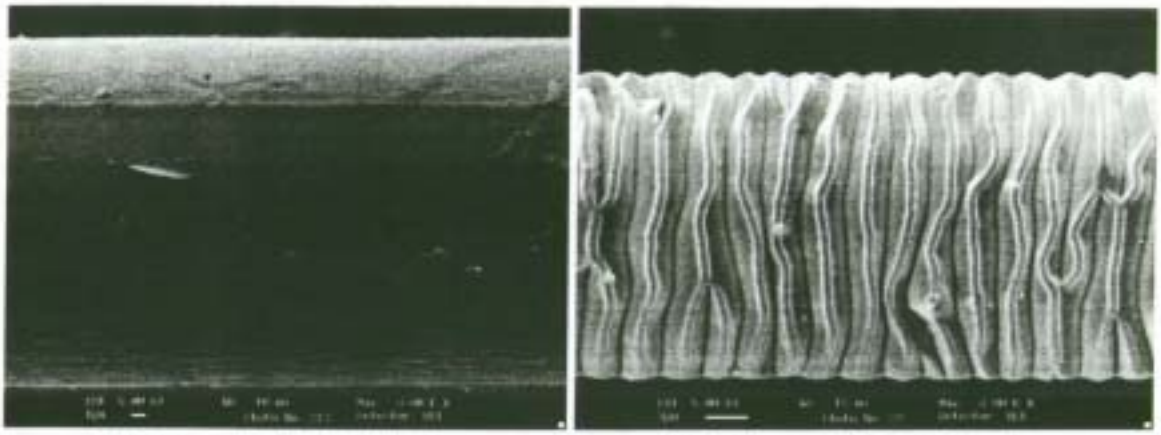

(a) 150 mJ cm^{-2} and 100 pulses (b) 100 mJ cm^{-2} and 50 pulses

Figure 2.8: The SEM images of nylon 66 after (a) 248 nm and (b) 193 nm excimer lasers irradiations.

On the other hand, PET fibers can form LIPSS with both of wavelengths, but only with different ripple spacing. Figure 2.9 shows two typical examples of PET fibers treated with same fluence and number of laser pulses, but for two different laser wavelengths, i.e. 193 nm and 248 nm. In the images, 248 nm laser has induced a greater spacing between ripples compared with the that produced by 193 nm laser. The detailed relationship between the mean ripple distance and the number of laser pulses at different laser wavelengths is shown in Figure 2.10 which shows the obvious difference in ripple spacing formed by two kinds of laser irradiation. As the number of laser shot increases, the ripple distances increase gradually. Afterwards, the growth of LIPSS becomes saturated by a certain amount of radiation dosage, and the mean ripple distance tends to a certain values, which depends on the radiation wavelength. For the shorter wavelength, the saturated value is relatively lower than the longer wavelength, about 1.6 μm for 193 nm laser and 3.6 μm for 248 nm laser. One of the explanations is due to the difference in penetration depths for 193 nm laser (about 0.034 μm) and for 248 nm laser (0.062 μm). Hence there is more involvement of materials when fibers are treated with 248 nm laser than with 193 nm irradiation.

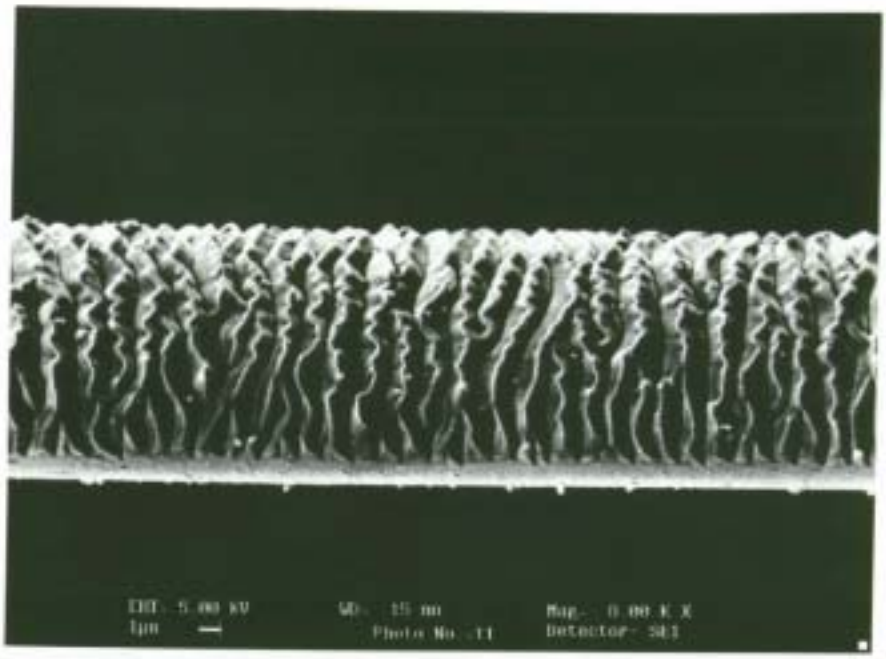

(a)

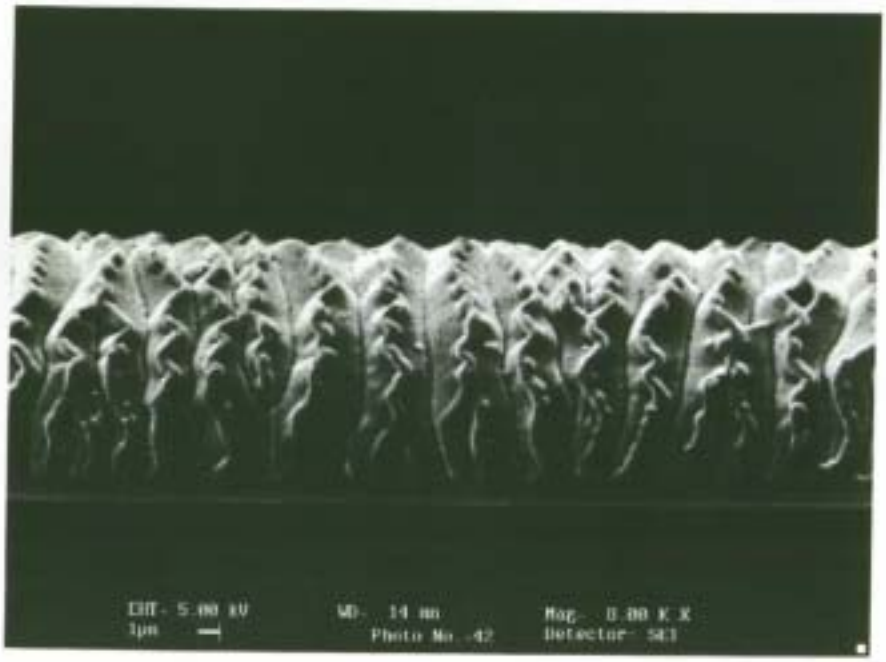

(b)

Figure 2.9: The periodic structures formed by (a) 193 nm and (b) 248 nm laser radiation on PET fibers with fluence of 50 mJ cm^{-2} and 50 pulses.

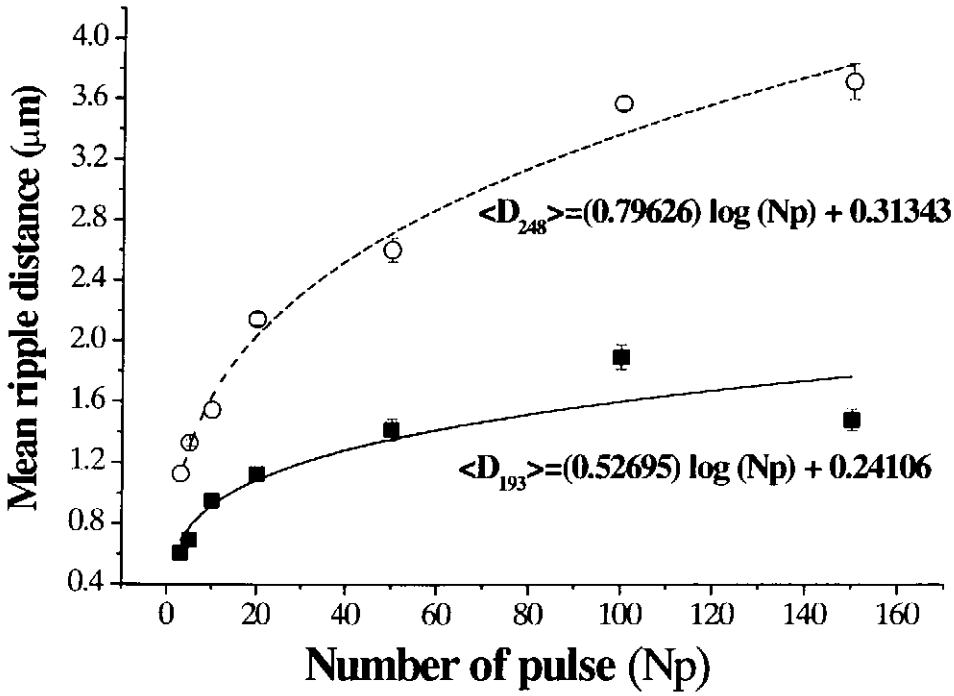

Figure 2.10: Comparison of the mean ripple distance of LIPSS formed by (■) 193 nm laser irradiation and (○) 248 nm laser irradiation with different laser pulse.

The tendency of the curves also obeys a logarithmic model function suggested by Knittel D [Knittel D. *et al.*, 1997a], where the value of K_1 is very sensitive to the absorption depth of the irradiation. As mentioned before, absorption depth on the same material is different for laser with different wavelengths.

Laser fluence dependence

The laser fluence dependence was studied by using laser irradiation with same number of shot and same wavelength. SEM images were taken and the mean ripple distances were compared. Figure 2.11 shows the SEM images of the PET fiber treated with 193 nm excimer laser for the same number of pulses but different fluence of 200 mJ cm^{-2} and 500 mJ cm^{-2}. It can be seen that shorter ripple distance has resulted from lower fluence of laser irradiation. More information of the fluence dependence on ripple spacing is provided in Figure 2.12, by varying the number of irradiating pulses at two different fluence of 71 mJ cm^{-2} and 163 mJ cm^{-2}. Similar to the relationship between the different wavelength and number of pulses, the curves also increase gradually and then saturate at a certain values.

One of the explanations is energy content carried by higher fluence laser. Such energy will be absorbed and transferred into the bulk materials. Therefore, the higher the fluence is the deeper the melt zone can be obtained. Finally a greater ripple distance can be achieved.

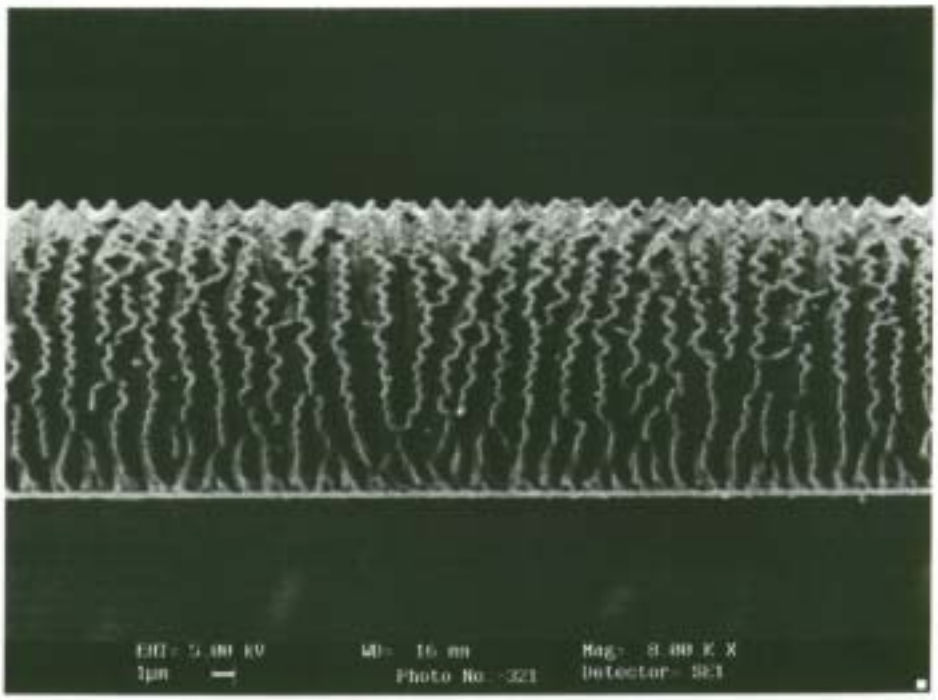

(a)

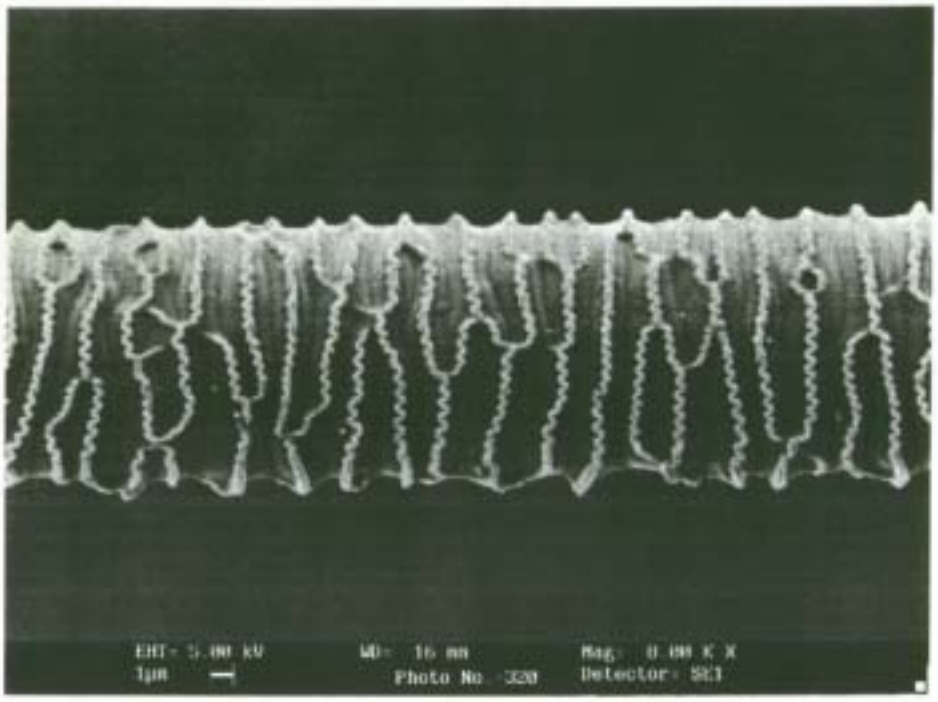

(b)

Figure 2.11: The periodic structures formed by 193 nm laser irradiation with fluence of (a) 200 mJ cm^{-2} and (b) 500 mJ cm^{-2} at 20 pulses.

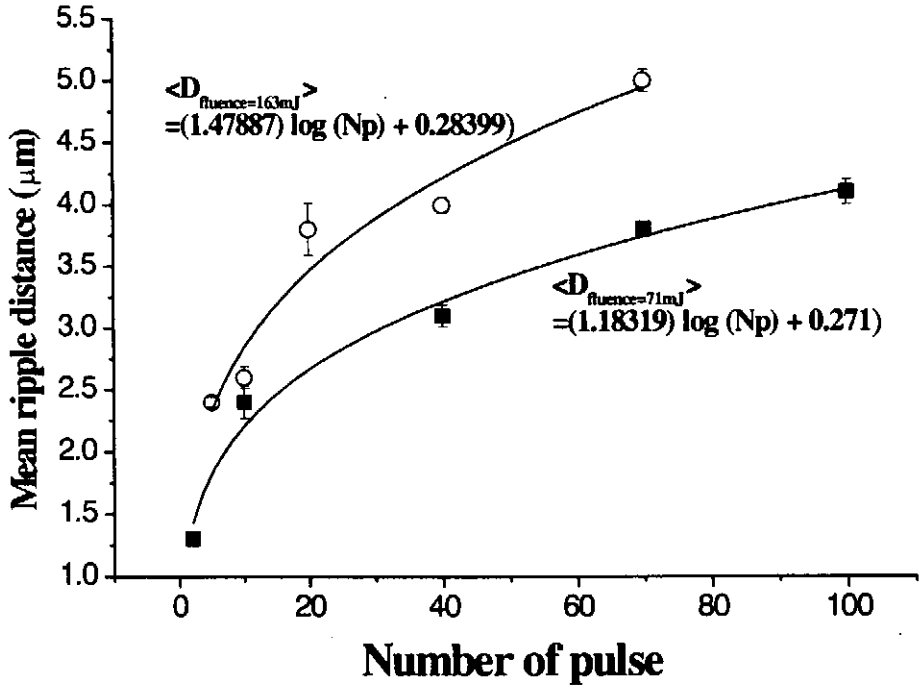

Figure 2.12: Comparison of the mean ripple distance of LIPSS formed by 248 nm excimer laser with fluence of (■) 71 mJ cm^{-2} and (○)163 mJ cm^{-2} at various number of laser pulses.

Number of pulses dependence

The hill and valley structure is formed on the PET fibers after excimer laser irradiation. These structures grow gradually as the number of pulses increases. For one shot of laser pulse with fluence higher than the material ablation threshold, a fine, but rather irregular structure is generated. This uneven structure is enlarges on further laser irradiation, giving a larger mean ripple distance between hills. The measured values already shown in Figure 2.10 and 2.12. A series of the SEM images of laser treated PET fibers are shown in Figure 2.13, both in fluence of 50 mJ cm^{-2} but different number of laser pulses (from 1 pulse to 300 pulses).

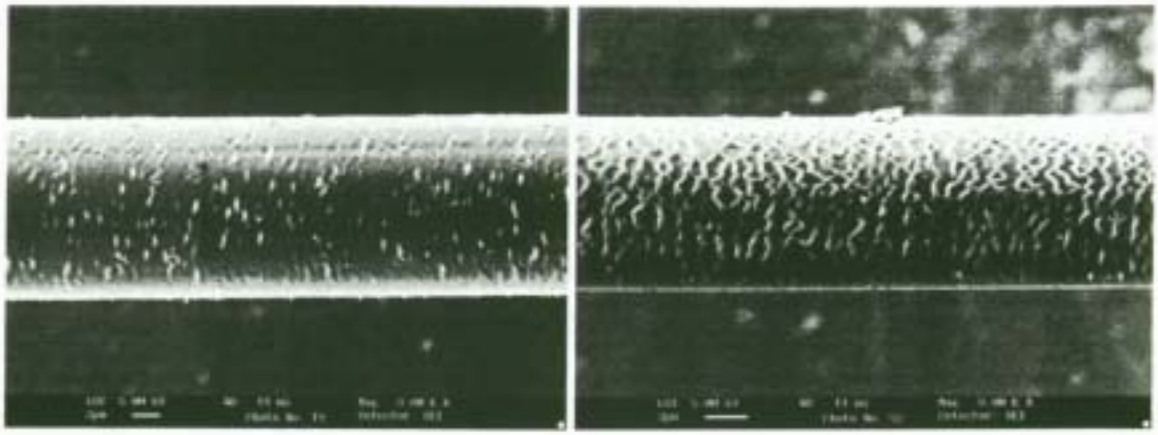

(a) (b)

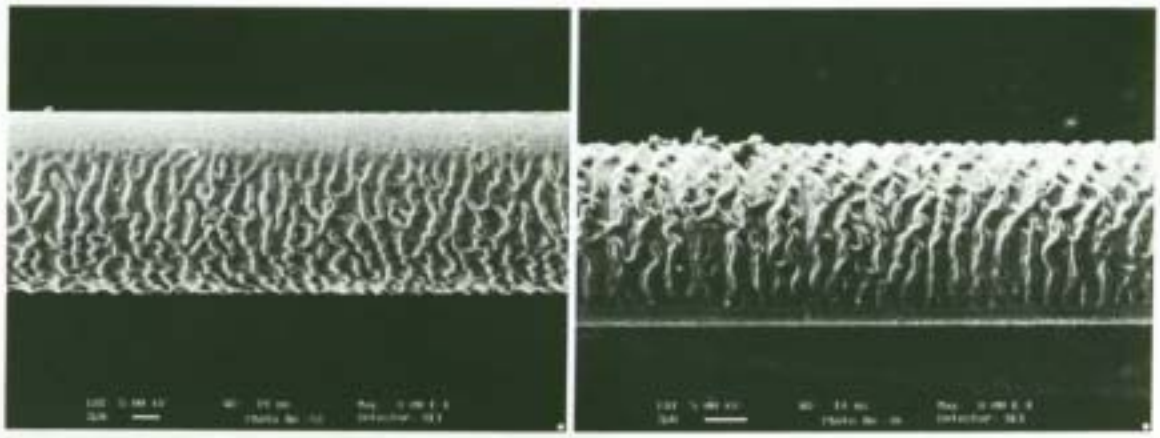

(c) (d)

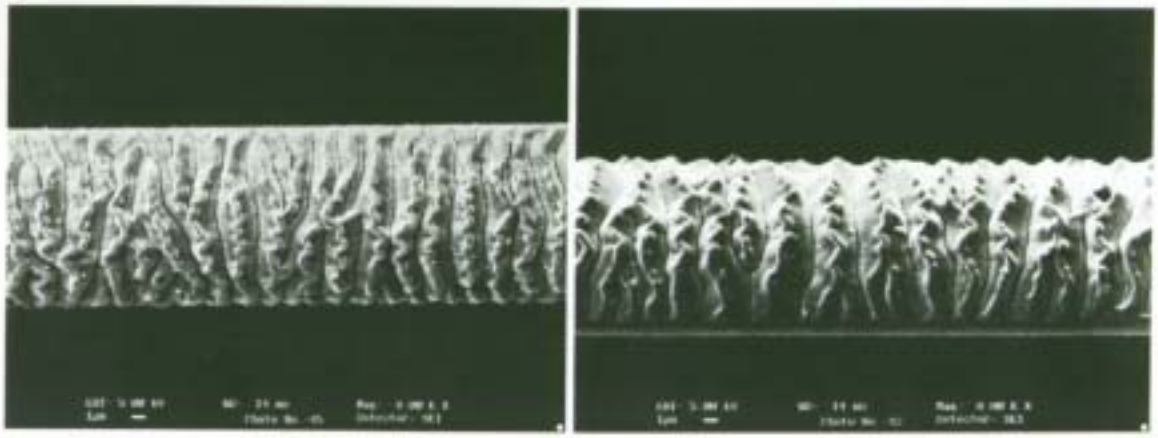

(e) (f)

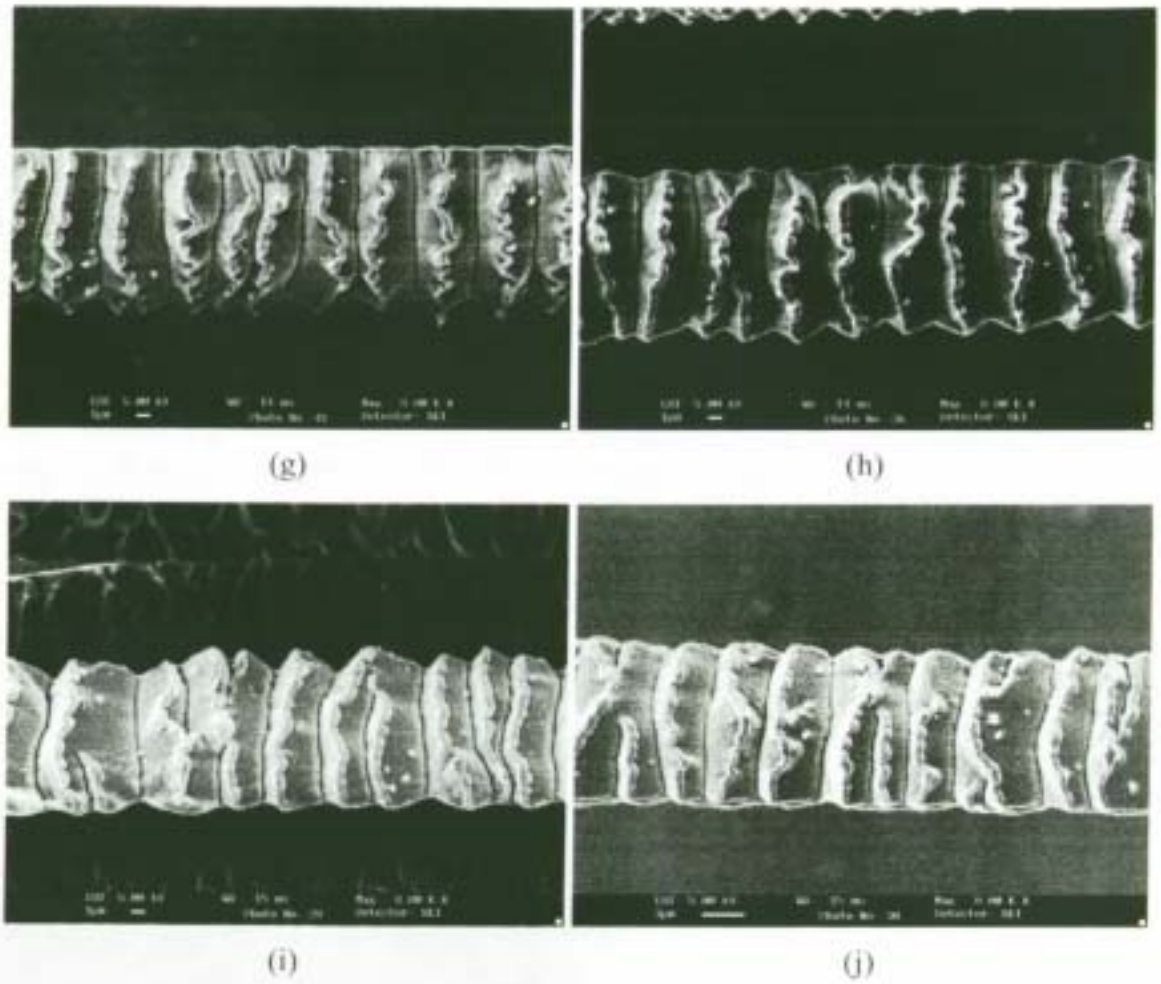

Figure 2.13: A series of SEM images of PET fiber treated with 248 nm excimer laser with fluence 50 mJ cm^{-2} at different laser pulses. (a) 1 pulse, (b) 3 pulses, (c) 5 pulses, (d) 10 pulses, (e) 20 pulses, (f) 50 pulses, (g) 100 pulses, (h) 150 pulses, (i) 200 pulses and (j) 300 pulses.

After about 20 to 150 pulses, the ripples become sharp and all of them are also aligned perpendicular to the fiber axis. Hills and valleys of the surface structure almost approach parallelism. No further changes can be observed by continuous laser irradiation. This result also coincides with the curves shown in Figure 2.10 and 2.12. It is believed that the structure is formed by means of thermal effect. During laser irradiation, the material is heated up by photothermal process. The upper layer of the material melts and then restructures in a very short time interval. Since stress has built

inside the fibers during the manufacturing process, therefore stress relaxation will occur if the material melts. The details of the formation mechanism will be discussed in the mechanism and theory sections.

2.2.2 Morphological study of low fluence laser treated PET fibers

The effects of low fluence laser treatment on PET fibers are reported in this chapter. Laser induced periodic surface structures are formed on the fibers by using 248 nm UV excimer laser with fluence below the ablation threshold of the materials so that no materials removals are involved in the treatment. The optimum conditions for forming a successful periodic ripple structure on PET fibers are 6 mJ cm^{-2} of laser fluence and 2000 shots of laser pulses. Other than the fluence and pulse number of the laser, the degree of polarization of the laser, its direction of polarization and the curvature of the fiber surface also play an important role in the formation of LIPSS. All these effects are reported in this work with highlight on the distinctive features in comparison with those of LIPSS on PET fibers due to high-fluence lasers and LIPSSs on PET films due to low-fluence lasers.

Laser beam polarization dependence

The effect of the degree of polarization of the irradiating laser was studied using the partially polarized and highly polarized laser beams as described in Chapter 1. The laser fluence at the sample and the number of pulses were kept at 6 mJ cm^{-2} and 2000 respectively. Figure 2.14 shows the SEM images of the treated PET fibers, with the fiber axis parallel to the direction of polarization. Both of the partially and highly polarized beams produce periodic ripple and / or granule structures with spacing about 200 nm. Figure 2.14a shows the fiber surface that has been irradiated by partially polarized laser. The surface structure is mainly granular, with a slightly oriented pattern along the fiber axis. However in the case of highly polarized light as shown in Figure 2.14b, a highly oriented ripple structure dominates, aligning with the direction of

polarization along the fiber axis.

Mechanisms for the formation of LIPSSs in general, and for the sub-micron structures due to low-fluence laser on polymer films in particular, have been proposed by a number of researchers [Csete M. *et al.*, 1998; Lippert T. *et al.*, 1997]. The pattern formed is believed to be due to the action on a semi-molten selvedge region of a modulating field, which is the interference resultant of the direct and scattered laser light. The pattern will align to the direction of polarization. The intensities of the two components for slightly polarized light perpendicular and parallel to the polarization direction differ only by a small amount. Therefore a granular pattern will develop. For highly polarized light, asymmetry results in a stronger field in the direction perpendicular to that of the polarization. Consequently, a ripple pattern will develop parallel to the direction of polarization (or the direction of the fiber). The mechanism is basically applicable to polymer fibers, as we shall discuss in the following sections.

(a)

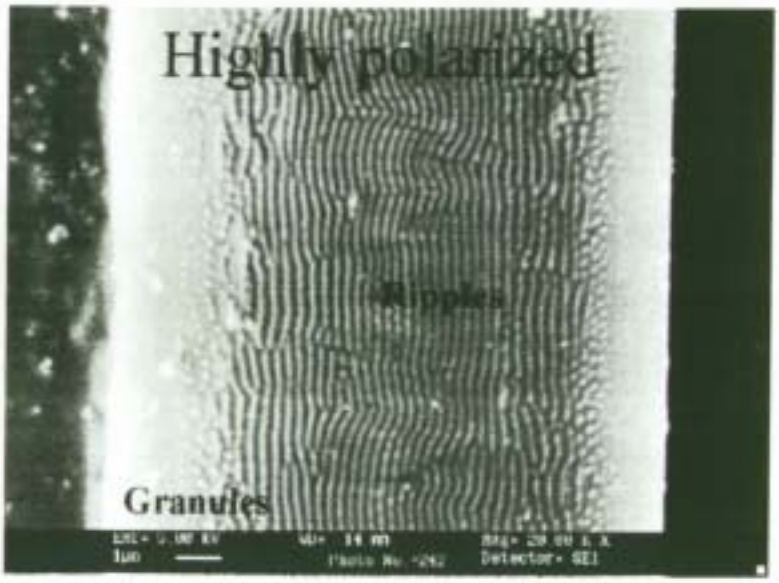

(b)

Figure 2.14: The dependence of the degree of polarization in formatting the LIPSS on PET fibers. (a) PET fiber irradiated by partially polarized laser and (b) PET fiber irradiated by highly polarized laser.

Fiber orientation dependence

The highly polarized beam was used to study of the relationship between the periodic structures and the direction of polarization relative to fiber orientation. Under the same fluence (6 mJ cm^{-2}) and number of laser pulse (2000 pulses), fiber samples were irradiated with different fiber orientation relative to the polarization direction of the beam. The results at inclination angles of 0, 45, 90 and 135 degrees are shown in Figure 2.15. It can be concluded from these SEM micrographs that the ripple direction tends to align with the polarization direction of the incident polarized laser beam and is independent with the fiber orientation. It is very different with the pattern formed due to high fluence laser treatment, indicating different forming mechanism.

As stated in the previous section, it is an established fact that the ripple patterns will align to the direction of polarization for polymer films under low-fluence irradiation. The result shows that this property persists for polymer fibers, of which the internal tensile stress of the fibers does not play a role in the ripple orientation. However, for polymer fibers under high-fluence irradiation, the ripple pattern is invariably perpendicular to the fiber axis. [Lazare S. *et al.*, 1993]

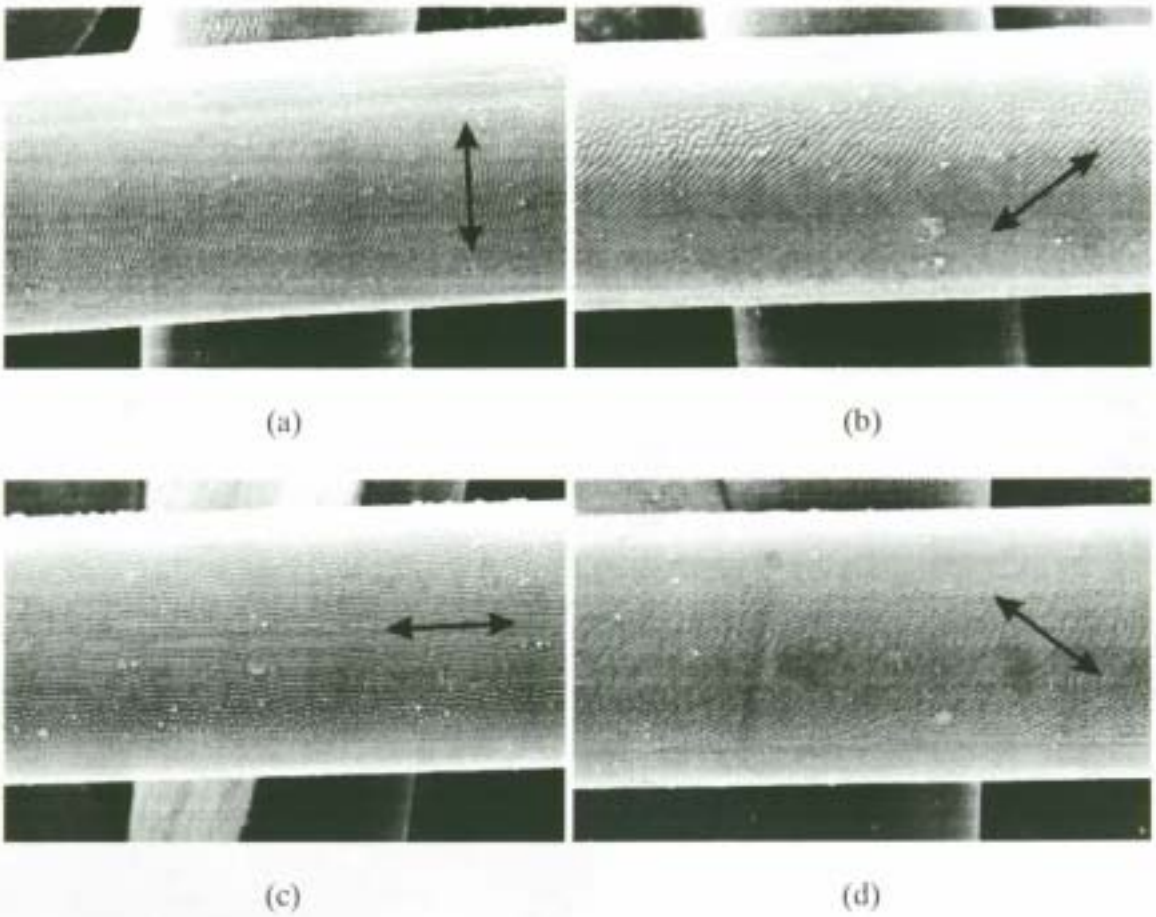

Figure 2.15: PET fiber irradiated by 248 nm excimer laser with fluence of 6 mJ cm^{-2} and 2000 pulses with the polarization direction (the arrow) at (a) 0°, (b) 45°, (c) 90° and (d) 135° to the fiber axis of the fiber.

Laser fluence dependence

In low-fluence polarized laser treatment, the fluence used is far below the ablation threshold of the irradiated polymer, which is about 20-30 mJ cm^{-2} for our PET fibers. Therefore fluence between 3 to10 mJ cm^{-2} was selected in this study. Figure 2.16 shows the effect of fluence in structuring the PET fibers. Figure 2.16a shows at a low fluence of 3 mJ cm^{-2}, the surface is free of modification even after the irradiation of 50,000 laser pulses. For higher fluence greater than 10 mJ cm^{-2}, however, the high fluence completely melts a surface layer and prevents periodic structures to developed as shown in Figure 2.16c. Between the two fluence limits, say 6 mJ cm^{-2}, successful ripple structures can be formed, as shown in Figure 2.16b. It can be concluded that in order for successful LIPSS formation on PET fibers, a narrow window of laser fluence (roughly 4-9 mJ cm^{-2}) should be used. M. Csete *et al.* and Sendova M. *et al.* reported a similar result for low-fluence laser on PET film in 1998 [Csete M. *et al.*, 1998 and Sendova M. *et al.*, 1994]. No similar window has been reported for high-fluence laser treatment on PET fibers.

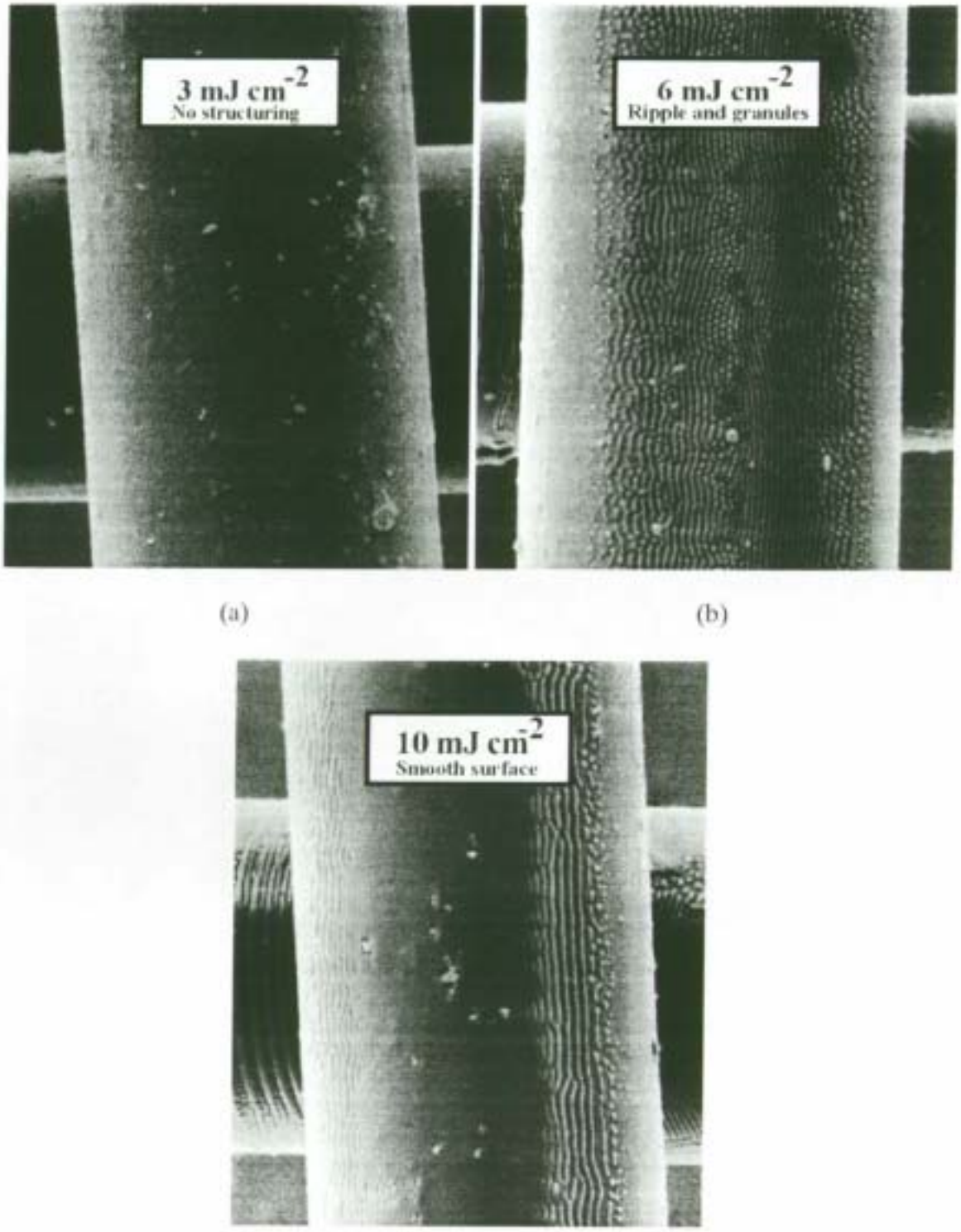

Figure 2.16: The dependence of the fluence used in forming sub-microns LIPSS on PET fiber. (a) 3 mJ cm^{-2}, (b) 6 mJ cm^{-2} and (c) 10 mJ cm^{-2}.

The cumulative effect of the laser pulses

Within the fluence window there should be sufficient dosage of irradiation in order to produce surface structure. The highly polarized laser beam with fluence maintained at 6 mJ cm^{-2} was used to study the dosage effect by varying the number of laser pulses for a given exposure. Figure 2.17 shows the dependence of the number of pulses in structuring the fiber surface. Initial structures appear on the fiber surface of Figure 2.17a, after the treatment of 500 laser pulses. These initial structures lie on the sides of the fiber (regions of greater angle of incidence, α) and most of them originate around some surface defects. After irradiation of about 2000 pulses, successful ripple structures have fully developed as seen from Figure 2.17b. By increasing the number of pulses to 5000 pulses, granular structures appear randomly between ripples, as shown in Figure 2.17c. Finally, if the number of pulses exceeds a certain value, about 10,000 pulses, all the ripples change to granules (Figure 2.17d).

Surface scattering is enhanced at the region of greater angle of incidence. Therefore ripple structures first appear at both sides of the fiber and then develop over the whole surface. For the same reason, the granules first appear at sides of the fiber thereafter and the granular structure then spreads over the whole surface. Prolonged low-fluence treatment of highly polarized beam produces similar granular structures as those due to the treatment of partially polarized beam. For partially polarized beam, scattered light in either direction differs only slightly and granular pattern develops right from the beginning.

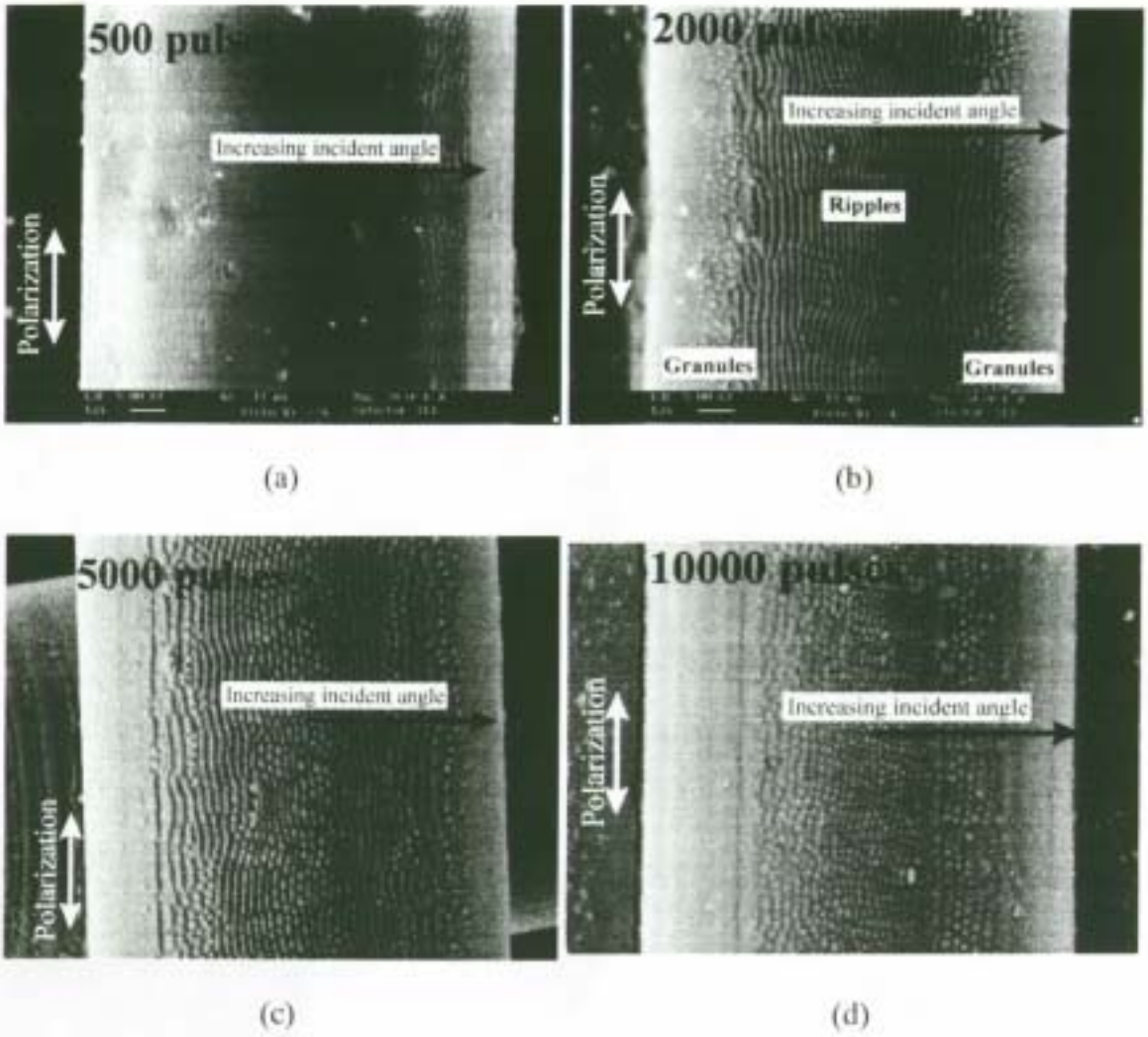

Figure 2.17: The dependence on the number of laser pulse in structuring the polymer surface with fluence of 6 mJ cm^{-2}. (a) 500 pulses, (b) 2000 pulses, (c) 5000 pulses and (d) 10000 pulses.

2.3 Mechanism of LIPSS formation

2.3.1 High fluence laser treatment

In the previous section, morphological study of the laser induced periodic surface structure have already been described in terms of the influence of excimer laser parameters such as laser wavelength, fluence and number of laser pulses. The ripple structures produced in separation of a few microns and basically perpendicular to the fiber axis. Thermal effect was believed to predominate the forming mechanism. High UV absorption coefficients and existence of stress fields also plays important roles.

Temperature profile of the PET fiber during high fluence laser irradiation

Energy input to the material surface is restricted to a small volume, at least during the time scale of the laser pulses. Since the relaxation rate for the change of an electronic state to a thermal vibrational state R' (~10^{11} s^{-1}) leading polymer heating is markedly higher than thermal diffusion into the bulk polymer (~10^{5}-10^{7} s^{-1}). Temperatures within the surface may reach values up to 10^{3} K. [Knittel D. *et al.*, 1997]

In order to estimate the temperature of the irradiating PET surface, the one-dimensional heat conduction equation was solved by substituting the physical parameters of PET. [Csete M. *et al.*, 1998]. The one-dimensional heat conduction equation is shown below:

$$\frac{\partial^2 T(x,t)}{\partial x^2} - a^2 \frac{\partial T(x,t)}{\partial t} = -\frac{\alpha}{\kappa} P(t) \exp(-\alpha x) F_0$$

Where $a^2 = \rho c/\kappa$, $\rho = 1.39\times10^3$ kg m^{-3} (the density of PET), $c = 1.165\times10^3$ J kg^{-1} K^{-1} (specific heat of PET), $\kappa = 1.47\times10^{-1}$ W m^{-1} K^{-1} (thermal conductivity of PET), $\alpha = 2.3\times10^5$ cm^{-1} (absorption coefficient of PET at 248 nm wavelength); $F_0 = 50$ mJ cm^{-2} (the fluence used in the laser treatment), and $P(t) = 2t / (\tau^2) \exp[-(t/\tau)^2]$ describes the typical shape of the excimer pulse, where $\tau = 13.24$ ns as calculated from the known FWHM = 15 ns of the pulse. The pulse shape is shown in Figure 2.18.

Taking into consideration of the initial room temperature of 20 °C, and also the boundary condition of $\partial T/\partial x = 0$, the relationship between temperature and time at different depth of PET was solved by using the appropriate Green's function. Figure 2.19 shows the time dependence of the temperature at different depths of the polymer. The temperature reaches about 3500 °C when the surface has been irradiated by a single shot of 248 nm excimer laser with fluence 50 mJ cm^{-2}. The value is very close to 10^3 K that mentioned by Schollmeyer.

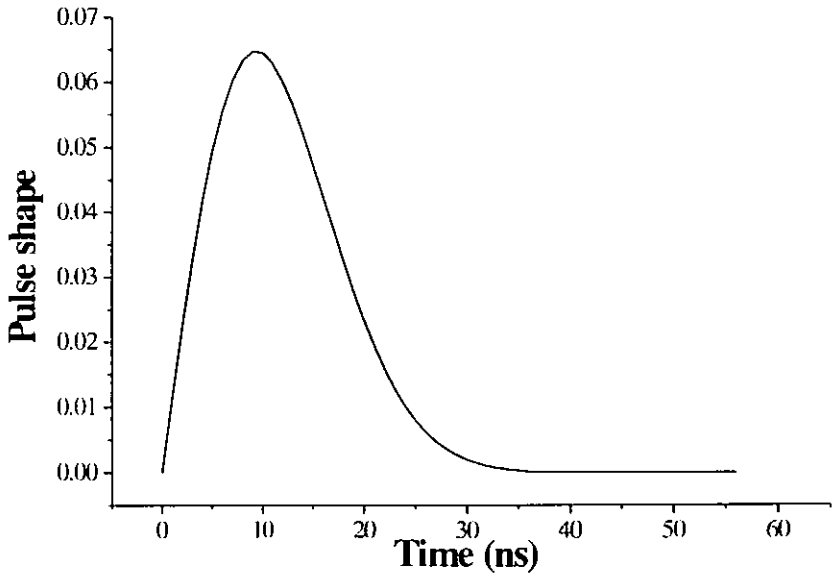

Figure 2.18: The temporal shape of the laser pulse, described by the function P(t).

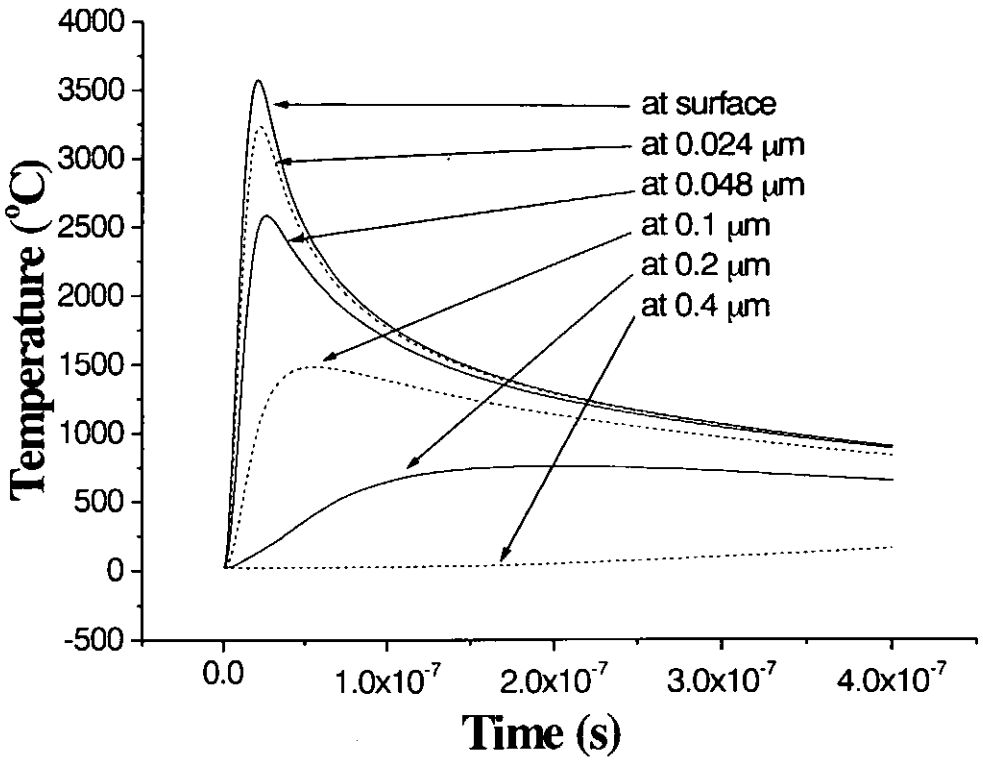

Figure 2.19: The time dependence of the temperature at different depths in the PET materials treated by 248 nm excimer laser with fluence of 50 mJ cm^{-2}.

In fact, polymer cannot reach such high temperature without any degradation. Although the profiles shown just indicate the temperature when all the thermal energy has been accumulated in the polymer without any loss, including loss to surrounding and due to the removal of polymer fragments, in the case of that high fluence laser treatment, the energy is always large enough to ablate part of the materials during laser exposure. Therefore an etching process should be involved at the beginning of ripple formation under high fluence laser treatment.

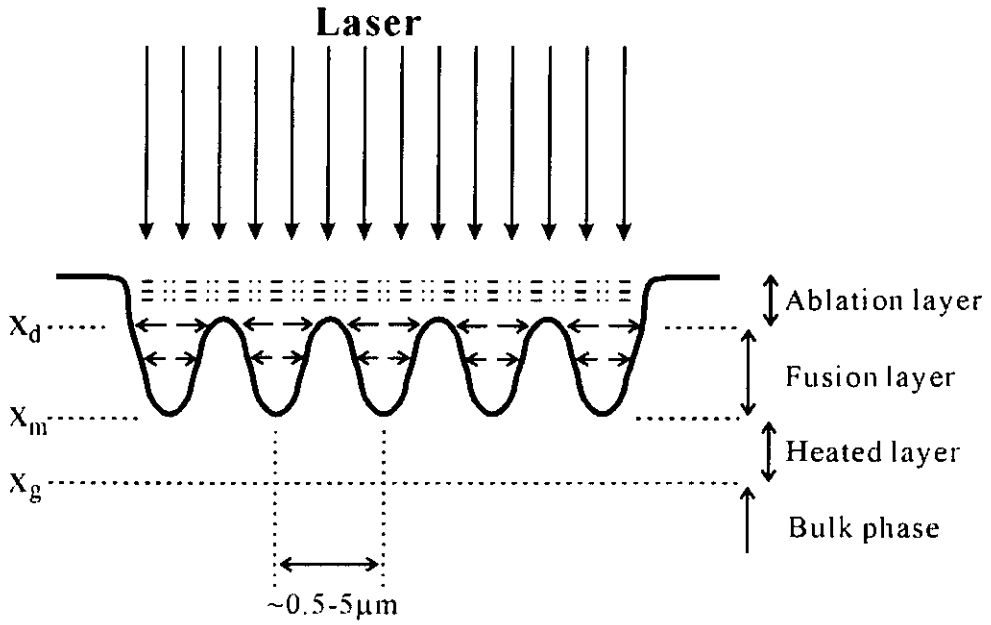

Figure 2.20: Model of the formation of LIPSS on PET fiber surface under high fluence excimer laser irradiation.

Mechanism of the LIPSS formation under high fluence laser treatment

Figure 2.20 shows a schematic model of the ablated polymer surface, which was given originally proposed by Knittel *et al.* [Knittel D. *et al.*, 1997b and Bahners T., 1993]. The structure consists of the ablation layer (surface to X_d in diagram), the fusion layer (X_d to X_m), and the layer which was heated above the glass transition temperature (X_m to X_g). Regions further inside the polymer do not contribute to the phenomenon of structuring.

Bahner & Schollmeyer suggested that synergistic phenomena between the internal stress field and the high temperature gradient (6×10^7 K cm^{-1} [Kesting W. *et al.*, 1993]) created in the surface layer of the polymer would lead to self-organizing materials convection and formation of ripples, which solidify when energy input ceases. No interpretation of the evolution of surface structures with increasing laser irradiation was

given.

After a certain number of laser shots, the surface layer is molten within a depth of a few microns and temperature gradients build in due to the high laser energy. Because of the temperature influence, gradient of viscosity of the molten region and gradients of polymer chain mobility within the underlying (still solid) polymer exist. Within such a region, shear induced shrinkage and the flow phenomena start. (As indicated in Figure 2.20, the arrows show the direction of the shrinkage). Reorganization of polymer chains is accompanied by the ablation of polymer fragments. Thus incoming irradiation pulses will drive the melt zone continuous into the fiber. The shrinkage is also caused by stress relaxation. The stress can be induced by drawing the fiber or elongating the fiber by mechanical method. Fibers with higher draw ratios show higher mean ripple distance after laser irradiation [Knittel D. *et al.*, 1997b].

The top of the ripples after solidification consists of almost amorphous polymer material, where no internal stress or tensions can be expected. These parts will survive in further laser irradiation, but the height will decrease because of ablation.

The forming mechanism also manifests under SEM images. Figure 2.21 shows the laser treated PET fibers. In Figure 2.21a, branching (indicated by arrows) appears on all the irradiated area. As the number of laser pulses increases, the number of branches becomes diminished. After a certain number of laser shots, no more branches appear (shows in Figure 2.21b) and the mean ripple distance becomes unchanged. This confirms that the merging effect is important in the formation of ripples with greater spacing and a cumulative effect of laser dosage [Knittel D. *et al.*, 1997a]. After the

saturation, no more sites can be merged, then the mean ripple distance become constant.

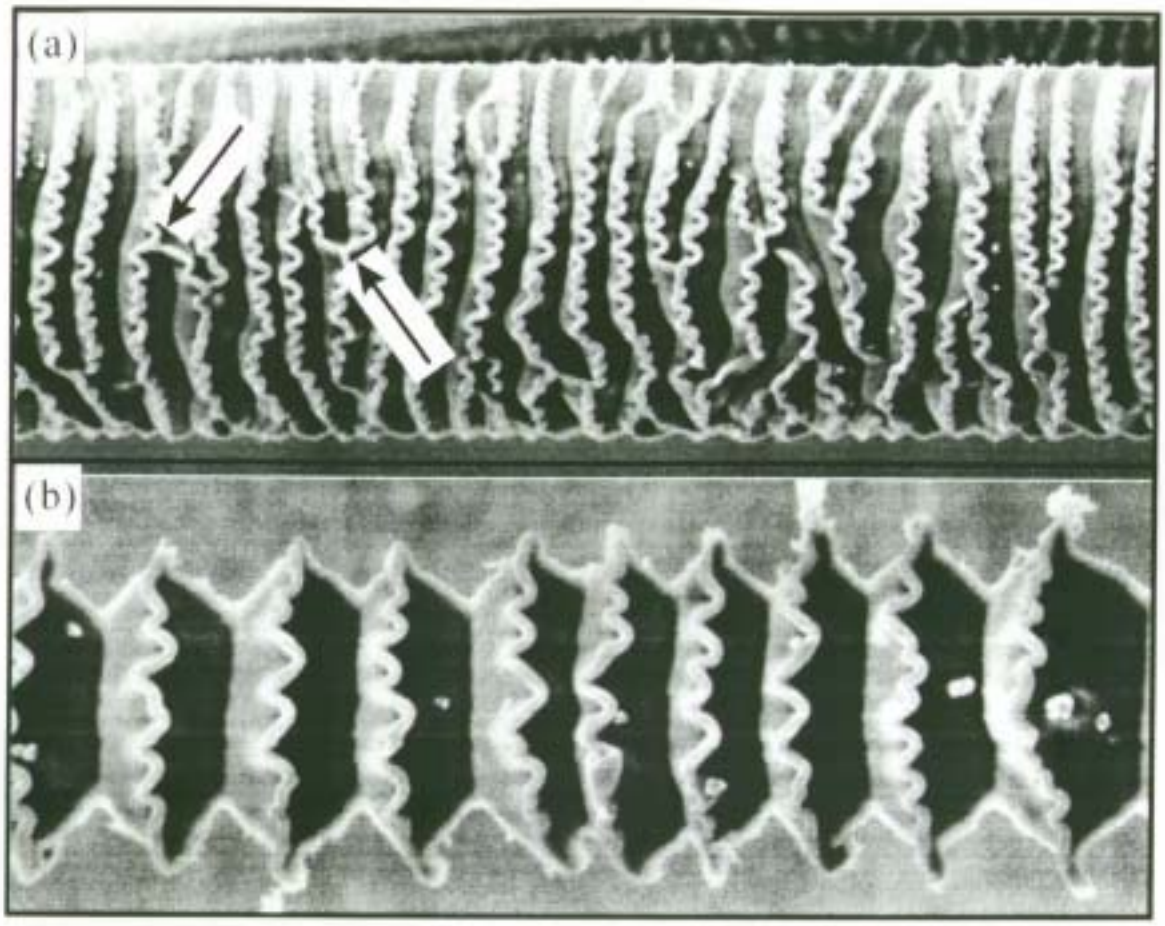

Figure 2.21: The laser treated PET fiber. (a) Branching (indicated by arrows) and (b) without branching.

If the fluence and the number of laser pulses are great enough, the fiber will disintegrates into elliptical segments mainly due to the continuos etching on the fiber, especially at the valleys (stress also exit in the untreated material just below the valleys).

2.3.2 Low fluence laser treatment

For the low fluence laser treatment on the polymeric materials, a periodic surface structure is formed after the laser irradiation. The final appearance of such kind of laser treatment is very difference from the LIPSS induced by high fluence irradiation, mainly in the magnitude of dimensions and also the formation mechanism. Figure 2.22 shows the schematic diagram of the treated sample surface. The periodicity of the ripples is about 200 nm, and the depth of such fusion layer is also very thin. It is very different from the ripples with microns-sized spacing and depth after high fluence laser treatment. Because the fluence used in low fluence laser treatment is far below the ablation threshold of the materials, therefore, it is believed that no material removal is involved in the treating process. That means no ablation layer existing in the schematic diagram.

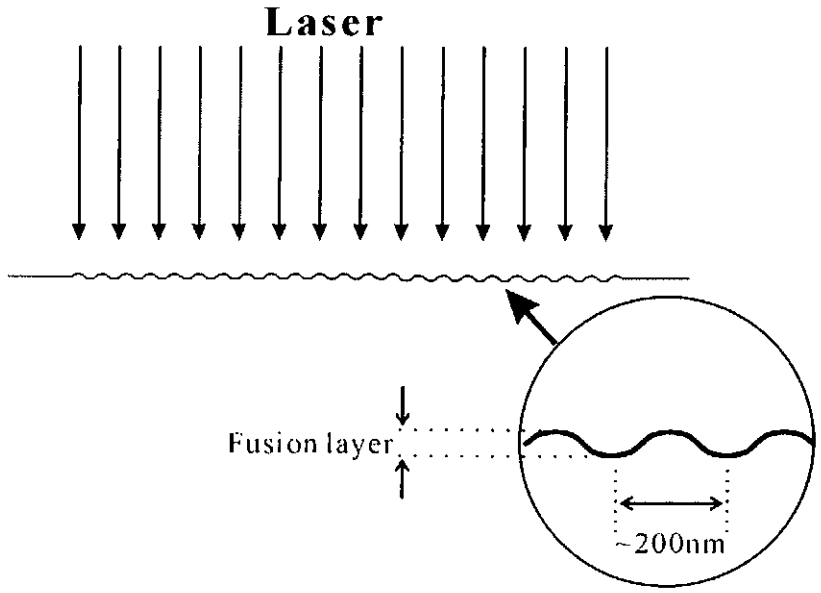

Figure 2.22: Schematic diagram of the periodic surface structure formed by low fluence laser irradiation.

Temperature profile of the PET fiber during low fluence laser irradiation

As mentioned in section 2.2, a "window" of fluence is needed to form the successful LIPSS on PET surface under low fluence laser treatment. Therefore, to understand the temperature distribution is a first and important step in realizing the whole mechanism of LIPSS formation. One-dimension heat conduction equation (same with the equation applied in the previous section) was employed in order to understand how the photon induced thermal energy distributed in the polymer. PET has undergone two important phase transition temperatures in the temperature region: the glass transition tewmeprature: T_g = 125 °C for crystalline and oriented structuring, and melting point: T_m = 250-265 °C [J. Brandrup *et al.*, 1975].

Based on the curve obtained in Figure 2.23, the maximum temperature attained (160 °C) due to 248 nm excimer laser with fluence 2 mJ cm^{-2} cannot reach the minimum temperature (melting point T_m) required for melting PET material. Therefore no periodic surface structure can be formed, as already shown in SEM images of section 2.2. On the other hand, when fluence of 6 mJ cm^{-2} (shows in Figure 2.24) is used in the laser treatment, the maximum temperature can reach to 450 °C, which is high enough to melt the materials in the upper surface layer. This upper surface layer is about 70 nm below the surface. During the laser irradiation, this molten layer has enough energy in undergoing self-organization and rearrangement them under specified conditions. That will be discussed in the mechanism section. If higher fluence was used, e.g. 8 mJ cm^{-2}, the fusion layer becomes relatively thick and therefore the resulting surface will have only melting features but no LIPSS is formed.

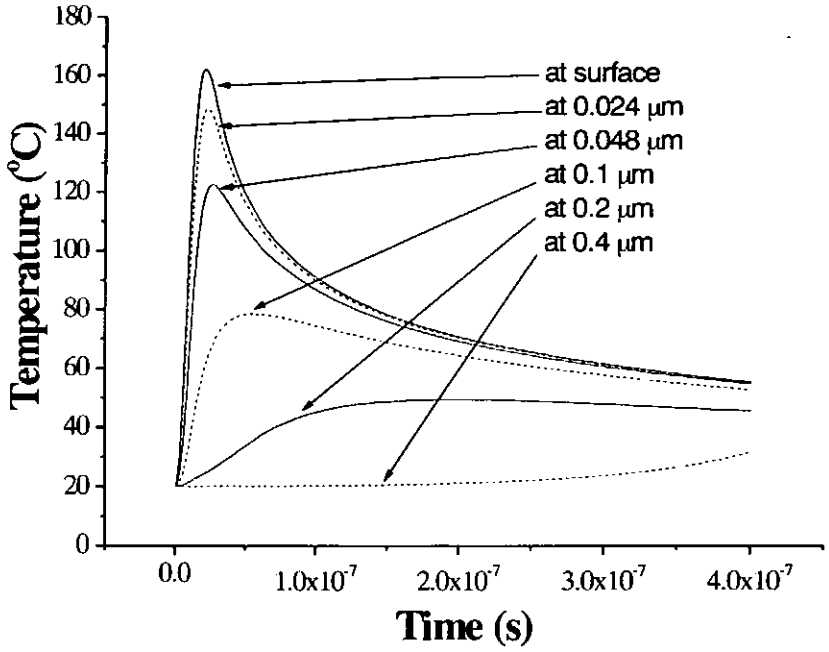

Figure 2.23: The time dependence of the temperature at different depths in the PET materials treated by 248 nm excimer laser with fluence of 2 mJ cm^{-2}.

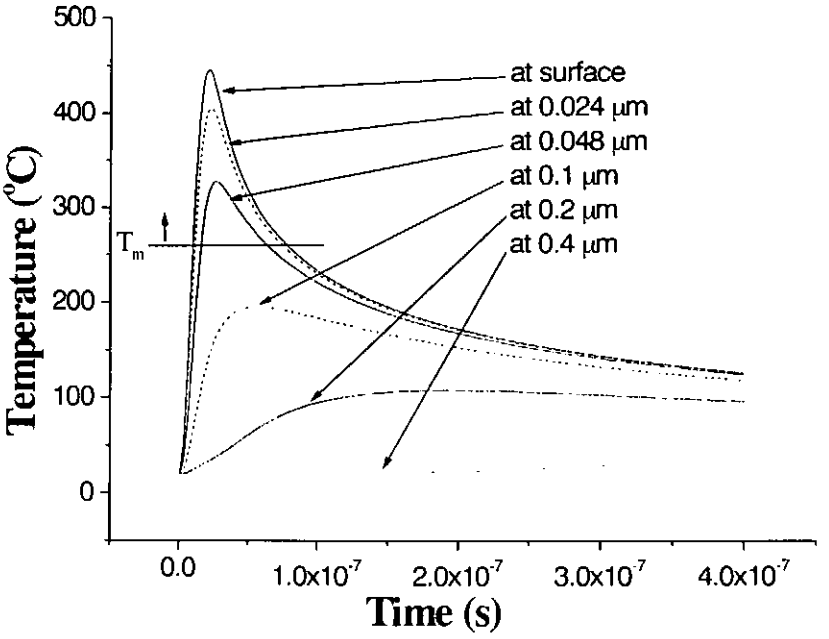

Figure 2.24: The time dependence of the temperature at different depths in the PET materials treated by 248 nm excimer laser with fluence of 6 mJ cm^{-2}.

Mechanism of the LIPSS formation under low fluence laser treatment

During low fluence laser treatment, the whole surface of PET has undergone some kind of phase-transition, which alters the optical parameters of the polymer. Because the upper layer of the materials melts due to the thermal energy, the molten layer and the original PET will be different in refractive index. For the molten layer, the refractive index n_i is 1.33 and the original PET has index n_o = 1.64 [Bolle M. *et al.*, 1993]. Laser waves can be scattered by any rough sites on the surface. Even in the very beginning, the waves are scattered by the nano-meters scaled roughness. These scattered waves coupled with the nearby incident waves will produce interference pattern [Siegman E. Anthony *et al.*, 1986] and then propagate onto the surface. As mentioned before, the upper surface layer has already melted due to sufficient high energy of the laser, and therefore, materials can be easily flow and self-rearrange.

As shown in Figure 2.25, the incident wave couples with the scattered wave and then produces interference pattern with spacing about Λ. In the insert of the Figure, α is the incident angle of the laser corresponding to the materials surface, β is the angle between the normal and the refracted wave. The relation between α and β is "$\sin\alpha = n_i \times \sin\beta$". ϕ is defined as $\frac{90^\circ - \beta}{2}$ that is the half angle between the two interfering waves. λ is the wavelength of the incident laser beam. By using a simple calculation, the relationship between the ripples spacing and the parameters is obtained in Equation 2.1. [Dyer P. E., 1990]

$$\Lambda = \frac{h}{\sin\phi} = \frac{\lambda}{2n_i \sin\phi} = \frac{\lambda}{2n_i \times \frac{1}{2}(1-\cos 2\phi)} = \frac{\lambda}{n_i - n_i \sin\beta} = \frac{\lambda}{n_i - \sin\alpha}$$

Equation 2.1

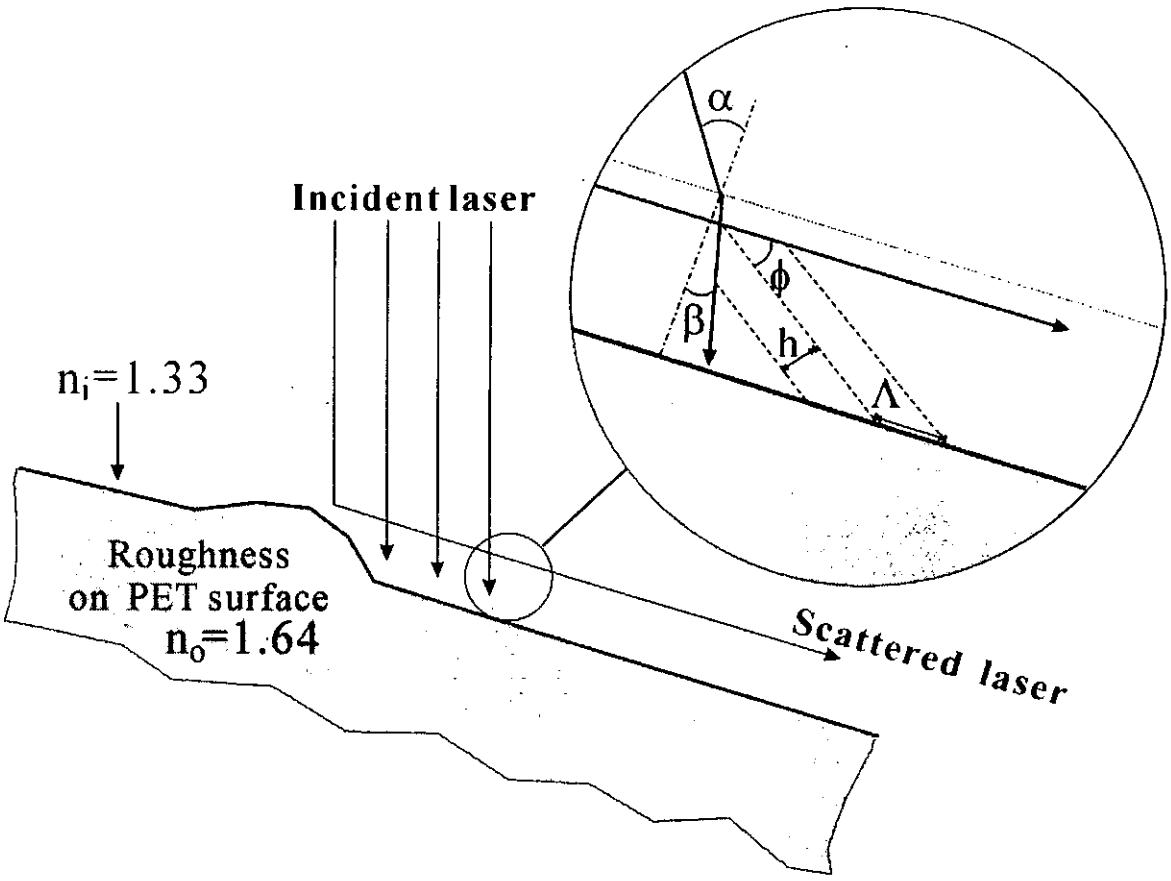

Figure 2.25: The physical model of the submicron-sized periodic structure formed by low fluence laser treatment.

The periodicity mainly depends on the wavelength of the pulsed laser and the angle between the sample and incident waves, with minor effect from the refractive index of the materials. Thus, with the highly polarized 248 nm excimer laser, the periodicity of about 200 nm is obtained on PET fiber surface.

The effect of fiber curvature

Different from the thin film, fibers have a curvature due to the cylindrical surfaces. Therefore the angle of incidence varies across the fiber circumference and according to Equation 2.1, the ripples spacing should increase gradually from center to either side.

The SEM micrographs, however, can only record the projection of the curved surface, Equation 2.1 should then be modified to Equation 2.2 as shown:

$$\Lambda(\alpha) = \frac{\lambda \cos\alpha}{n_i - \sin\alpha}$$

Equation 2.2

Figure 2.26 shows a plot of the average measured values of the ripple spacing obtained from SEM images and the expected values obtained from Equation 2.2. The experimental values agree reasonably well to the expected values especially in the central part of the fiber.

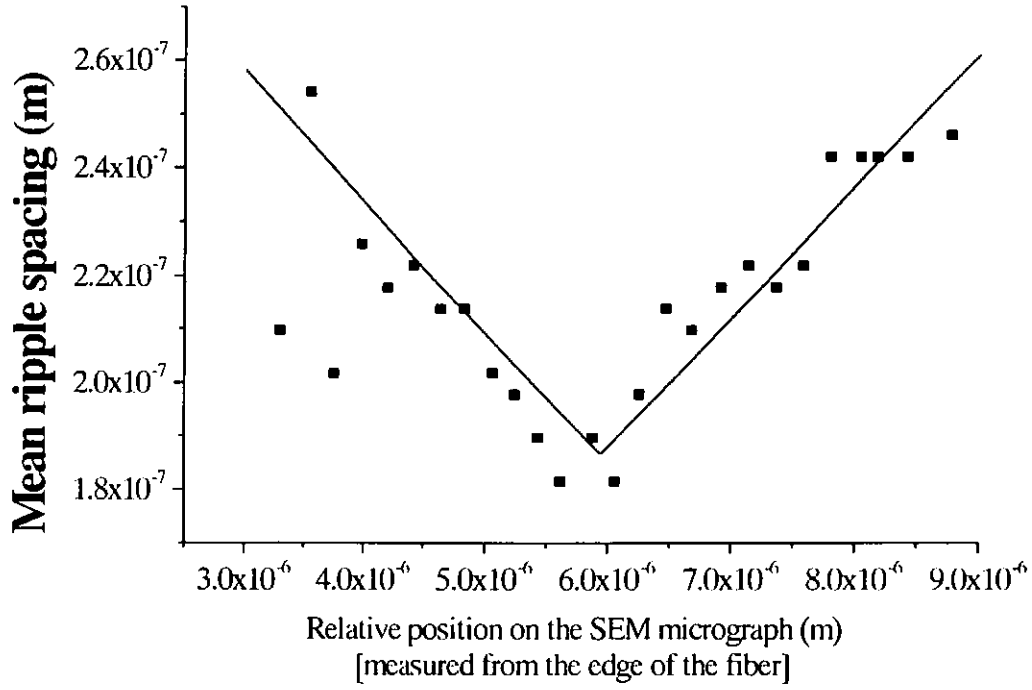

Figure 2.26: The relation of the mean ripple spacing in different position of the laser treated fiber. (■) Experimental measured values and (——) simulated values based on the modified equation 2.2.

Chapter 3 Chemical Modifications

Laser treatment on materials is often accompanied by physical and chemical changes of the surface. Physical modifications occur in the form of a certain regular surface structure (granular structure or ripple-like structure) of the irradiated area using high or low fluence laser treatment. Due to the extremely high absorption coefficient of polymer materials under the short wavelength laser, the reacting volume is very thin. A great portion of laser energy is converted to heat (with the simulated temperature profile mentioned in chapter 2). This kind of thermal effect can introduce many photochemical and photo-thermal reactions. Therefore, in this chapter various analysis methods, including XPS, FTIR and UV spectroscopy are described to characterize the irradiated polymer surfaces / materials in order to study the chemical changes due to different laser treatments.

3.1 Experimental Techniques

3.1.1 X-ray Photoelectron Spectroscopy

X-ray photoelectron spectroscopy (XPS) was used to determine the composition and the chemical structure of the laser treated PET materials. The spectrometer employed was PHYSICAL ELECTRON Phi 5600.

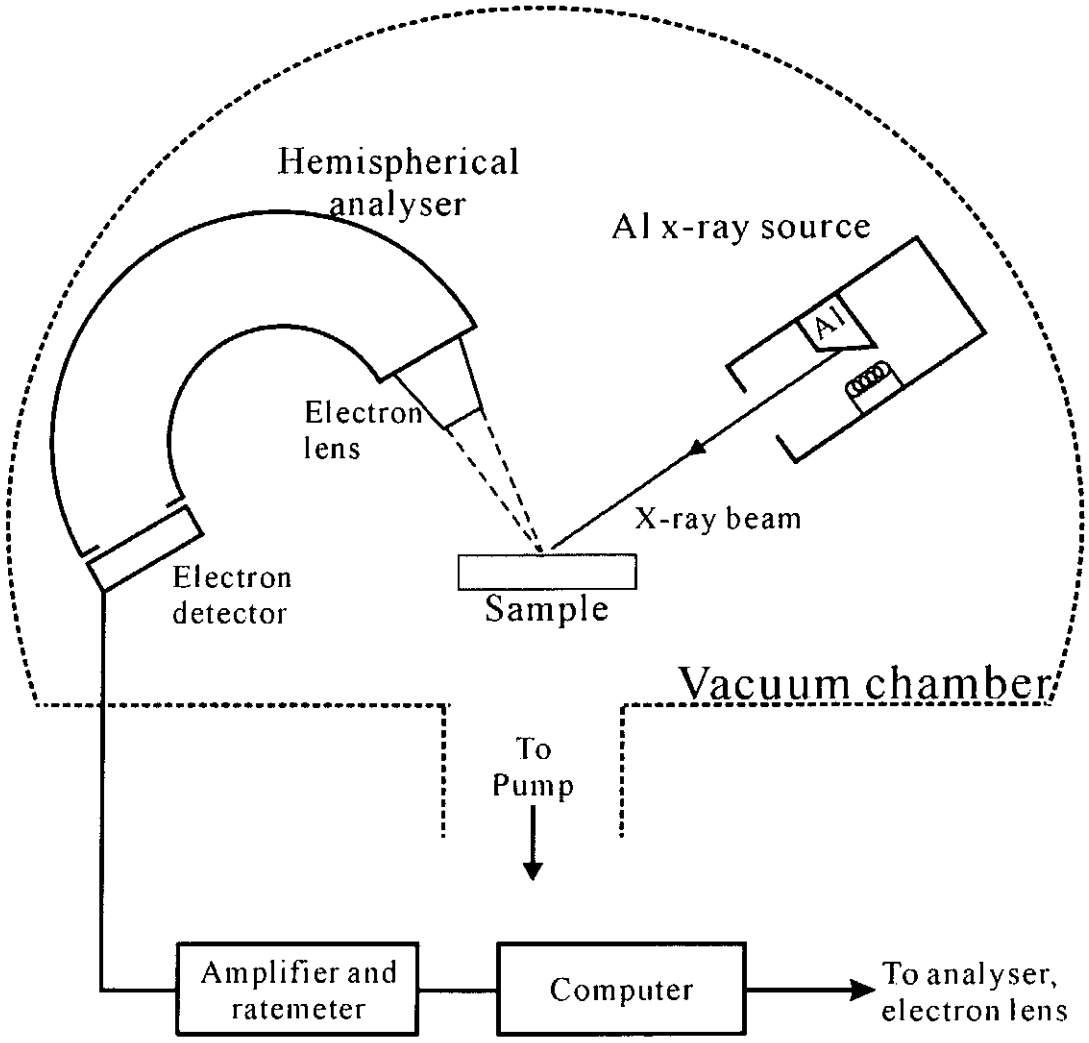

Figure 3.1: Schematic diagram of an XPS system.

Figure 3.1 is a schematic diagram of the XPS system. The chamber is kept at base pressure of 7.3×10^{-9} Torr. X-rays are generated by bombarding an Al $K\alpha$ anode with 10 keV electrons. The X-ray photons ($h\nu$ = 1486.6 eV and 350W) hit and knock out the core electrons of the atoms in the sample. Basically the kinetic energy of a knocked out core electron is $E_K = h\nu - E_B$, where E_B is the binding energy of the electron. To determine E_B, E_K is measured by a hemispherical electron energy analyzer and the relative intensity of the electron flux is counted by an electron detector. Indeed, E_B of the photoelectron is (Equation 3.1):

$$E_B = h\nu - E_K - w$$

Equation 3.1

Where, w is the work function of the spectrometer, a factor that corrects the electrostatic environment in which the electron is formed and measured. Various methods are available to determine a value for w, such as some calibration procedures. From the characteristic values of E_K of the photoelectrons emitted from different kinds of elements in the sample, the composition of the sample can be determined.

The relative content of a specific element, denoted as F_i for instance, can be calculated from the integrated areas of the spectra of all the elements after removing the Shirley background, according to the following formula (Equation 3.2):

$$F_i = \frac{A_i / f_i}{\sum_j (A_j / f_j)} \times 100 at.\%$$

Equation 3.2

Where A_j and f_j are the area of the spectrum and sensitivity factor of the jth kind of element. The sensitivity factors, f_j, of the elements involved in this study are tabulated in Table 3.1.

Table 3.1: The XPS sensitivity factors of carbon (C) and oxygen (O).

Sensitivity factor of C1s (f_{C1s})	Sensitivity factor of O1s (f_{O1s})
0.314	0.733

In addition, because the peak position of a photoelectron spectrum is influenced by the chemical environment of the atoms, by observing the peak shifts of the spectra, one

may examine the chemical change of the sample. However due to charge accumulation on the surface of the insulating samples, the peak of a spectrum may be erroneously shifted without relating to any structural information. This shift can be reduced by a charge neutralizer, which imposes some electrons to the sample to compensate the loss of negative charge due to the emission of photoelectrons. Furthermore, graphite C1s peak usually appears at 285 eV, and can be used as a standard for correcting this systematic error.

The obtained spectra are deconvoluted into certain single core levels after background subtraction. The individual components are taken as mixed Gaussian-Lorentzian functions. Concentrations of the different elements are determined by integration of the area under each individual peak.

3.1.2 Infrared Absorption Spectroscopy

Other than the XPS, Fourier Transform Infrared Spectroscopy (FTIR) is also a common and cost-saving instrument in studying chemical modification of materials, especially polymeric materials. A Nicolet's, Magna-TR^{TM} system 760 was used to investigate the IR absorption spectra of the samples, with the wavenumber varying in the range of 400 to 4000 cm^{-1}. An absorption band occurs when the incident photons are absorbed by the sample to excite the constituent molecules. The frequency of the photon to be absorbed is equal to a natural frequency of the molecules, and so the absorption spectra provide useful characterization information of the materials' structure. Furthermore, the relative intensities of the absorption bands can reflect the abundance of the structural phases associated to the characteristic vibrations.

3.1.2.1 Study on fabric samples

Diffuse reflectance infrared Fourier transform spectrometry (DRIFTS) is an effective way of obtaining infrared spectra directly on non-transparent samples with minimum sample preparation. In addition to time saving in sample preparation, it permits conventional infrared spectral data to be gathered on samples that are not appreciably altered from their original state. The widespread application of diffuse reflectance measurements was possible until the general availability of Fourier transform instruments in the mid-1970s because the intensity of radiation reflected from powders is too low to be measured at medium resolution and to provide adequate signal-to-noise ratios with dispersive instruments.

Diffuse reflectance is a complex process that occurs when a beam of radiation strikes a rough surface of a finely divided sample. Specular reflection occurs at each plane surface. However, since there are many of these surfaces randomly oriented, radiation is reflected in all directions. (Figure 3.2). Typically, the intensity of the reflected radiation is roughly independent of the viewing angle.

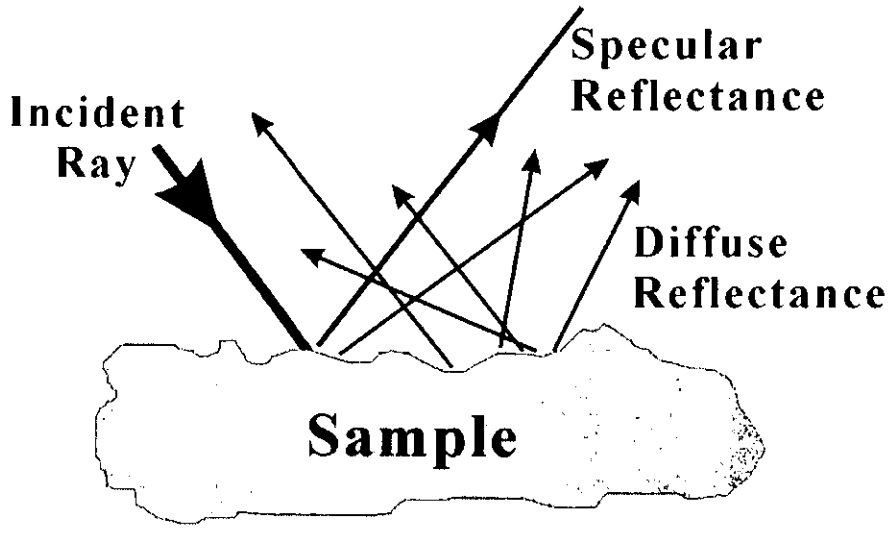

Figure 3.2: Two types of reflected energy after the infrared radiation irradiated on a solid sample.

A number of models have been developed to describe in quantitative terms the intensity of diffuse reflected radiation. The most widely used of these models was developed by Kubelka and Munk. According to their derivation the relative reflectance intensity (KM) for a tested sample is given by

$$KM = \frac{(1-R)^2}{2R}$$

Where R is the ratio of the reflected intensity of the sample to the reflected intensity of the standard.

If one compares a conventional infrared absorption spectrum with a diffuse reflectance spectrum of a same material, the peak locations are the same in two kinds of spectra but the relative peak heights differ considerably. The differences are typical, with minor peaks generally appearing larger in diffuse reflectance spectra.

3.1.2.2 Study on fiber samples

Fiber samples with Laser Induced Periodic Surface Structure (LIPSS) patterns were examined by FTIR with polarized light (The mechanism in forming the LIPSS has been discussed in chapter 2). Because the patterns have been obtained by polarized laser pulses, polymer functional groups may align with the direction of the electric field [Wong W. Y. Y. *et al.*, 1997]. Therefore, in order to study the alignments of the functional group, a polarized reflected FTIR absorption spectroscopy was employed. Figure 3.3 shows the experimental setup.

Fiber samples irradiated by a polarized low-fluence laser beam were used in the study. During irradiation the polarization direction of laser beam was set along the fiber

axis. In the study of the laser treated fibers, IR polarizer was set at 0° (parallel to the LIPSS) and 90° (perpendicular to the LIPSS) respectively in order to study the chemical modifications of the PET fiber along and perpendicular to the fiber axis.

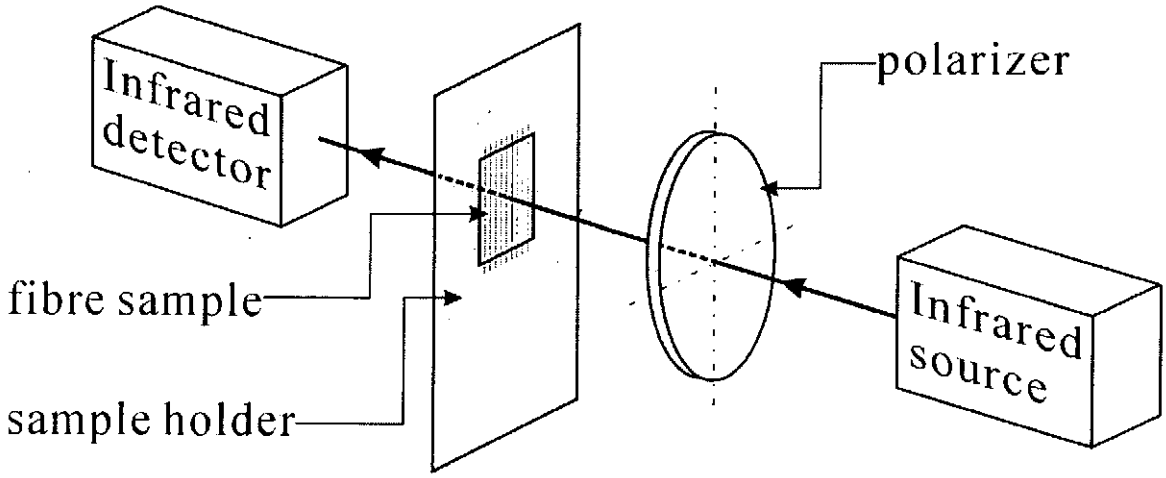

Figure 3.3: The experimental setup of polarized FTIR.

3.1.3 Ultra Violet absorption Spectroscopy

As mentioned in Chapter 1, high absorption coefficient is one of the necessary conditions in forming ripple structure on the irradiated surface. Therefore in order to study the effect on absorption properties of laser treated fabrics, a UV-VIS absorption spectrometer (PERKIN ELMER; Lambda 18 with a Reflectance Spectroscopy Accessory, labsphere, RSA-PE-18) was employed in the measurement of the fabrics. Figure 3.4 shows the schematic diagram of the accessory employed. All the fabrics were scanned in a range from 240 nm to 450 nm in 1 nm interval.

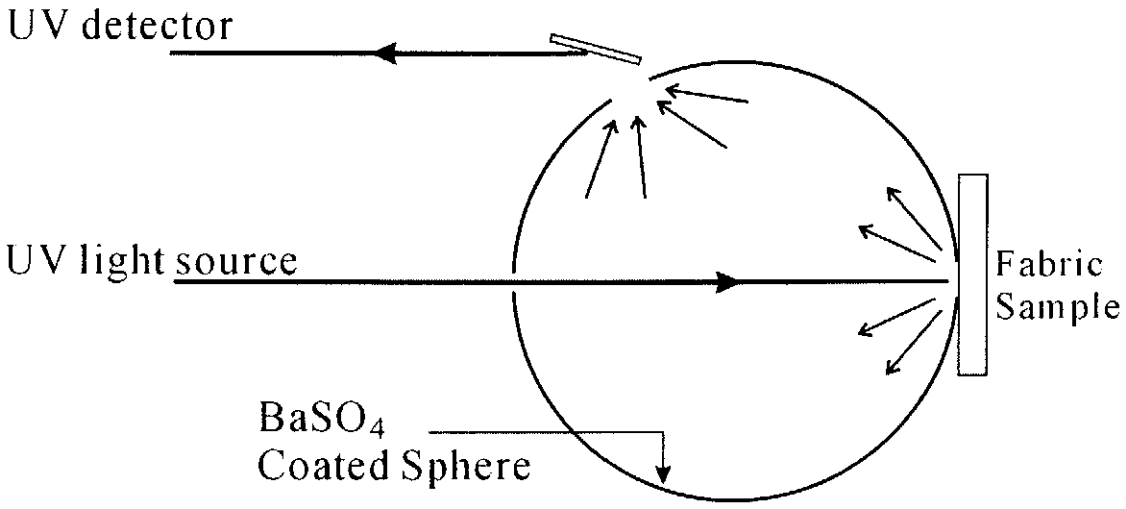

Figure 3.4: Schematic diagram of the Reflectance Spectroscopy Accessory, labsphere, RSA-PE-18, of UV-VIS absorption spectrometer.

3.2 Results and Discussions

3.2.1 X-ray Photoelectron Spectroscopy

The content of carbon (C1s) and oxygen (O1s) atoms on the PET surface after 248 nm excimer laser irradiation was analyzed by XPS. C1s and O1s scanning spectra were obtained and analyzed by examining each of peak size, intensity and position. For the C1s spectra, the 284.7 eV peak is normalized before comparisons. Under each spectrum, either carbon or oxygen, several peaks can be resolved / deconvoluted by curve fitting into a sum of single-core peaks. Each peak corresponds to a certain chemical bond, for PET, C1s 284.70 eV aromatic carbon (C-C), 286.24 eV bearing a single oxygen (C-O-C), 288.66 eV carboxylic carbon (C=O); O1s 532.3 eV π-bonded oxygen (C=O), 533.9 eV σ-bonded oxygen (C-O-C). The shape of these C1s spectra was carefully examined for fibers according to the number of laser pulses and major differences were found mainly at the 286.24 eV (C-O-C) and 288.66 eV (C=O) peaks. The details will be discussed in the following sections.

3.2.1.1 High fluence laser treated PET surface

PET is a polymer containing aromatic moieties within their polymer chain. High fluence laser treatment frequently results in debris of yellow to black materials, on the treated surface. The origin of such debris can been seen as the incomplete burning of ablation products within the ablation volume.

Figure 3.5 (a) and (b) show the change of carbon and oxygen peak shape due to different number of high fluence laser irradiation. For the C1s spectra, the peak intensity of both 284.7 eV and 288.66 eV peaks decreases gradually as the number of pulses

increases. In addition, the C=O peak (288.66 eV) has shifted to a higher binding energy level, that indicates a certain polymer chain is cross-linked with each other and formed a more complex network structure with high energy on the irradiated surface. Besides the shifting and decreasing of the C1s peaks, widening of the peak also shows the chemical composition have been changed during the laser irradiation. With increase the accumulation of laser pulses, the peak near 286.24 eV becomes smaller with apparently greater dissociation of ester bonds. These findings, along with the fact that the peak of O1s spectra (Figure 3.6) decreases at the same time, indicate deoxidization reaction on the surface of PET. Groups such as CO, CO_2 and others may be scattered from the treated surface as a result of laser ablation.

Oxygen content of the irradiated area also shows a significant decrease after just one pulse of laser irradiation. This means the laser has provided sufficiently high energy to decompose the bonds between carbon and oxygen.

Figure 3.8 shows the atomic concentration of carbon (C1s) and oxygen (O1s) of high fluence laser treated PET surface with different number of pulse. As the number of irradiation pulse increases, the carbon content also increases gradually while the oxygen content decreases. This is in agreement with the result obtained by Lazare and Srinivasan [Lazare S. *et al.*, 1986].

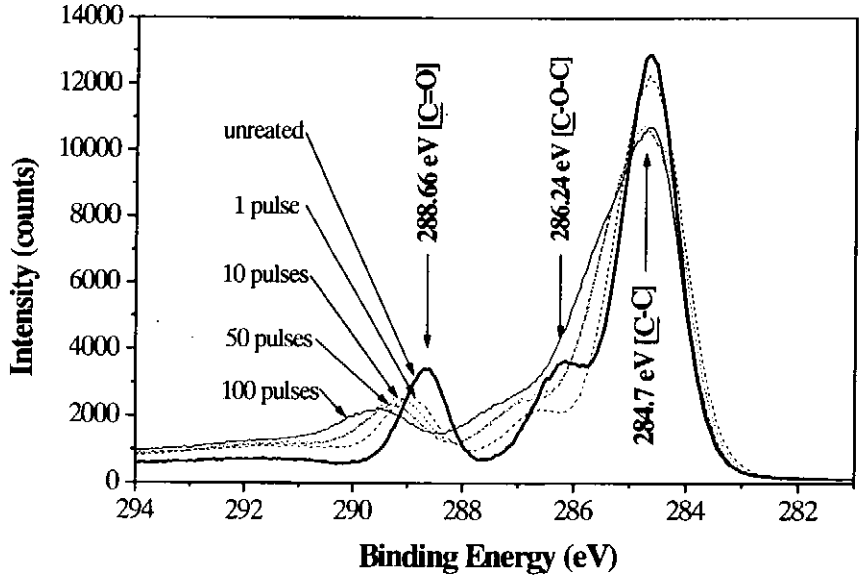

(a)

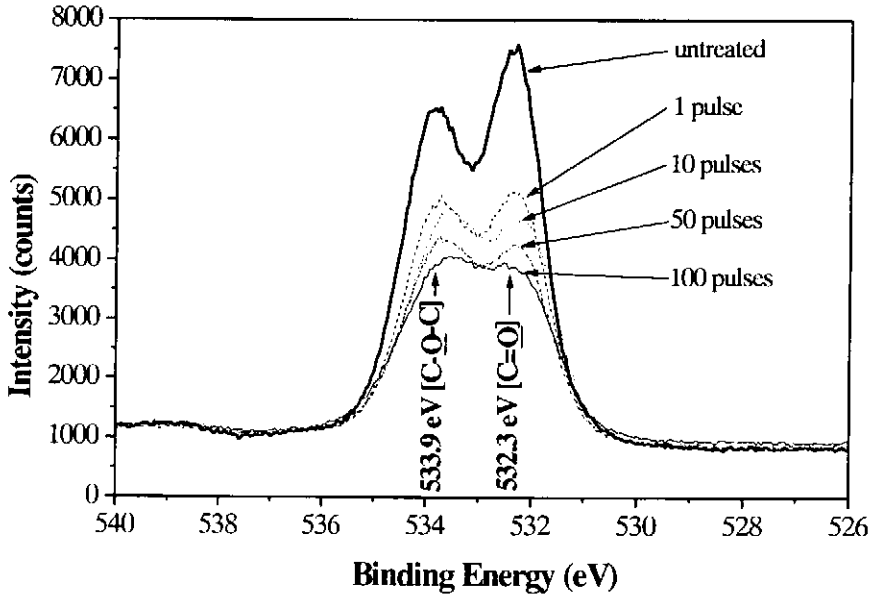

(b)

Figure 3.5: (a) C1s and (b) O1s XPS spectra on PET surface after irradiation of different number of high fluence laser pulses.(100 mJ cm^{-2})

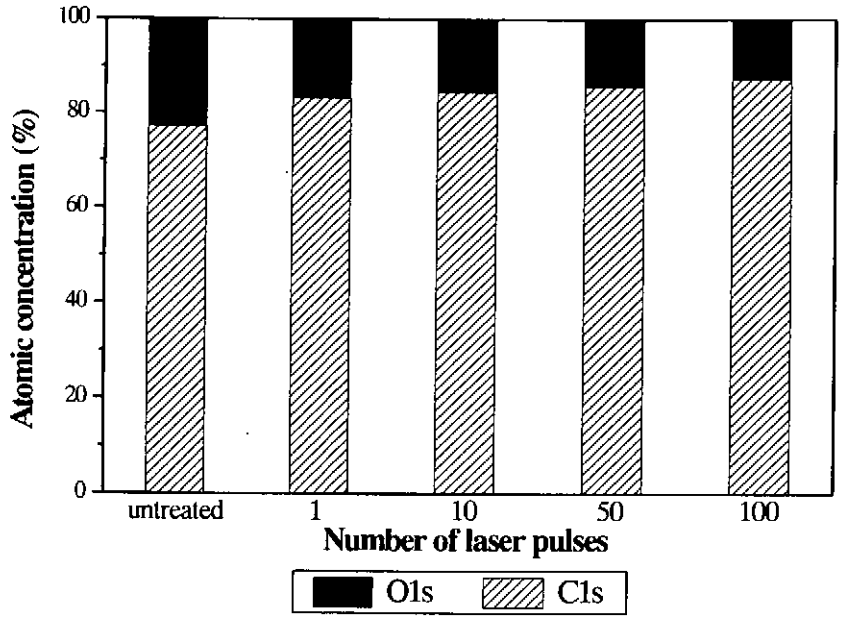

Figure 3.6: The atomic concentration of carbon (C1s) and oxygen (O1s) of high fluence (100 mJ cm^{-2}) laser treated PET samples

3.2.1.2 Low fluence laser treated PET surface

For the low fluence laser treatment, the 284.7 eV peak decreases as the number pulse increases. However, 288.66 eV and 286.24 eV peaks remain constant both in intensity and position, but widen in the full width half maximum (FWHM). These two peaks indicate the bond of carbon formed with oxygen atoms. As the same time, the O1s spectra of low fluence treated PET has a significant increase compared with untreated sample. These two observations indicate the process has rendered the sample more oxidized. The phenomenon is very different from the deoxidization in high fluence laser treatment.

Both C1s and O1s spectra also tend to a certain position after the first 1000 pulses. This means the oxidized surface is formed and stops further photochemical reaction of the PET surface. Therefore, prolonged laser irradiation will not induce any further

chemical composition modification even a 10,000 laser pulses have been used.

Figure 3.8 shows the relationship between the ratio of C and O atoms and the number of irradiation pulses with fluence far below the ablation threshold (6 mJ cm^{-2}). With increase of irradiated pulses, the C content decreases while the O content increases. The C to O ratio drops by about 15% in the first 1,000 pulses and remains unchanged for further irradiation. The reduction of C/O ratio indicates the high and low fluence laser treatments have a very different mechanism. It also provides a supporting explanation for many textile property modifications (The details will be discussed in Chapter 4). Experimental results suggest that the processing of low fluence laser treatment is an oxidization of the irradiated surface, leading to increased oxygen content as the laser dosage increases. Similar results also obtained in irradiation of polymers including labile triazeno group [Lippert T., 1997] and PEEK [Laurens P. *et al.*, 1999] This is very different from the high fluence laser treatment, in which the C/O ratio of high fluence treatment has a significant increase.

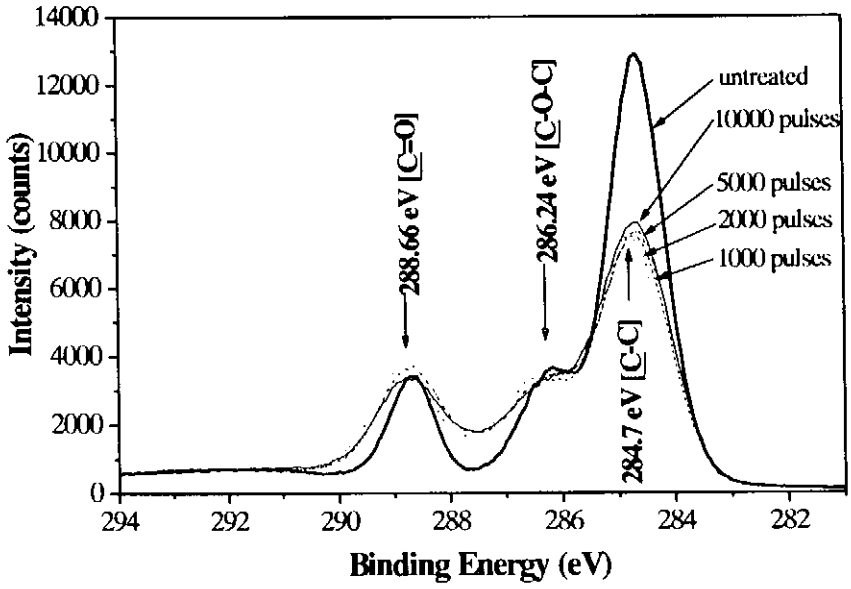

(a)

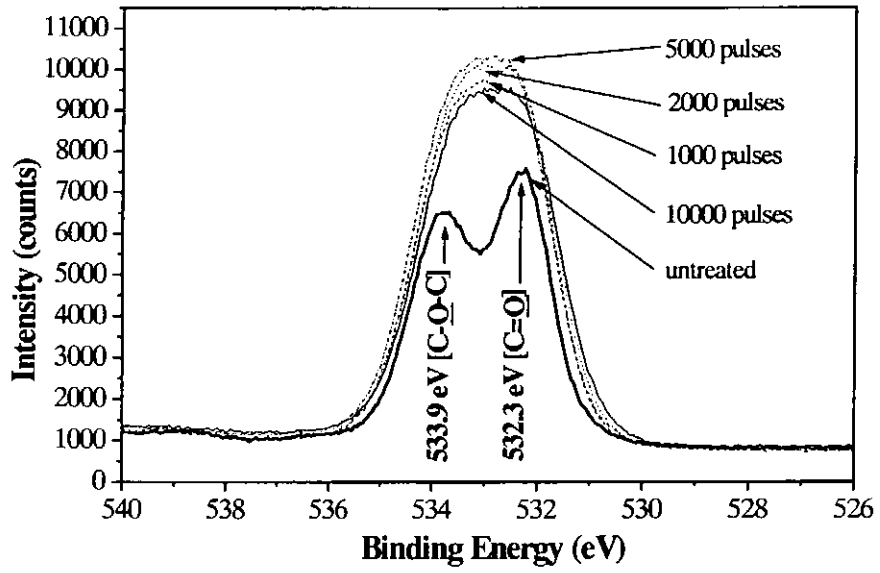

(b)

Figure 3.7: Peak shape change in XPS spectra of (a) C1s and (b) O1s of PET surface after different number of low fluence laser irradiation.(6 mJ cm^{-2}).

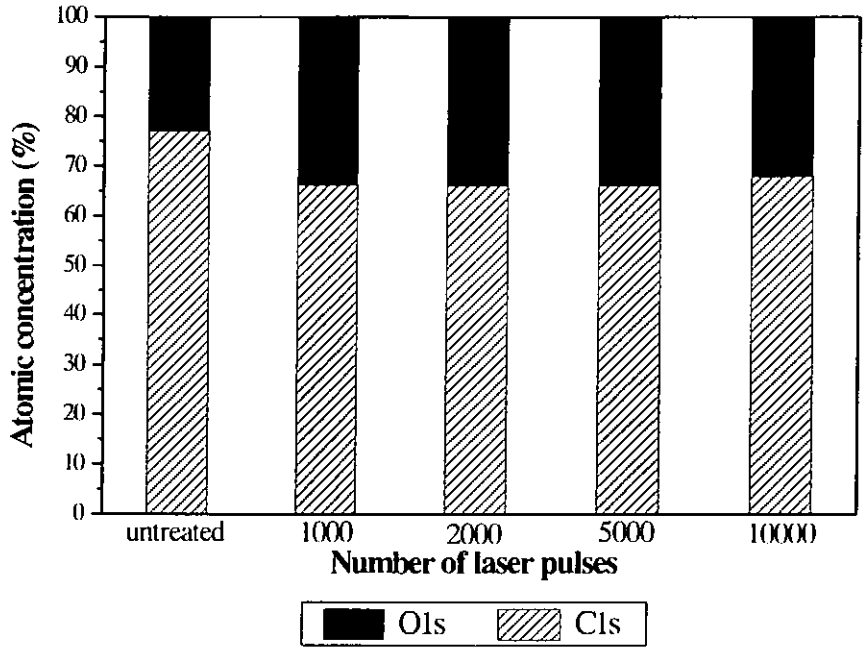

Figure 3.8: The atomic concentration of carbon (C1s) and oxygen (O1s) of low fluence (6 mJ cm^{-2}) laser treated PET samples

3.2.1.3 Comparison of high and low fluence laser treatments

Chemical modifications of high and low fluence laser treatments have already been presented in the previous sections. Figure 3.9 shows the comparison of the (a) C1s and (b) O1s XPS spectra of high and low fluence laser treated PET surfaces. For the carbon / carbon bond (284.7 eV), intensity reduces for both kinds of laser treatments, but much more for low fluence. On the other hand, the intensity of carbon / oxygen bonds (288.66 eV and 286.24 eV) in low fluence laser treatment remains constant, but is widened the FWHM. This is very different from the high fluence treatment in which the peaks have shifted and decreased in intensity. As mentioned before peak shifting mainly appears on high fluence treatment due to cross-linking and decomposition processes on the irradiated surface. These two processes do not occur in low fluence treated sample.

Significant differences also exist in the O1s XPS spectra (Figure 3.9b). Although the two oxygen peaks remain at the same positions, the oxygen content increases after irradiation for while decreases for high fluence laser treatment. This indicates the amount of C-O and C=O bonding has increased after low fluence laser treatment and decreased after high fluence laser treatment.

From the above observations, it may be concluded that oxidization is the process during low fluence laser treatment and deoxidization is the one for high fluence laser irradiation on the PET surface. The following is a more quantitative treatment of the results to indicate the differences. Table 3.2 shows the atomic concentrations (at.%) of C1s and O1s for laser treated PET samples under different fluences and number of pulses. Carbon to oxygen ratio is also listed. The ratio is a commonly used method to compare the difference of chemical modification. For the untreated samples, the C/O

ratio is about 3.4, under high fluence laser irradiation, the ratio gradually increases with the number of laser pulses, since the content of oxygen decreases gradually. On the other hand, this ratio decreases under low fluence treatment within the first 1000 laser pulses, and remains constant at around 2 even 10 times of pulses accumulated (10000 pulses). This might be an interesting discovery, C/O ratio changes long before the occurrence of any physically observable changes.

Table 3.2: The atomic concentration (at.%) of laser treated PET surface under different conditions determined by XPS.

	Atomic Concentration		C/O ratio
	C1s (%)	O1s (%)	
Untreated PET surface	77.26%	22.74%	3.40
High fluence laser treated PET surface (100 mJ cm^{-2})			
1 pulses	83.27%	16.73%	4.98
10 pulses	84.62%	15.38%	5.50
50 pulses	85.83%	14.17%	6.06
100 pulses	87.56%	12.44%	7.04
Low fluence laser treated PET surface (6 mJ cm^{-2})			
1000 pulses	66.28%	33.72%	1.97
2000 pulses	66.08%	33.92%	1.95
5000 pulses	66.25%	33.75%	1.96
10000 pulses	67.99%	32.01%	2.12

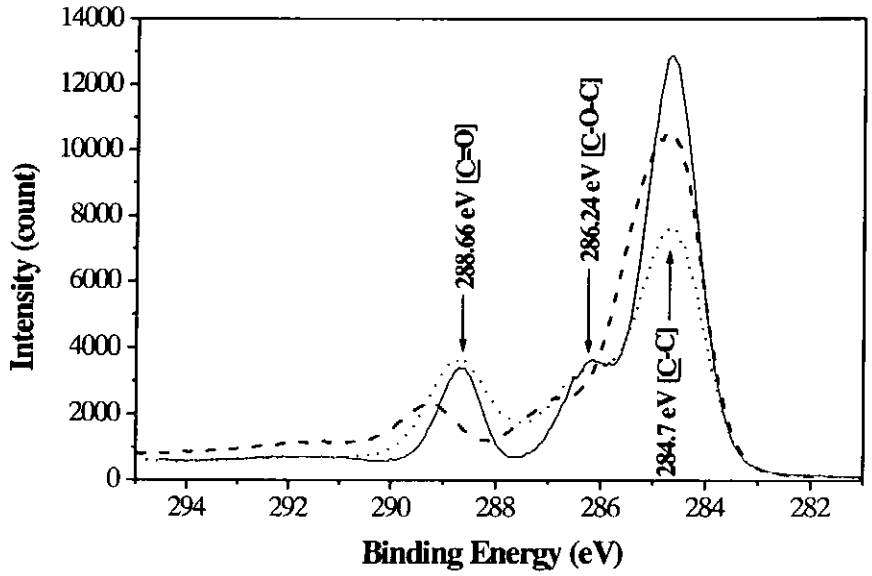

(a)

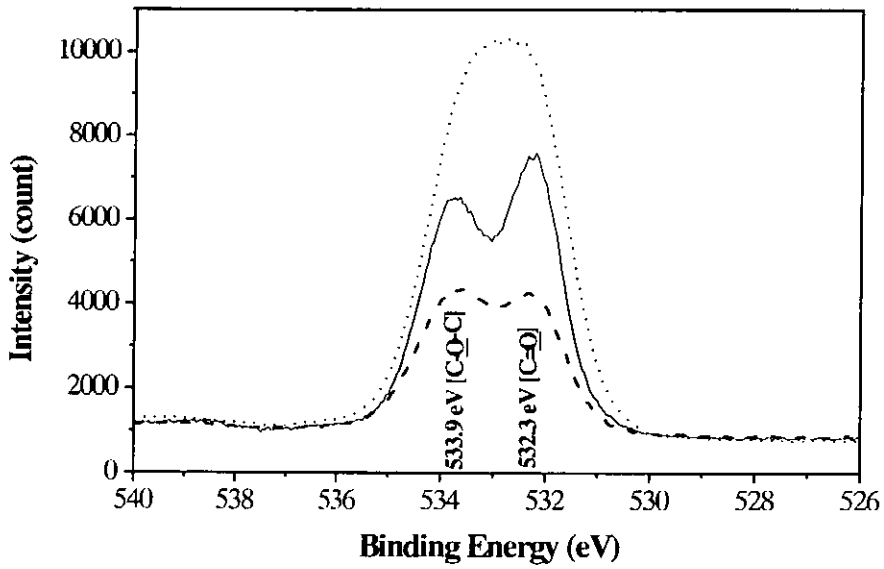

(b)

Figure 3.9: Peak shape change of (a) C1s and (b) O1s of PET surface by XPS after 248 nm excimer laser irradiation. (—) non-irradiated; (- - -) high fluence treatment:100 mJ cm^{-2}, 50 pulses; (·····) low fluence treatment: 6 mJ cm^{-2}, 5000 pulses.

3.2.2 Infrared Absorption Spectroscopy

Polyester fabrics and fibers treated with high (100 mJ cm^{-2}) and low (6 mJ cm^{-2}) fluence laser irradiation with different number of pulses were further tested with diffusion reflectance FTIR spectrometry and polarized FTIR spectrometry to study the chemical modification of the laser exposed PET surface. Due to different working principles of XPS and FTIR, the indicated chemical changes have different interpretations. In XPS, x-ray is used to stimulate electrons from the surface (below 10 nm) and then analyzed after the collection. Therefore XPS indicates the chemical change of a very thin layer on the tested surface. However, infrared has a relatively deeper penetration depth into the testing samples and therefore the information show by FTIR spectra is at least several microns deep from the surface of the sample.

3.2.2.1 High fluence laser treated PET surface

PET fiber surfaces treated by high fluence laser irradiation were analyzed by diffusion reflectance FTIR. Two ranges (2500 cm^{-1} to 3500 cm^{-1} and 1500 cm^{-1} to 2000 cm^{-1}) were selected from the original spectra (400 cm^{-1} to 4000 cm^{-1}) and are shown in Figure 3.10 and 3.11.

Figure 3.10 shows the position of C-H (~2970 cm^{-1}) and O-H (3440 cm^{-1}) groups on the surface of PET materials. With increased number of pulses, peak intensity increases 10 times from untreated sample to 100 pulses treated sample in both peaks. The increased signal is mainly due to the roughness induced by laser. Absorption property is also improved by the high fluence laser treatment. However, peak intensity of both peaks decreases after further irradiation (200 pulses and 500 pulses). This dramatic change is especially significant at wavenumber of 2970 cm^{-1}, the C-H bond

vibration. The results suggest possible dissociation on the irradiated area, or formation of a new structure on the top surface to block the IR signal.

Similar phenomena also appear in Figure 3.11, which shows diffusion reflectance FTIR spectra between the range of 1500 cm^{-1} and 2000 cm^{-1}. By increasing the number of pulses from 0 to 100, the adsorption property of the whole surface also improved gradually just like that in the range of 2500 cm^{-1} to 3500 cm^{-1} especially at 1745 cm^{-1} (C=O). However, when the pulses is over 200 shoots, peaks intensity having a significant decrease, The peak position also shifts to a lower wavenumber. This shifting is mainly due to the decomposition of C=O of the irradiated area and formation of carbon-richen surface that blocks the IR signal from penetrating the sample.

In order to easier comparison, Figure 3.12 shows the relationship between the number of irradiation pulse and the relative percentage change of peak intensity at 1745 cm^{-1}(C=O), 2970 cm^{-1}(C=H) and 3440 cm^{-1} (O-H) compared with the intensity at 1170 cm^{-1} where the KM value remains substantially constant. Hence, for each individual spectrum

$$\text{Relative percentage change} = \frac{I_x - I_{1170}}{I_{1170}} \times 100\%$$

where I_x and I_{1170} are respecting intensities at different peak positions and at 1170 cm^{-1}). As the pulse number increases, the relative percentage bonding vibration also increases, that means the increment at the peak is not just induced by roughness or absorption improvement, it is also due to the increment of certain amount of molecules on the test surface.

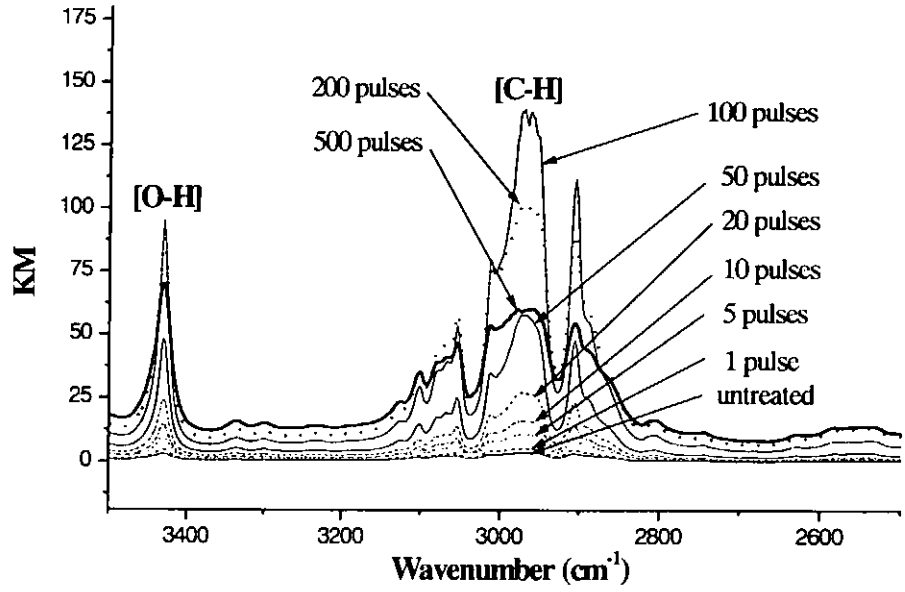

Figure 3.10: The pulse number dependence of the high fluence treated PET fiber spectra of diffusion reflectance FTIR between the range of 2500 cm^{-1} and 3500 cm^{-1}.

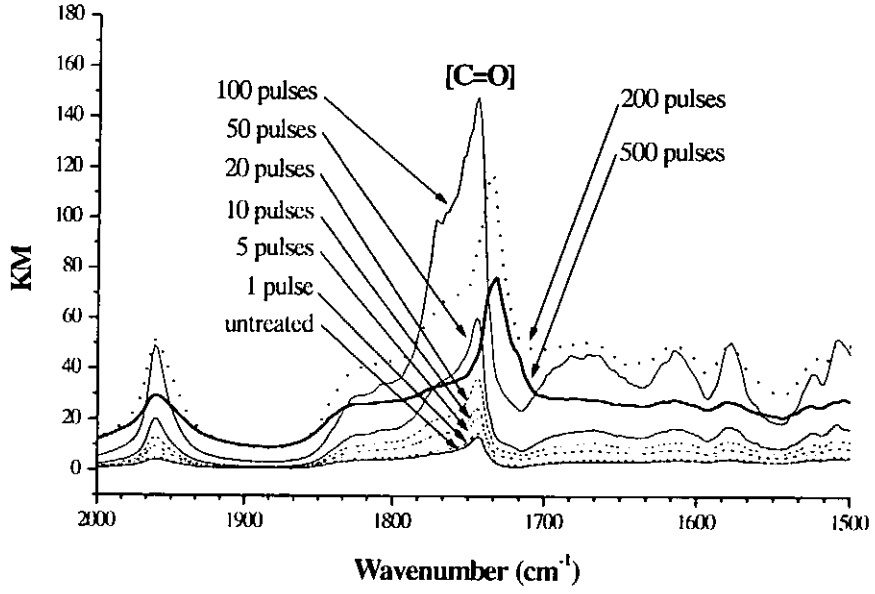

Figure 3.11: The pulse number dependence of the high fluence treated PET fiber spectra of diffusion reflectance FTIR between the range of 1500 cm^{-1} and 2000 cm^{-1}.

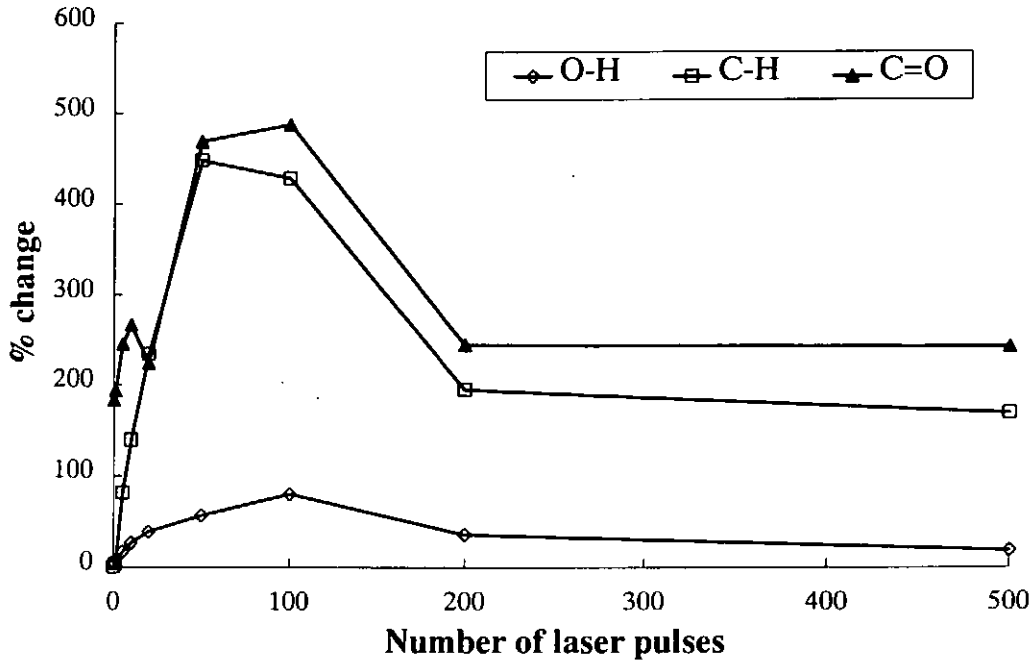

Figure 3.12: The relative percentage change at 1745 cm^{-1}, 2970 cm^{-1} and 3440 cm^{-1} (compared with 1170 cm^{-1}) of high fluence laser treated PET fibers from FTIR spectra.

In order to detect possible alignment of polymer chain, polarized FTIR was employed to analyze the irradiated fibers. Figure 3.13 shows the polarized IR spectra of the high fluence laser treated PET fiber compared with those of he untreated samples with the fiber axis parallel (0^o) and perpendicular (90^o) with the easy axis of transmission of the polarizer. In high fluence laser treatment, all the ripple structures were induced perpendicular to the fiber axis. As mentioned in Chapter 2, the formation mechanism of the LIPSS under high fluence irradiation is mainly due to thermally relaxation of the internal stress. Therefore the peak of 3000 cm^{-1} (C-H bond vibration) at 0^o polarized is relatively weak after irradiation. But the overall IR absorption increases due to the surface roughness produced. At 1745 cm^{-1}, both directions polarization result in a sharper and intensity enhanced peak after high fluence laser treatment, especially in the case of 0^o direction where a greater increase is observed.

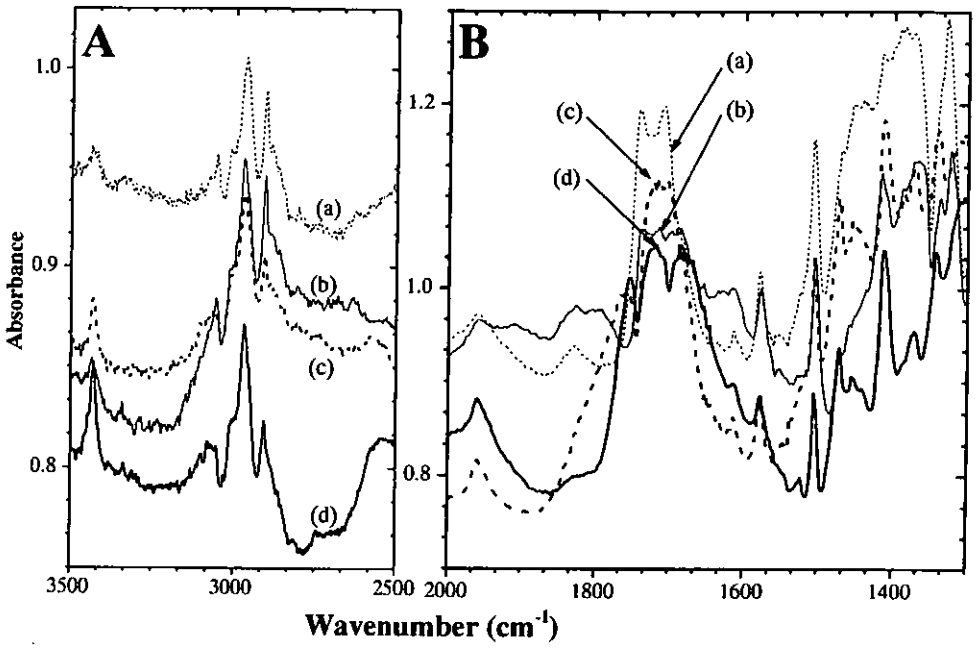

Figure 3.13: Polarized FTIR spectra of PET fibers (A) The spectra between 2500 cm^{-1} and 3500 cm^{-1}; (B) The spectra between 1300 cm^{-1} and 2000 cm^{-1}.
(a) 20 pulses 100 mJ cm^{-2} laser treated surface at 0°,
(b) untreated surface at 0°,
(c) 20 pulses 100 mJ cm^{-2} laser treated surface at 90° and
(d) untreated surface at 90°.

3.2.2.2 Low fluence laser treated PET surface

As mentioned before, because the working principles of XPS and FTIR are very different, therefore, FTIR is suitable in detecting high fluence laser treated sample, but not for low fluence laser treated sample. This is because the LIPSS formed by low fluence is very thin, in nano-meters scale. Therefore, compared with the indicating signal of IR spectrometry, the bulk materials (volume under the LIPSS) contribute mainly to the spectrum feature.

As shown in Figure 3.14, three IR absorption spectra (untreated sample, 500 and 10000 pulses irradiated samples) are plotted together in a range of 1500 cm^{-1} to 2000

cm^{-1}. As the dosage increased, the absorption signal at the peak of 1745 cm^{-1} only changes by a small value (5 KM units) from the original one, but the other parts of the spectra almost overlap. The increase of the peak intensity indicates that the vibration of C=O bond become stronger due to the oxidation of the treated surface. This result also coincides with the result obtained from XPS. On the other hand, the little increment at C=O bond vibration and the overlapping among the curves are mainly due to the stronger signal from the bulk materials.

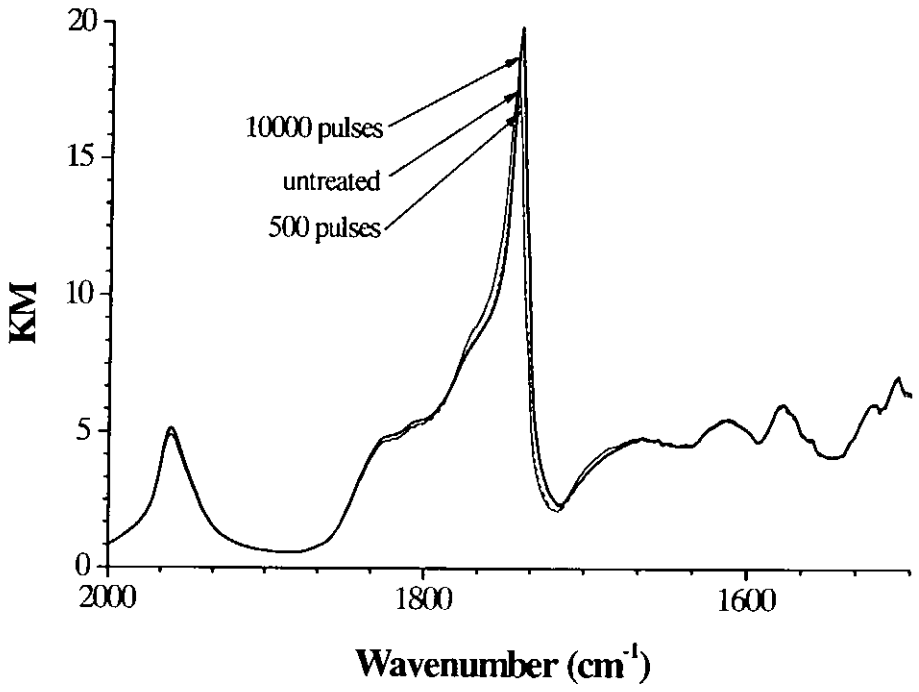

Figure 3.14: The pulse number dependence of the low fluence treated PET fiber spectra of diffusion reflectance FTIR between the range of 1500 cm^{-1} and 2000 cm^{-1}.

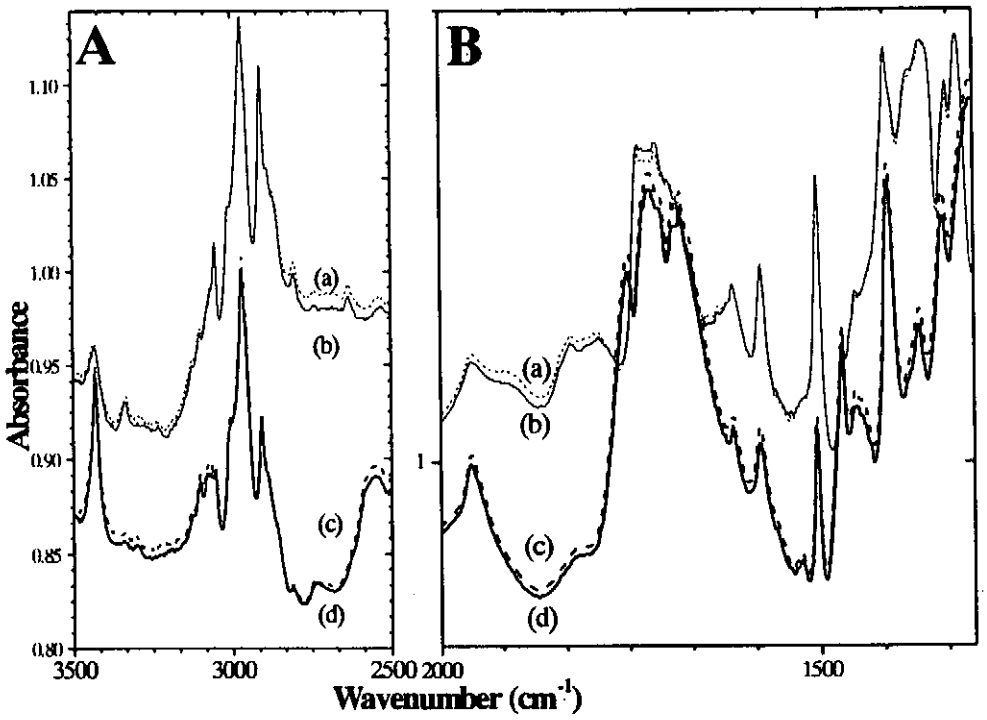

Figure 3.15: Polarized FTIR spectra of PET fibers (A) The spectra between 2500 cm^{-1} and 3500 cm^{-1}; (B) The spectra between 1300 cm^{-1} and 2000 cm^{-1}.
(a) 2000 pulses 6 mJ cm^{-2} laser treated surface at 0°,
(b) untreated surface at 0°,
(c) 2000 pulses 6 mJ cm^{-2} laser treated surface at 90° and
(d) untreated surface at 90°

After the low fluence irradiation, nano-meters sized LIPSS structure is formed on the surface. Results of some researchers (Wong W. Y. Y. *et al.*, 1997) would suggest possible alignment of the polymer chains on the treated surface relative to the polarization direction of the laser beam. Therefore polarized FTIR spectrometry was employed in study the chain alignment modification. Figure 3.15 shows the polarized IR absorption spectrum at 0° and 90° polarization. For this experiment, all the ripples were grown in the direction along the fiber axis.

Figure 3.15 shows the IR spectra in two different ranges with two polarization

orientations. No significant change can be observed. This is very different from the findings of Wong *et al.*. One possible explanation is the sample shape. Our sample is fiber form whereas that of Wong *et al.* is in film form. The fiber form has a highly orientated polymeric structure and therefore, it is very difficult to reveal the little modification.

3.2.3 Ultra-Violet (UV) Absorption Spectroscopy

3.2.3.1 High fluence laser treated PET surface

When the PET fabric is irradiated with excimer laser at fluence of 100 mJ cm^{-2} in atmospheric condition, the surface color of the sample gradually changes from originally white to yellowish brown with the increase in the number of laser shots. Figure 3.16 shows the UV spectrum of high fluence laser treated PET fabrics in different number of pulses and Figure 3.17 is the comparison of the absorbance at 248 nm for samples irradiated with different number of laser pulses. In the far UV range (240 nm-300 nm), the absorbance decreases in the first few laser shots and then increases after further irradiation. This tendency also obtained in PVDC film [Niino H. *et al.*, 1998]. These characteristics may be due to oxidization on the fabrics' surface. The first few shots of laser serve to clean up or etch away the thin layer of contamination on the sample. After the cleaning processing, the overall absorption is improved especially in the range of visible and near ultra violet region. The increased absorption bands in this range indicate the formation of long conjugated chains of carbon multiple bands on the surface. However, the photochemical reaction of the laser irradiation is limited to the upper layer of the fabrics (several microns) because the laser beam could not transmit through the modified surface layer that have a higher absorption. Hence the absorbance shown in Figure 3.17 tends to level off as the number of pulses increases.

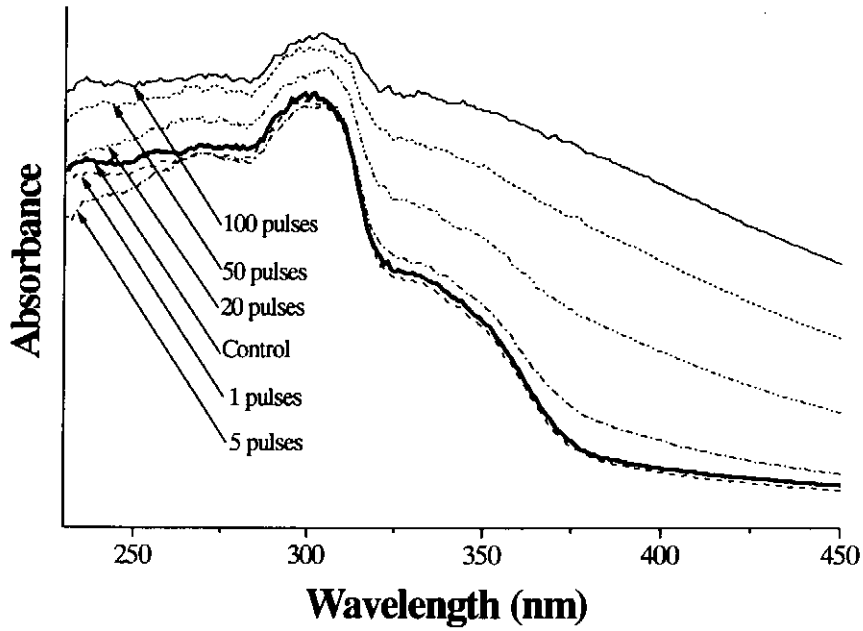

Figure 3.16: Ultra-violet absorption spectrum of high fluence laser treated PET fabric.

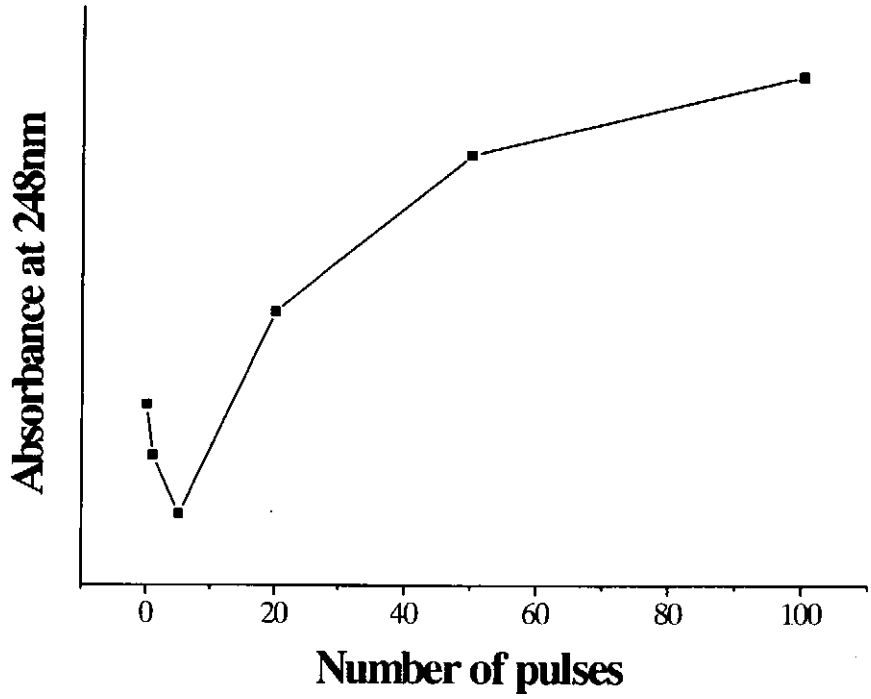

Figure 3.17: Comparison of absorbance at 248 nm for different number of high fluence laser pulses on PET fabrics.

3.2.3.2 Low fluence laser treated PET surface

Figure 3.18 displays the ultraviolet absorption spectra of low fluence laser treated PET fabrics with different number of laser shots. The absorbance is plotted against wavelength in the range of 230 to 450 nm. This figure shows the change of the absorption curves mainly occurs at the range of far UV region (240 nm to 300 nm), whereas the visible and near UV region have no significant enhancement. Figure 3.19 shows the absorbance of 248 nm for samples treated with increasing number of laser shots. Similar to the case of high fluence laser treatment, the absorption has a great drop in value from untreated sample to 200 pulses and then increases gradually. This indicates the surface is cleaned after a few hundred shots. Afterwards, an increase in the number of shots leads to an increase in the absorbance of the treated samples especially at far UV region because of chemical modification. As the number of the laser pulses has increased to 10000 shots, the spectrum becomes very similar to the untreated one. One of the explanations is the re-oxidation of the surface after cleaning process.

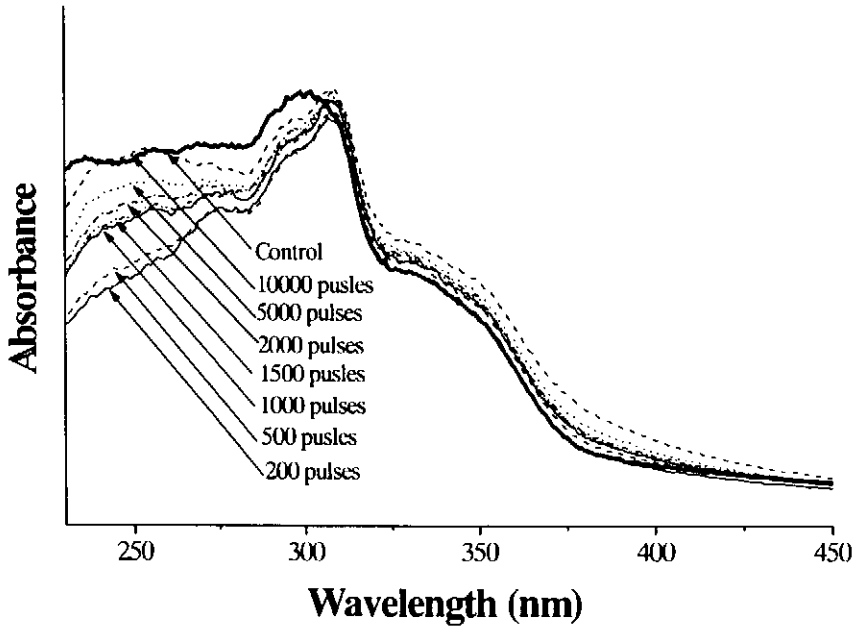

Figure 3.18: Ultra-violet absorption spectrum of low fluence laser treated PET fabrics.

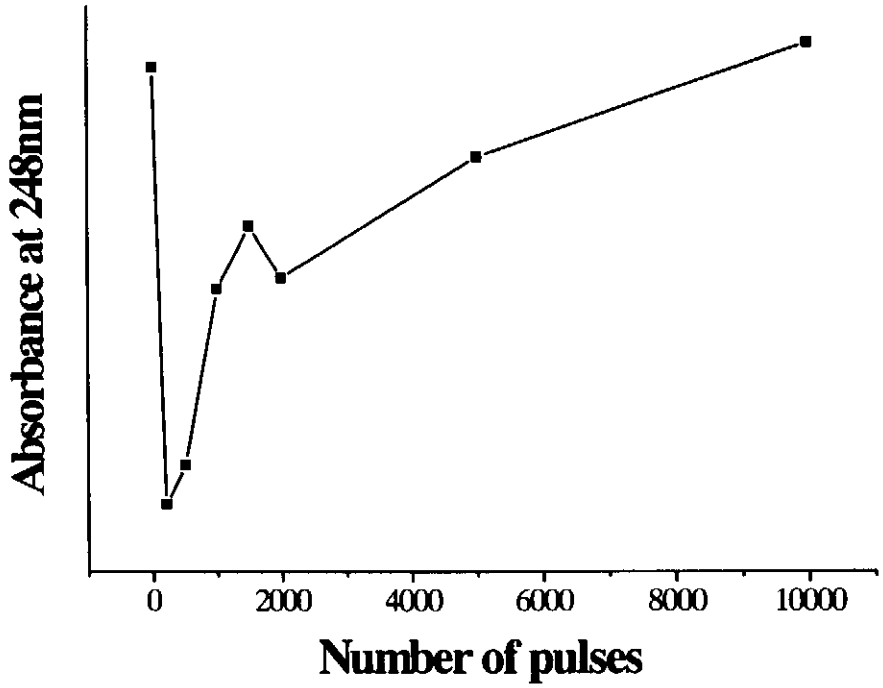

Figure 3.19: Comparison of absorbance at 248 nm for different number of low fluence laser pulses on PET fabrics.

Chapter 4 Textile Properties Modifications

Laser Induced Periodic Surface Structure (LIPSS) was formed after the excimer laser irradiation on polymeric materials. This kind of structure induces many textile properties modification on the irradiated fabrics' surface, such as luster, wettability, dyeability and stability. In order to find out the advantages and disadvantages of the laser irradiated PET fabrics, different instruments were used to characterize the treated samples.

4.1 Experimental Techniques

4.1.1 Glossiness measurement

Compared with natural materials, untreated synthetic fabric has an unnatural glossy appearance due to the smooth surface of the treated fibers. A Digital Variable Angle Glossmeter (model VGS-1D, made by NIPPON DENSHOKU KOGYO CO., LTD., JAPAN) was used to measure the glossiness of the samples.

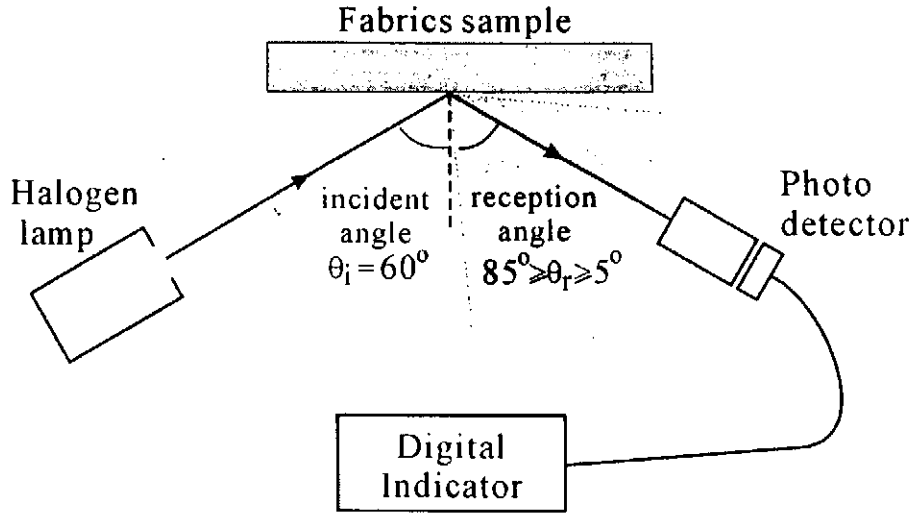

Figure 4.1: The schematic method of Digital Variable-Angle Glossmeter

Figure 4.1 illustrates the working principle of measurement. This apparatus is designed according to JIS Z-8741 (Japanese Industrial Standard, method of measurement for specular glossiness) and the glossiness index obtained is the glossiness percentage of standard black glass with refractive index of 1.576, therefore all the measured values can be used to evaluate the glossiness of fabric surface.

In the study of the laser treated samples, the incident light was fixed at 60° (θ_i) and the receiving angle (θ_r) is varied from 5° to 85° in step of 5°. This Angle Variation method has been widely adopted because the mechanism is similar to that of subjective evaluation in which the incident light and fabric sample are fixed while the position of the observer is variable.

4.1.2 Whiteness measurement

In textile industry, white fluorescent or non-fluorescent samples have a considerable economic significance. Since about 1950, before fluorescent optical whiteners were available, people have tried to describe white samples with a single number for the degree of whiteness. Many formulas were suggested for whiteness. For whiteness evaluation the differences in the sensitivities of the observers and also the consumer preference for certain shades or tints are important. The preferred white is also product-dependent. Several researchers have compiled and compared many formulas. After years of investigation CIE decided to recommend a formula for whiteness, which is

$$W = Y + 800(0.3138 - x) + 1700\,(0.3310 - y)$$

Where Y is one of the tristimulus values. It is a measure that relates to the lightness of the sample. The values of x and y are the coordinates of the chromaticity diagram,

called chromaticity coordinates. The CIE limited the use of the formula to whiteness larger than 40. Therefore if the measured value is greater than 40, the sample surface is no longer white. (Anni B.S., 1994)

Changes in fabrics' whiteness after laser irradiation were quantified by CIE whiteness index. Fabric whiteness was measured by Spectrophotometer (DataColor International, model Spectraflash ® 600 Plus) with an integration sphere (apparatus with angle of incidence 8°) and D65 light source (daylight with the standardized color temperature of 6500 K). All the sample values were averaged with 4 different position and 4 flash numbers in both warp and weft directions. Figure 4.2 shows the schematic diagram of Spectraflash ® 600 Plus.

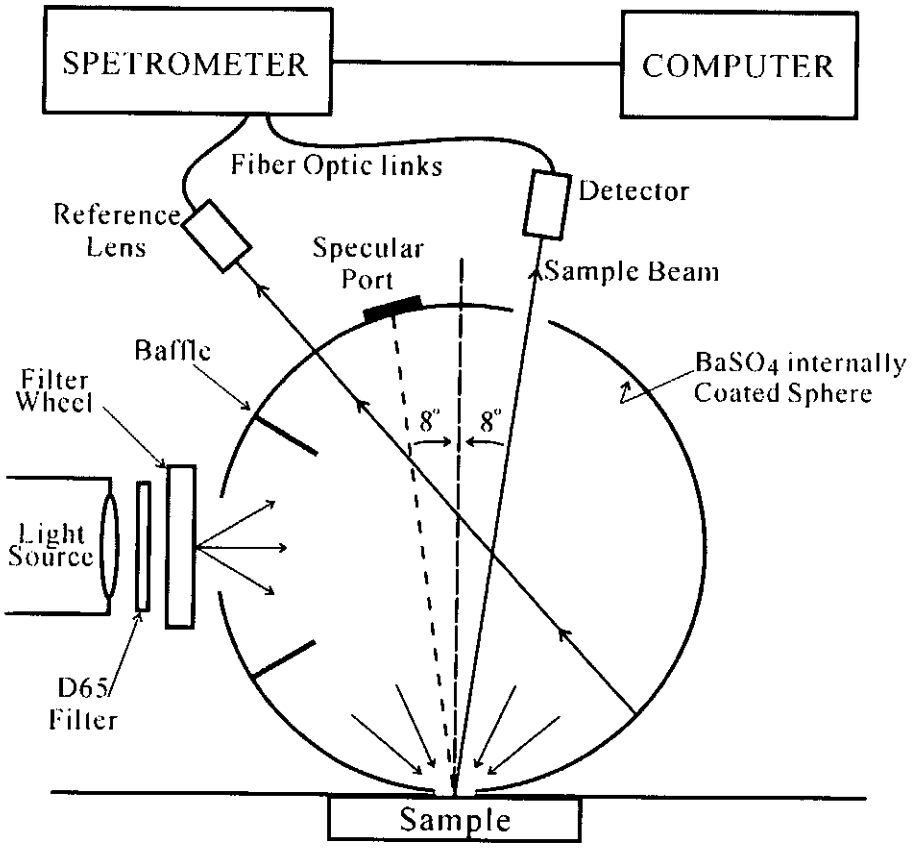

Figure 4.2: Schematic diagram of Spectraflash ® 600 Plus for measuring whiteness.

4.1.3 Contact angle measurement

Contact angle measurements of liquid droplets on substrate surface are used to characterize surface wettability. The contact angle is defined as the angle between the substrate support surface and the tangent line at the point of contact of the liquid droplet with the substrate (Figure 4.3).

This value is related by Young's equation to the surface energy of the substrate. The value of the contact angle of the liquid droplet will depend upon the surface energy of the substrate and the surface tension of the liquid. If complete wetting takes place between the liquid and the substrate surface, the droplet will spread out over the substrate and the contact angle will approach zero, whereas if wetting is only partial, the resulting contact angle will lie in the range of 0 to 180 degrees. In general, polymer materials have typically low energy surfaces. Liquids placed on these surfaces remain in the form of drops having finite contact angles, so long as surface energy of the substrate is less than surface tension of the liquid.

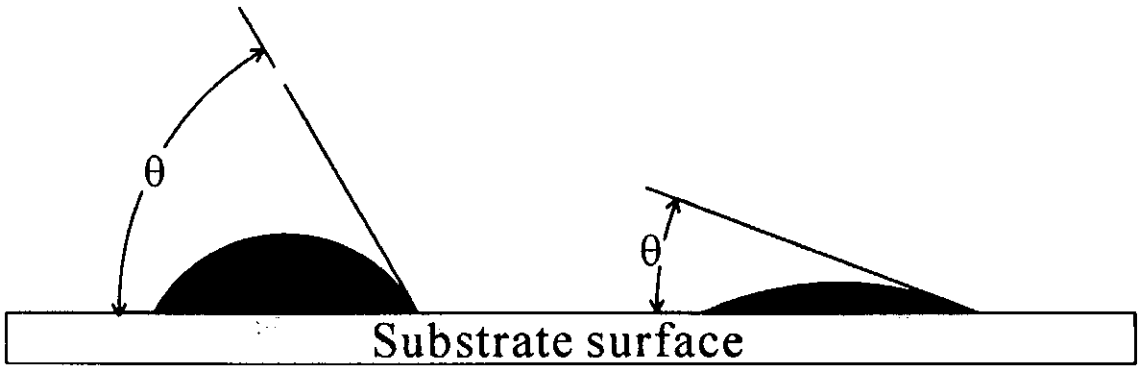

Figure 4.3: Angle between substrate and tangent line.

The actual time for a droplet to reach equilibrium with the surface depends upon the liquid being used. In this study, a de-ionized water droplet was used. Equilibrium always reaches in seconds. Contact angle reading should be taken at that moment. Prior

to equilibrium the angle is advancing. Once equilibrium has been reached the angle starts to recede.

Solid surface may not be completely homogeneous, so that their surface energies are not evenly distributed, especially on the fabric surface. Therefore, mean values were used in the plots after averaging more than 20 measurements in each treating condition. In order to have an accurate reading, all water content of the samples should be keep constant. Therefore, fabrics have been kept under BS 1051 standard condition (20 ±2 °C and 65% relative humidity) for 24 hours before each experiment.

Half-Angle ™ measuring method

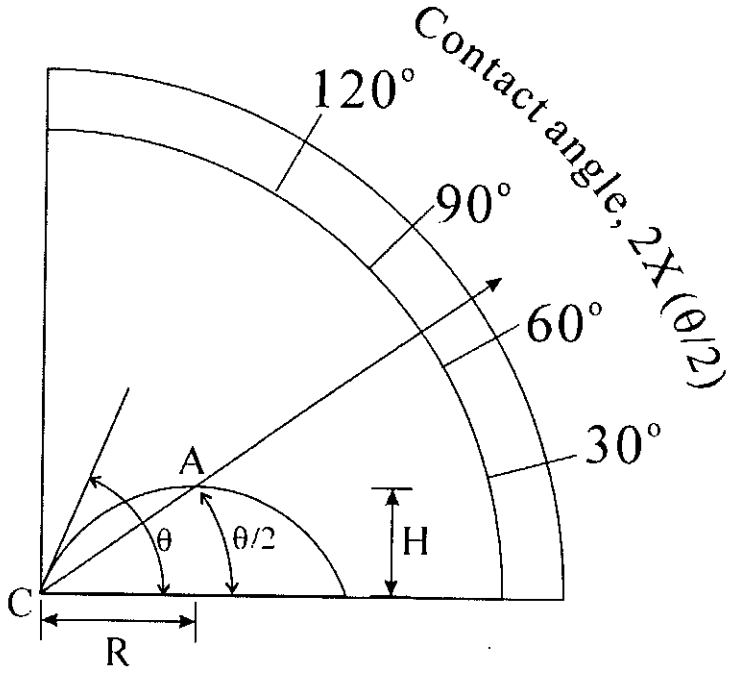

Figure 4.4: The scale on the screen of contact angle meter.

In this study, a contact angle meter (Tantec Inc., model CAM-MICRO) was used to measure the contact angles on different fabric surfaces. A method called Half-Angle™ measuring method was used for measuring the contact angles. This allows direct angle

measurements but eliminates errors associated with arbitrary tangential alignment of a hairline to the droplet image. The method is based on the formula for determining contact angles from the droplet dimensions:

$$\theta = 2 \times \tan^{-1}(H / R)$$

Where θ is the contact angle, H is the height of droplet, and R is the radius of the droplet's base (Figure 4.4).

4.1.4 Moisture Regain measurement

Other than the contact angle measurement that indicates how laser treatment can affect the wettability of PET fabrics, moisture regain is also a common method in determining the wettability of a sample. As mentioned in contact angle measurement, all the samples should be kept in a conditioned environment (20 ±2 °C and 65% relative humidity) for 24 hours before the experiment in order to get an equilibrium of moisture content in the bulk of materials.

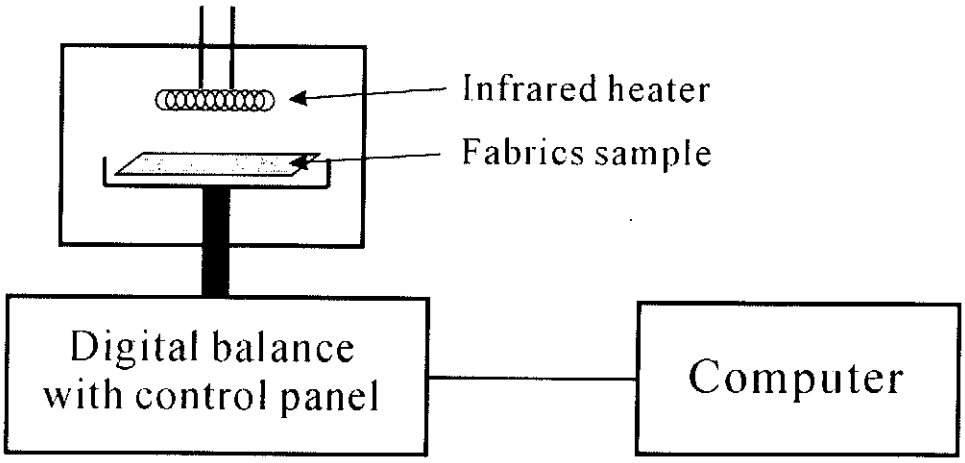

Figure 4.5: The schematic diagram of METTLER TOLEDO LJ16 Moisture Analyzer.

A METTLER TOLEDO LJ16 Moisture Analyzer was employed in the study. It contains two parts, an infrared heater and a digital balance with control panel. All the data are presented in a percentage format under the following formula.

$$\text{Moisture Regain (\%)} = \frac{\text{Wet weight - Dry weight}}{\text{Dry weight}} \times 100\%$$

Where wet weight is the weight before heating and the dry weight is the weight after heated.

4.1.5 Dyeing process

Because of the smooth surface of synthetic fibers, dark shades are difficult to obtain. However by using laser irradiation, the dyeability is improved especially for deep color [Knittel D. *et al.*, 1998]. Therefore, in this study, PET fabrics with different laser treatments were tried to dye and compare.

PET micro-fabrics were dyed with carrier dyeing. The following dyeing conditions were used in the dyeing experiment.

	Carrier dyeing
Material	1 g PET micro-fabrics
Laser treatment	(a) Untreated sample (b) 248 nm laser, 100 mJ cm^{-2} and 5 pulses (c) 248 nm laser, 6 mJ cm^{-2} and 2000 pulses (d) 193 nm laser, 100 mJ cm^{-2} and 5 pulses
Dyes used	C.I. Disperse Blue 56
Dyes concentration	1 %

Dispersing agent	Sandozol KB(10%), 0.5 c.c. per fabric
Carrier	Levegal DTE01(10%), 2.5 c.c. per fabric
Acetic acid (10% conc.)	0.25 c.c. per fabric
Liquor ratio	50 : 1

After the dyeing process, reduction-clearing process was used to clean the dyed fabrics. All the dyed fabrics were treated at 60 °C in the mixture (the content being shown in the following table) for 15 minutes, and then rinsed and dried.

	Reduction clearing
Sodium dithionite (10%)	2 g per liter
Caustic soda (10%)	2 g per liter
Dispersing agent	Sandozol KB(10%), 1 c.c. per fabric

The temperature during the dyeing process is shown schematically in the following temperature time curve (Figure 4.6).

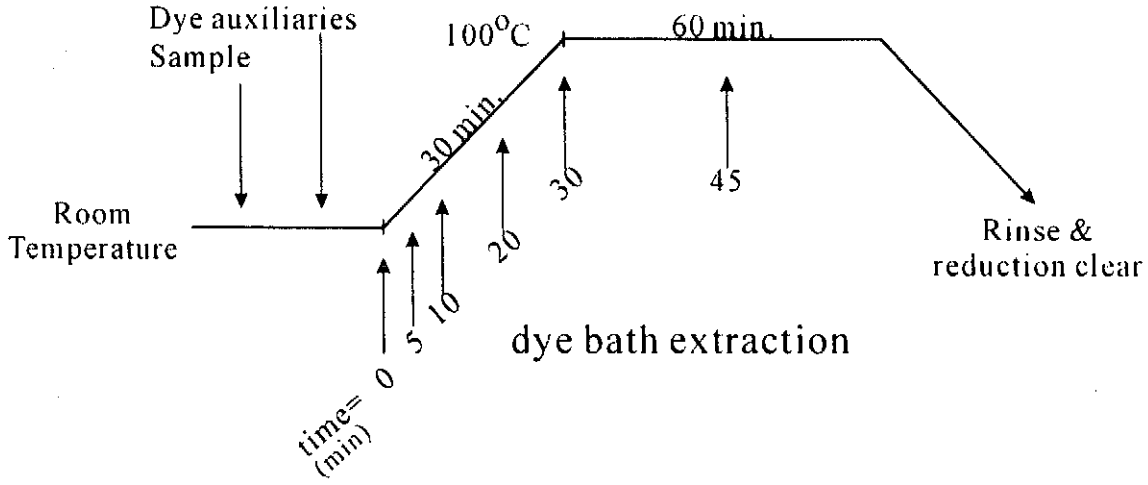

Figure 4.6: Schematic diagram of the carrier dyeing process

Determination of dyebath exhaustion

Dyebath exhaustion was determined by extracting residual dye liquor at prescribed times. In this study, the dye concentrations in the dyebath were determined at 0, 5, 10, 20, 30 and 45 minutes. The concentration of the residual dye was measured at the wavelength with maximum absorption λ_{max} using PERKIN ELMER UV / VIS Spectrophotometer. The following equation was used in calculating the percentage of exhaustion.

$$E = \frac{A_o - A_t}{A_o} \times 100\%$$

Where E is the percentage exhaustion at time t,

A_o is the absorbance of dye solution at 0 min and

A_t is the absorbance of dye solution at time t.

Determination of the color change of dyed fabrics

In order to compare the improvement of dyeability, Spectraflash ® 600 plus was used to determine the color change after dyeing. The laser treated samples were compared with the non-laser-treated fabrics, according to the CIE L*a*b standard. Positive value of delta E (△E) means darker / deeper color has been obtained on the fabrics compared with the non-laser-treated one.

4.2 Results and Discussions

4.2.1 Modification of Luster

4.2.1.1 Glossiness

Because of the slight difference in the weft and warp yarns, reflective glossiness was measured in both weft and warp directions. Glossiness indexes were plotted again the reception angle for each samples. In general, the weft direction has a greater reading compared with warp direction. It is because the sizes of the yarns used in weft and warp directions are not the same. Figure 4.7 shows the SEM image of the PET fabric under the testing. The yarns in weft direction have a greater surface area compared with those in warp direction. Therefore the glossiness obtained has a directional difference that is not due to the effect of laser treatment.

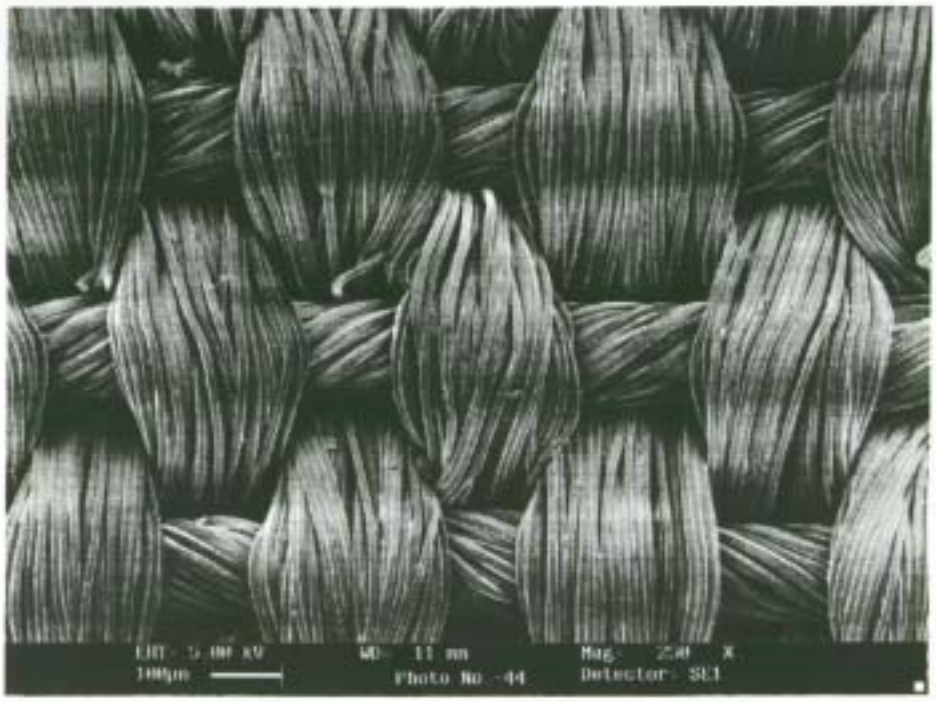

Figure 4.7: SEM image of the PET thick fabric

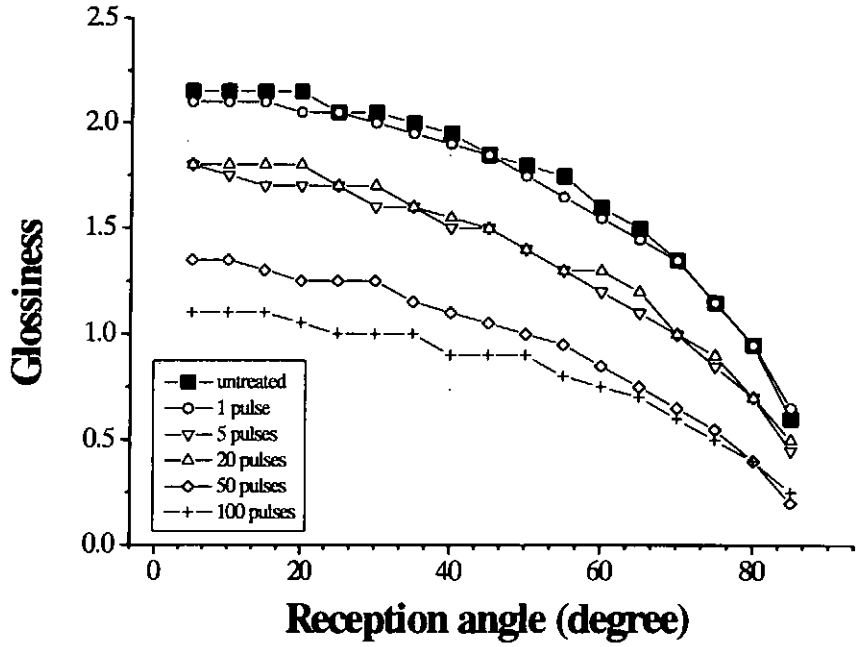

Figure 4.8: Glossiness distribution of the high fluence (100 mJ cm^{-2}) laser treated PET thick fabric in warp direction.

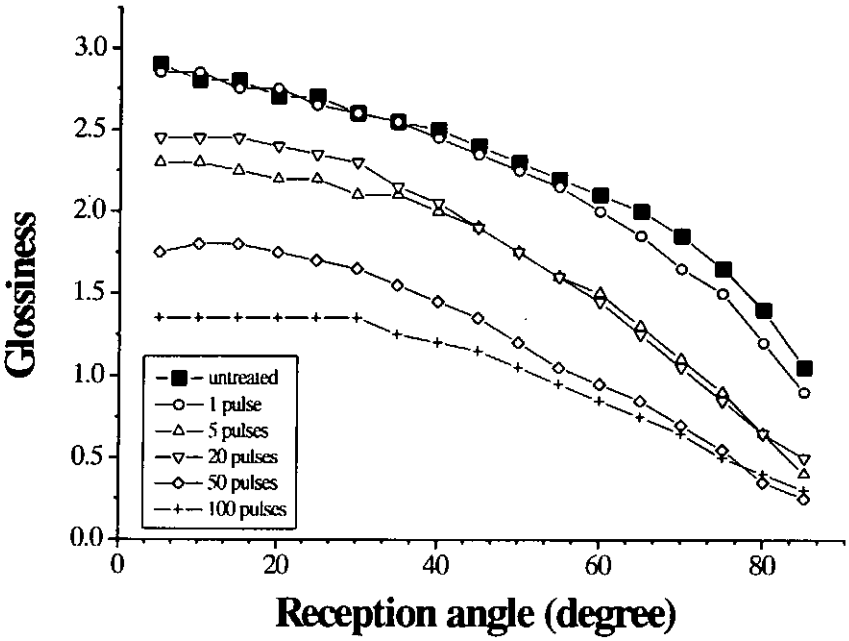

Figure 4.9: Glossiness distribution of the high fluence (100 mJ cm^{-2}) laser treated PET thick fabric in weft direction.

For the high fluence laser treated PET fabrics, the glossiness values decreases gradually with the increasing number of laser pulses. Figure 4.8 and 4.9 show the relationship between the glossiness values and the reception angles in different number of laser pulses. The decreasing in glossiness values is caused by the enhancement of surface roughness after the laser irradiation and also the color changes in high number of laser shot. Such enhancements increase the ability of light absorption, leading to smaller glossiness values of treated fabrics.

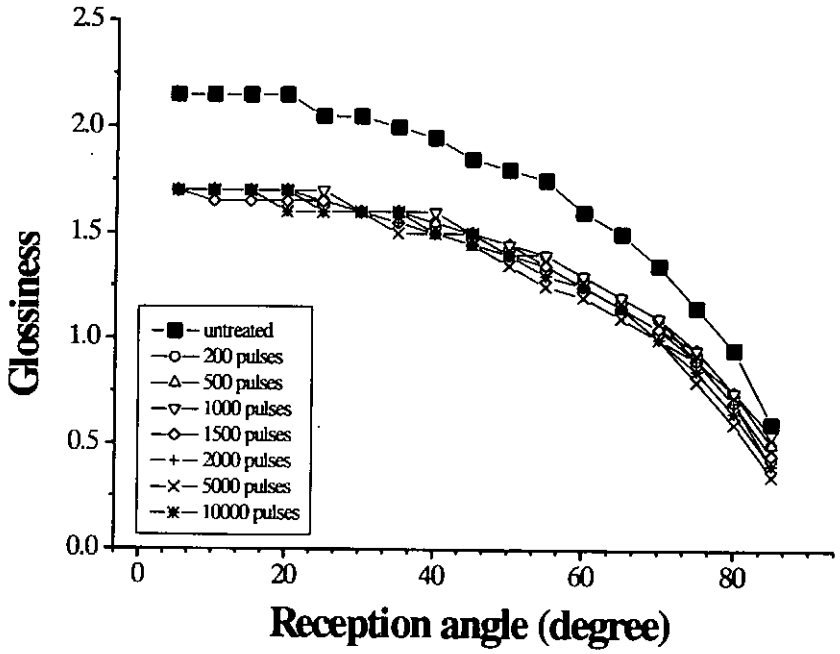

Figure 4.10: Glossiness distribution of the low fluence (6 mJ cm^{-2}) laser treated PET thick fabric in warp direction.

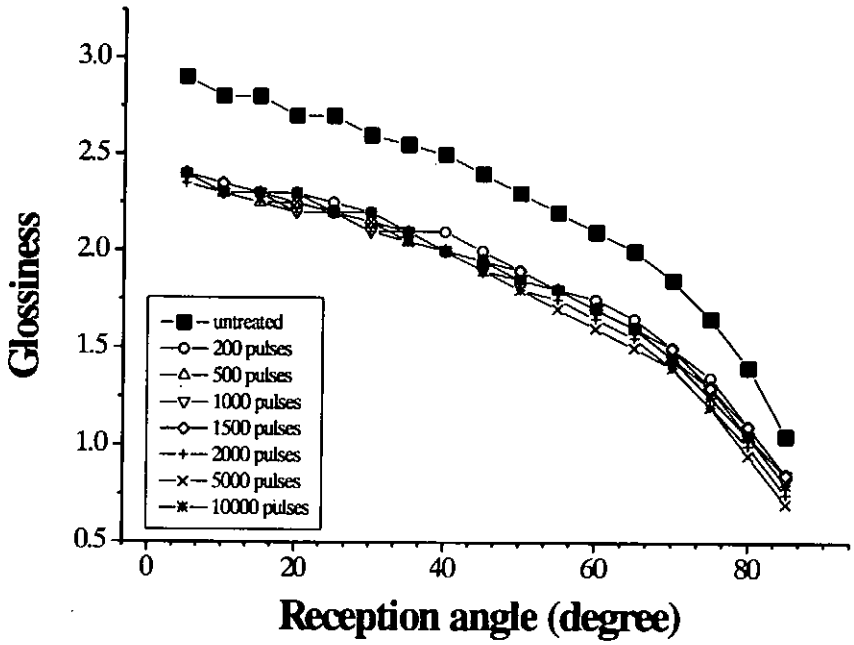

Figure 4.11: Glossiness distribution of the low fluence (6 mJ cm^{-2}) laser treated PET thick fabric in weft direction.

However, after the low fluence laser irradiation, the fabrics have no significant color changes. The treated fabrics remains white in color even irradiated with 10000 laser pulses. As shown in Figure 4.10 and 4.11, the low fluence laser treated PET surfaces have no significant drop in the value of glossiness due to increased number of laser pulses for both weft and warp directions. The decrement mainly caused by the increase of absorption property induced by surface structuring / roughness, but no contribution due to color change.

4.2.1.2 Whiteness

Figure 4.12 shows the reduction of fabrics' whiteness versus laser irradiation dosage (pulse fluence × number of pulse). The yellowness increases with higher fluence and greater number of laser shot. The increase in yellowness is less severe with low fluence laser treatment, even with prolonged exposure of 5000 pulses, but the surface is no longer white (value below 40) at 10,000 pulses.

In high fluence laser treatment, 5 pulses of laser shots of fluence of 50 mJ cm^{-2} are sufficient to lower the whiteness to a great extent. Therefore, high fluence or great number of pulses will limited the potential applications if the fabrics should be kept reasonably white.

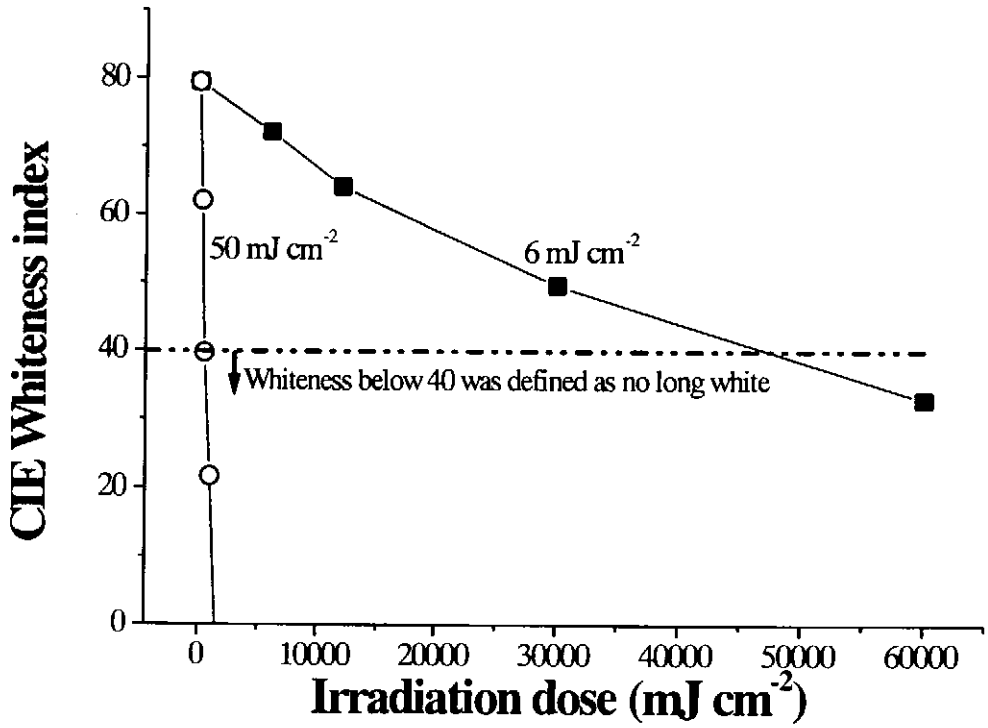

Figure 4.12: The CIE whiteness index of high and low fluence laser treated PET fabrics.

4.2.2 Modification of Wettability

4.2.2.1 Contact angle measurement

One of the methods in determining the wettability of a fabric is contact angle measurement. De-ionized water droplets were placed on the testing PET fabrics. From the shadows projected onto the protractor of the contact angle meter, the contact angle values were deduced.

Figure 4.13 shows the relationship between the contact angle and the number of pulses after high fluence laser treatment. The figure indicates that the contact angle increases with the number of laser pulses initially and then tends to a constant value for greater numbers of laser pulses. Similar results were obtained on PET film [Watanabe H. *et al.*, 1993]. This constant value depends on the wavelength and the fluence used in the laser treatment.

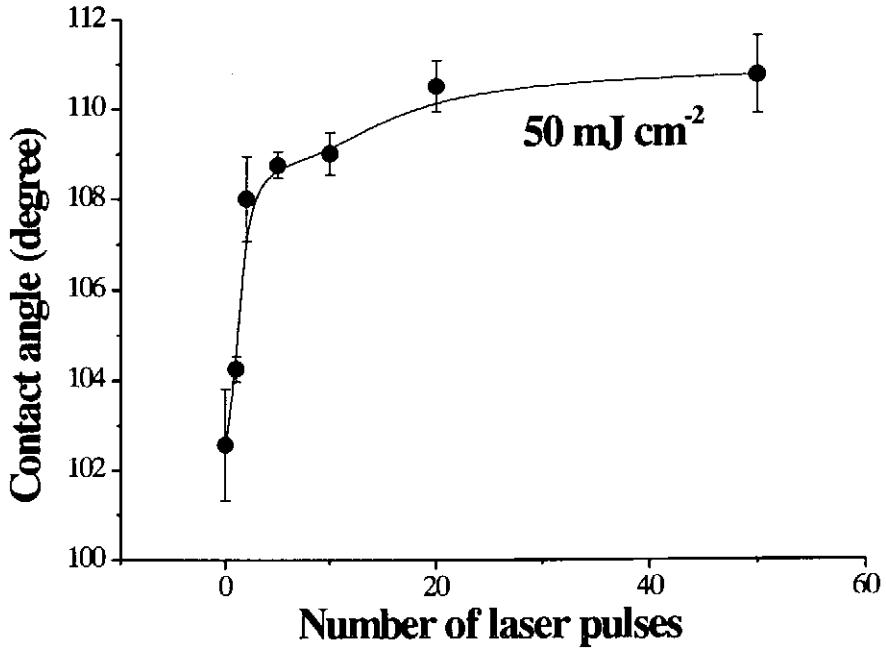

Figure 4.13: The contact angle of high fluence (50 mJ cm^{-2}) 248 nm laser treated PET fabrics for various number of laser pulses.

This increasing of the contact angle values is mainly caused by two reasons, first the periodic surface structure induced by the laser irradiation and secondly the chemical composition changes. Physically, the microns-sized ripples formed on the surface of the fibers are large enough for trapping air between them. The air may prevent the water droplet from direct contact with the fiber. Since ripple size increases with the number of laser pulses, this may explain why the contact angle increases with the number.

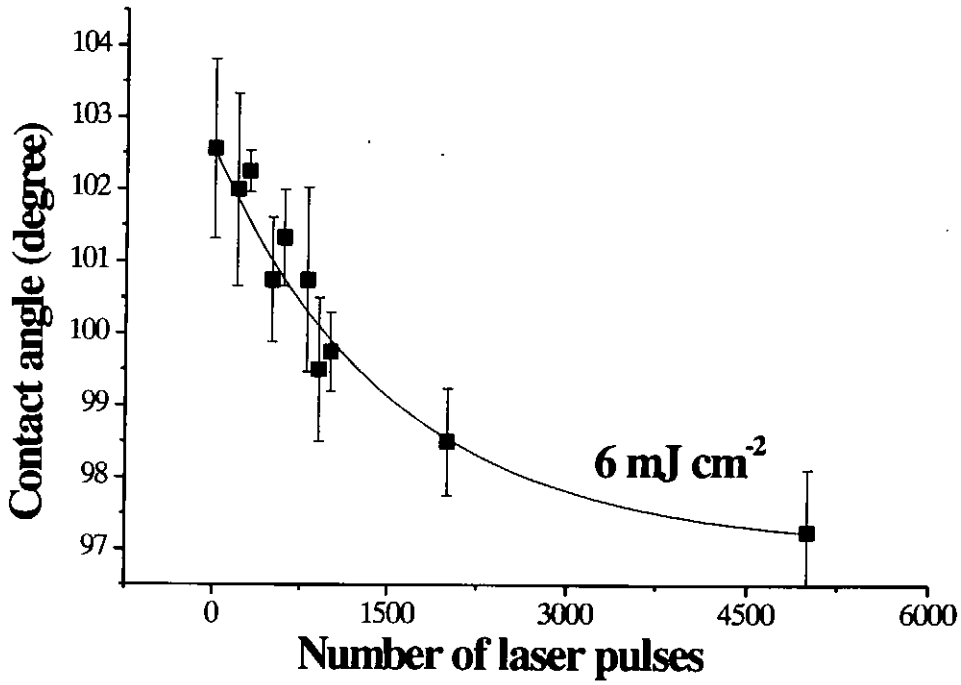

Figure 4.14: The contact angle of low fluence (6 mJ cm^{-2}) 248 nm laser treated PET fabrics.

On the other hand, XPS results show a significant increase in the carbon to oxygen ratio (C/O ratio) on the PET materials after high fluence laser treatment. This indicates that the carbon content of treated fabric surface is increased due to the formation of a highly carbonaceous surface layer. The yellowish-brown color on the treated fabric, especially after the irradiation of large number of laser pulses supports the formation of

this layer. Therefore the contact angle decreases due to the decrease in attraction between the non-polar carbonaceous surface and the polar waster molecules.

However, for low fluence laser treatment, the relation between contact angle and the number of laser pulses shows an extremely different tendency. PET fabrics after low fluence laser irradiation, increase in hydrophilicity because the contact angle decreases as the number of laser pulses. Similar to the high fluence case of laser treatment, both surface roughness and the chemical composition affect the wetting property. However in the low fluence laser treatment, the structures formed on the surface is about a hundred nano-meters size, and order of magnitude lower than those for high fluence. Therefore, this physical modification of surface roughness is less significant to change the contact angle. Chemically, according to the results of XPS chemical analysis, the C / O ratio decreases after low fluence laser irradiation. That means the oxygen content on the surface of the treated samples is increased. Such increasing also leads to the increase in the number of polar radicals. Since polar radicals increase the attraction between the modified surface and the polar water molecules wettability increases and the contact angle decreases accordingly. This effect accumulates as the number of pulses increases as shown. These tendency also obtained on the surface of polymer containing N=N-N< group [Lippert T., 1997] treated with low fluence excimer lasers and PET fabrics treated with UV excimer lamp [Praschak D. *et al.*, 1998].

4.2.2.2 Moisture regain measurement

Table 4.1 lists the moisture regain (MR%) of PET fabrics undergone different treatments.

Table 4.1: Results of the moisture regain (in %) of treated and untreated PET fabrics.

Sample	Percentage of Moisture Regain (MR %)	% difference compared with untreated sample
Untreated	1.29 %	//
Treated with 248 nm laser with fluence 100 mJ cm^{-2} and 5 pulses	1.10 %	-14.59 %
Treated with 193 nm laser with fluence 100 mJ cm^{-2} and 5 pulses	1.17 %	-9.03 %
Treated with 248 nm laser with fluence 6 mJ cm^{-2} and 2000 pulses	1.38 %	+7.53 %

As shown in the Table 4.1, the percentage of moisture regain (MR%) of PET fabrics, treated or untreated fabrics is around 1% to 1.5%. Water evaporated out from the fabrics is detected by the moisture analyzer. For the untreated samples, the MR% is about 1.29 %. After high fluence laser treatment, under both 248 nm and 193 nm, the values of MR% become 1.10 % and 1.17 % respectively, a decrease by 14.59% and 9.03% compared with that of the untreated fabric.

The negative values shown in the Table 4.1 indicate the wettability is decreased compared with the untreated samples. The results are compatible with those obtained in contact angle measurements, which have shown a decrease in hydrophilicity. More significant effect has been formed for 248 nm. One of the explanations is that the ripple

structures formed on the surface are deeper and larger with 248 nm laser treatment (due to deeper laser penetration depth). Therefore, greater volume has been modified on the material surfaces, to enhance the effect.

On the other hand, fabric subject to low fluence laser treatment has higher values of MR%, about 7.53% more than that for untreated sample (where the positive value of the difference indicates the increase in wettability). Similar to the results obtained in the contact angle measurements, low fluence treatment results in an increase in wettability, mainly due to the chemically increase in the oxygen content in the surface layer. These polar radicals increase the adhesion ability of water molecules to the treated surfaces.

4.2.3 Modification of Dyeing properties

The percentage exhaustion curves of laser treated dyed PET fabrics are shown in Figure 4.15. It can be observed that the exhaustion of the dye on PET micro-fabrics of different laser treatments, i.e. high fluence 248 nm laser treatment (100 mJ cm^{-2} and 5 pulses), high fluence 193 nm laser treatment (100 mJ cm^{-2} and 5 pulses), low fluence 248 nm laser treatment (6 mJ cm^{-2} and 2000 pulses) and untreated, have a slight difference for this kind of dye stuff, especially in the very beginning (first 20 minutes). The slopes of the exhaustion curves for laser treated fabrics are greater at the beginning of dyeing implying that the initial dyeing rate of high fluence laser treated fabrics is faster than that of the untreated one. But the time to reach the dyeing equilibrium remains the same. As suggested by many researchers [K. S. Lau *et al.*, 1995 and D. Knittel *et al.*, 1998], this is the effect the relatively faster of dye molecules diffusion into the treated samples and there are more available dyesites present on the treated surface. In general, the improvement of dyeability is believed to be closely related to the surface structures induced by laser irradiation and it is expected that dye particles are captured more easily in the ripple structures of the modified surface area.

At the same time the formation of the surface structure also induced more surface area on the fiber in both high and low fluence treatments, so that more contact areas are available for dyes molecules to diffuse into the fiber surface. The increased surface areas will also facilitate the swelling effect during the process of dyeing, resulting in faster diffusion rate. However, as the dispersed dye diffusing into the fibers' surface will have to diffuse through the surface to the bulk of the fiber. As the bulk is not affected by laser modifications because of the limited laser penetration, therefore, the exhaustion of dye in the bulk of fiber remains unchanged for treated and untreated fabrics.

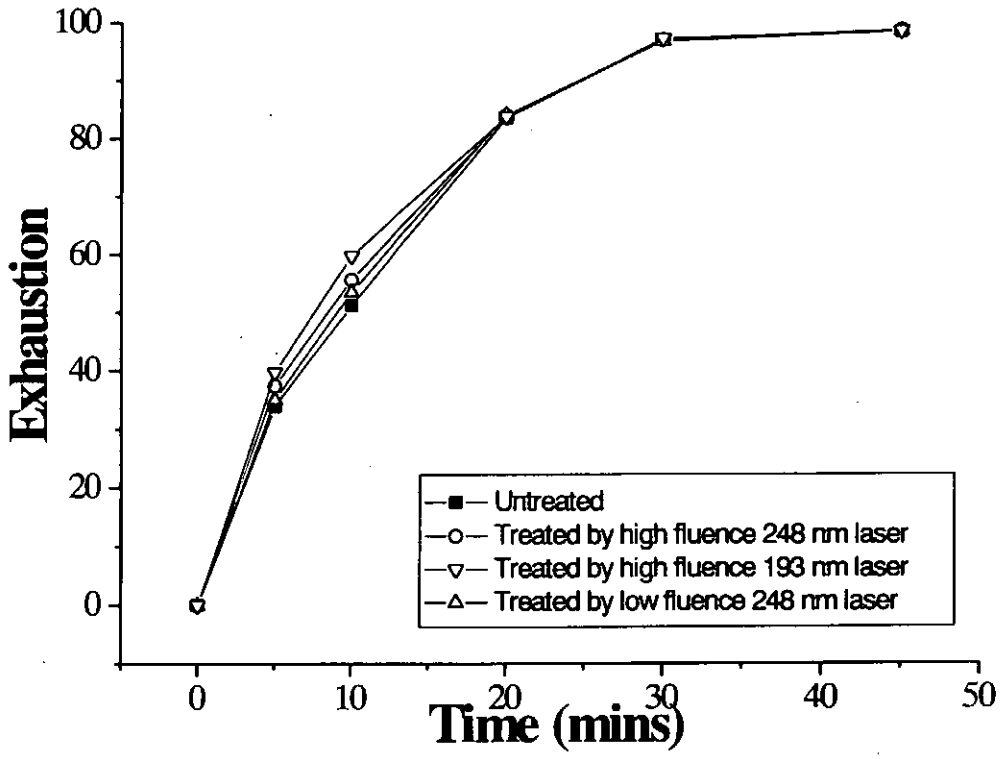

Figure 4.15: Dyebath exhaustion study of laser treated PET fabrics.
(■) Untreated (○) High fluence treatment of 248 nm laser
(▽) High fluence treatment of 193 nm laser (△) Low fluence treatment of 248 nm laser

In studying the appearance of the dyed samples, spectrophotometer was employed to measure the color differences of different dyeing conditions under CIE Lab standard. Figure 4.16 shows the color differences of the dyed fabrics with different laser treatments. All the fabrics were compared with the untreated one in each dyeing condition. Positive value of delta E (Δ E) means the color is darker / deeper than the reference (untreated samples). In the graphs shown, all readings are positive, meaning the color of the treated samples is darker than the untreated one. Color changes due to laser treatments also play a role.

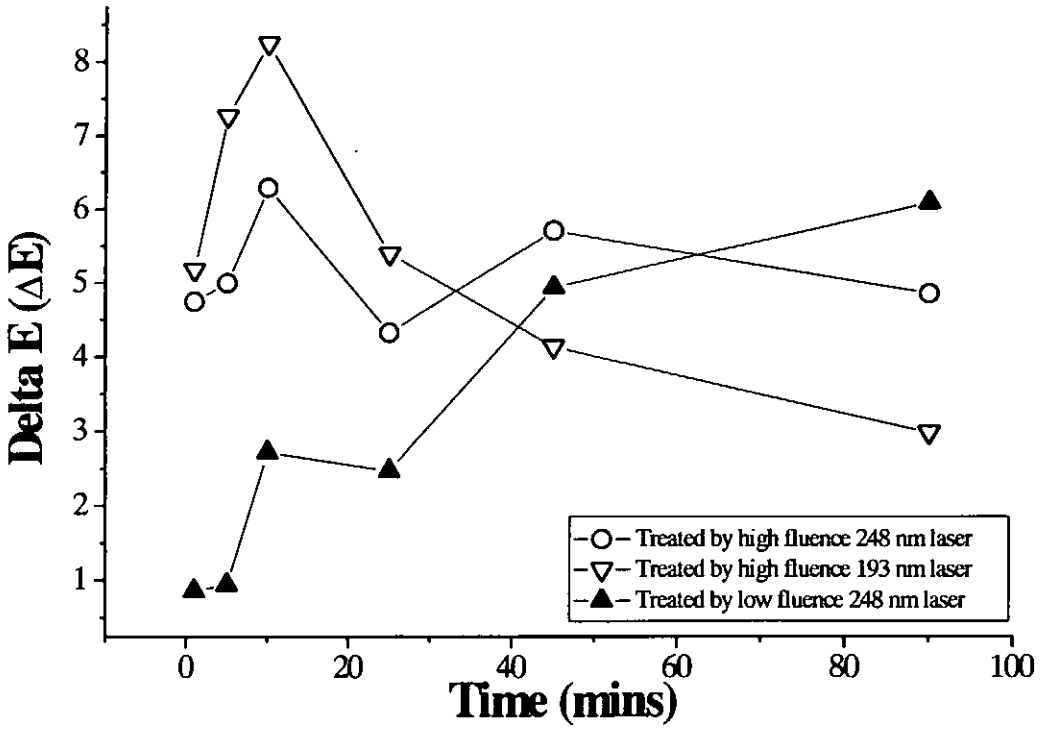

Figure 4.16: Color difference study of the laser treated PET fabrics compared with the untreated samples. (○) High fluence treatment of 248 nm laser
(▽) High fluence treatment of 193 nm laser (▲) Low fluence treatment of 248 nm laser

For the high fluence laser treatment, both 193 nm and 248 nm, there is a peak in the beginning (10 minutes). In this time interval, the dye uptake is not very high, so that the original yellowish color due to laser treatment dominates and larger value of △E is obtained when compared with the untreated samples. As dyeing time increases, the dye uptake becomes significant until around 90 minutes, the completion of the conventional dyeing process. The high fluence laser treated fabrics still kept a high positive value in delta E. This means a deeper color has obtained due to the improvement of dyeability.

On the other hand, the curve for low fluence laser treated PET fabrics dyed with the same kind of disposal dyes simply shows an increasing trend. Because the treated fabrics have no color changes after laser irradiation, no peak is present in the beginning

of the curve. The final high values of delta E indicate that the dyeability of the low fluence laser treated fabric is better than the untreated one.

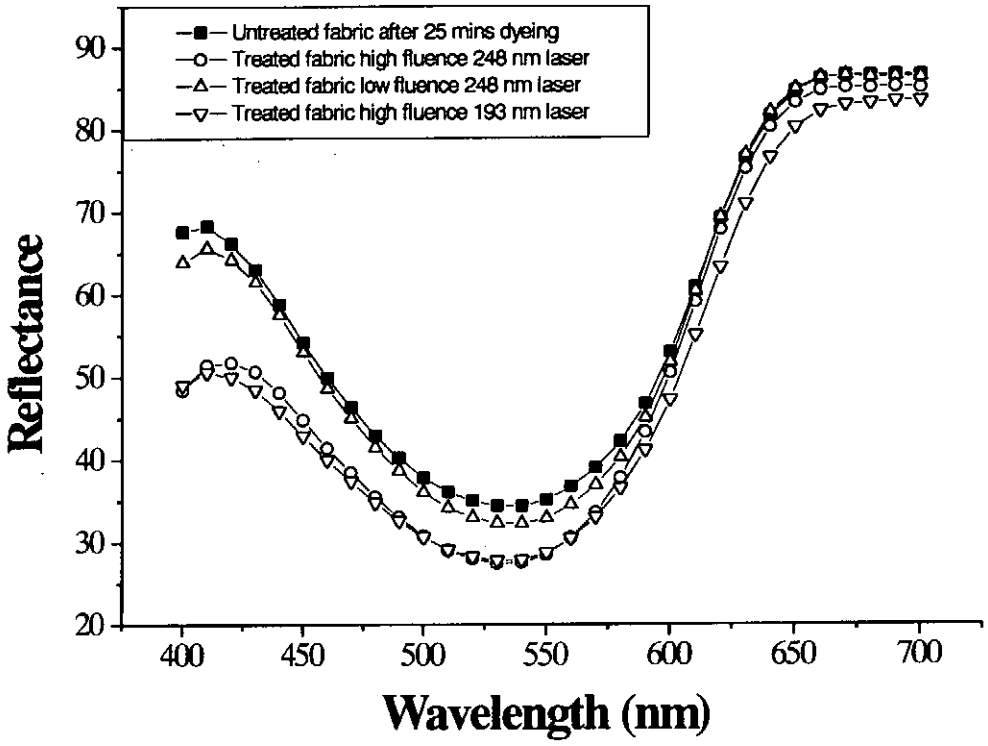

Figure 4.17: Spectral reflectance study of dyed PET fabrics with different laser treatments. (■) Untreated (○) High fluence treatment of 248 nm laser (▽) High fluence treatment of 193 nm laser (△) Low fluence treatment of 248 nm laser

Other than the delta E curve, spectral reflectance curve is also another common method in comparing color difference of the dyed samples. Figure 4.17 shows the spectral reflectance of the dyed fabrics at dyeing time of 25 minutes. Curves at different dyeing time also have similar pattern.

As can be clearly seen from the figure the treated samples give a lower values of spectral reflectance in the whole visible light range, especially at the region of blue color, implying deeper dyeing has achieved. For high fluence laser treatments, the

decrease of the reflectance is much more than that of low fluence laser treated samples. It is mainly due to the deeper structuring formed in high fluence laser treatments, so that better diffusion of dye is obtained.

4.2.4 Stability of modified surface

In textile industry, many processes involve chemicals and high temperature. Therefore for industrial applications of the LIPSS, the stability of the surface structures should be stable in several commonly used chemicals and hot water. SEM observations reveal that prolong treatment of the samples with chemicals and boiling water can only remove small part of the wall of the micro-trough or result in swelling of the wall structures. The SEM images of the samples untreated and treated by sulfuric acid (70%), sodium hydroxide (5%), acetone and boiling water are shown in Figure 4.18 and Figure 4.19. According to standard experimental results of textile testing, untreated PET fibers are insoluble in the above chemical solutions.

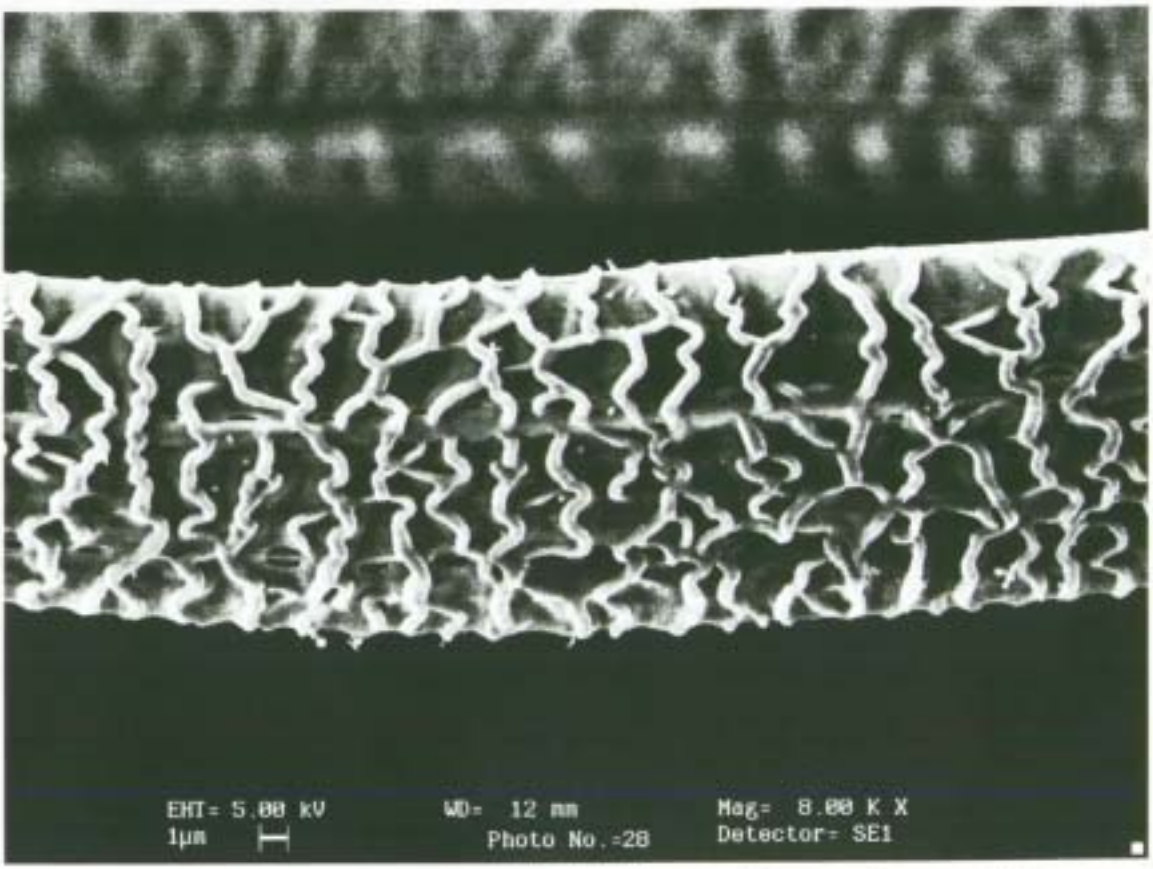

Figure 4.18: SEM image of PET micro-fiber treated with 248 nm laser with fluence of 100 mJ cm^{-2} and 5 pulses.

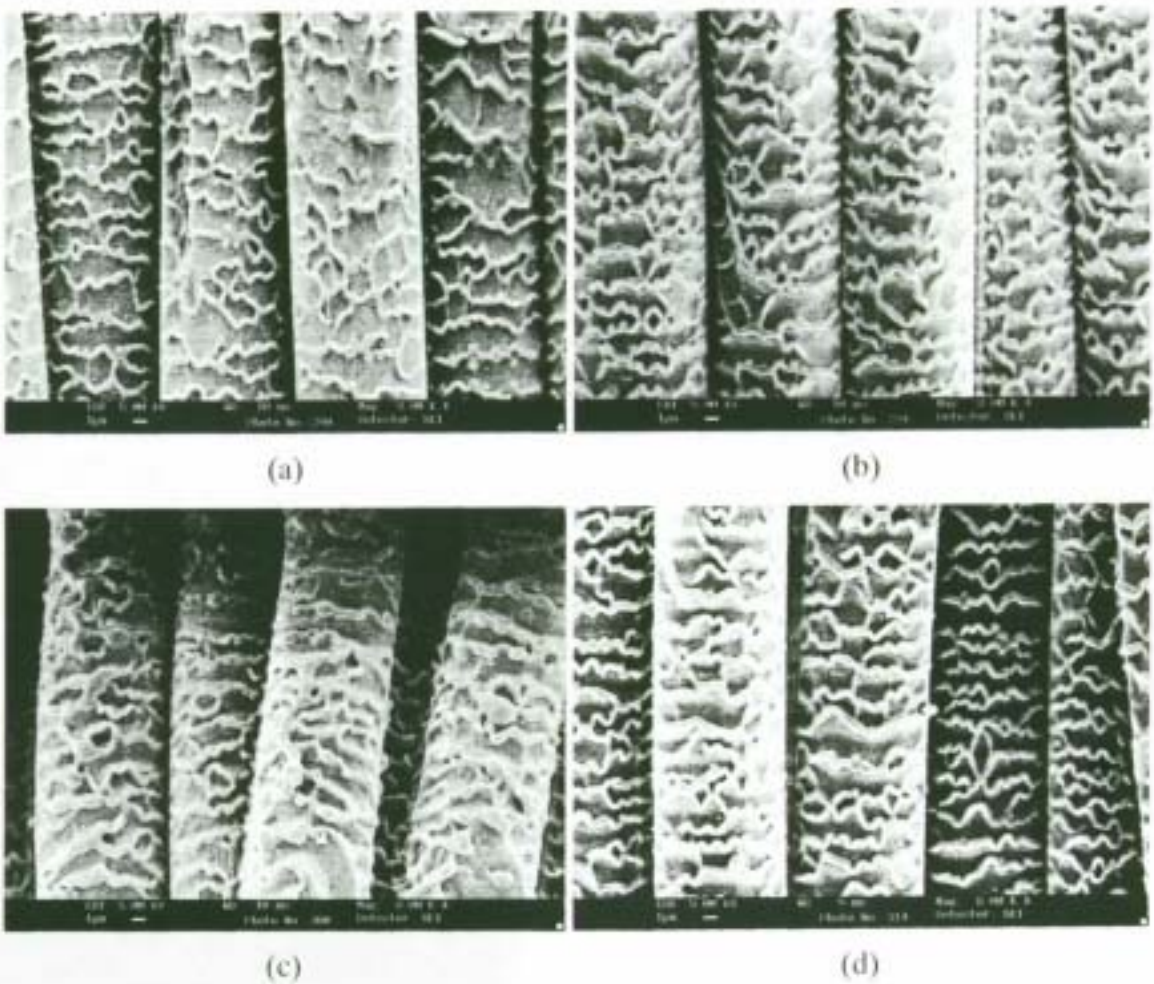

Figure 4.19: SEM images of PET micro-fiber treated with 248 nm laser with fluence of 100 mJ cm^{-2} and 5 pulses and further treated with (a) acetone, (b) boiling water, (c) 70% sulfuric acid and (d) 5% sodium hydroxide for one hour.

By compare the laser treated samples with the further treated samples, the LIPSS structures remain unchanged at all. Figure 4.18 is a treated sample of 248 nm laser with fluence of 100 mJ cm^{-2} and 5 pulses. Experiments on fibers undergone other types of laser treatment, i.e. high fluence 193 nm laser treatment and low fluence 248 nm laser treatment also give similar results. Therefore it can be confirmed that there are no significant changes of the laser induced surface structures in different environmental conditions, such as acidic, alkaline and also high temperature.

Conclusions

Laser irradiated synthetic fibers develop characteristic roughness in the form of granular or ripple like structures on the originally smooth surface. The structures depend on the nature of the materials, the irradiated laser fluence (laser power above or below the ablation threshold of the irradiated materials), dosage, wavelength and sometimes the polarization of the radiation.

In this report, poly (ethylene terepthalate, PET) and polyamide (Nylon) textile fibers and fabrics were used in the investigation. These samples were irradiated by excimer UV lasers of two different wavelengths, 193 nm and 248 nm. The UV absorption spectrum of each material is used to confirm the absorption band of materials. Spectra plotted show that the absorbance is above 90 % at both 248 nm and 193 nm wavelength for PET, but is about 60 % at 248 nm for nylon. Therefore LIPSS can be produced on PET for both wavelengths, but 248 nm laser cannot induce any LIPSS on nylon.

Surface morphological change was observed with scanning electron microscopy (SEM) and atomic force microscopy (AFM). For high fluence radiation, a single laser pulse is sufficient to generate a ripple like structure on the fiber surface. For PET, the threshold fluence of the pulse of width 15 ns and 248 nm is around 30 mJ cm^{-2}. Pulse of higher fluence produces more conspicuous pattern. Spacing of LIPSS increases as the number of pulses increases and becomes constant after certain dosage. The "saturated" spacing is wavelength dependent. For PET fibers, the spacing is about 3.6 μm for 248 nm laser and 1.6 μm for 193 nm laser. Also for high fluence irradiation, the ripple pattern is perpendicular to the fiber axis, i.e. the direction of the fiber frozen-in tension.

Formation of LIPSS on fibers with high fluence lasers is mainly caused by the synergic effect between the internal stress field and the high temperature gradient created in the surface layer of the fibers.

In low fluence laser treatment, the ripple/granular structures induced on the surface have spacing mainly around 200 nm. Furthermore, structures can only be formed with a sufficient number (up to 500) of laser pulses of low energy fluence in a narrow window of roughly 4 to 9 mJ cm^{-2}. Polarized laser light produces initially a ripple structure which is parallel to the axis of polarization. The structure direction is independent of the fiber axis. The ripple pattern becomes granular for increased dosage. Unpolarized laser light simply produces granular patterns. Because the fluence used is far below the ablation threshold of the materials, therefore, it is believed that no materials removal is involved in the process. The sub-micron sized LIPSS formed on the polymer surface is mainly caused by the coupling of interference pattern (between the incoming laser beam and the scattering beam) in the fused layer. Simulated temperature profiles show that during irradiation, only a thin upper surface layer is melted due to sufficient high photo-induced thermal energy, and therefore, materials can easily flow and self-rearrange. Measurement of the ripple spacing confirms the theoretical formula obtained from interference consideration.

In addition to physical measurements, chemical modifications due to laser treatment were also studied in this project. X-ray photoelectron spectroscopy (XPS), Fourier transform infrared spectroscopy (FTIR) and UV absorption spectroscopy were used to analyze the changes of the chemical composition of the laser irradiated surface. Again, these results reveal some significant difference between high and low fluence laser treated PET. For the untreated samples, the carbon to oxygen (C/O) ratio is about

3.4. Under high fluence laser irradiation, the ratio gradually increases with the number of laser pulses, since the content of oxygen decreases gradually. On the other hand, this ratio decreases under low fluence treatment within the first 1000 laser pulses, and remains constant at around 2 even 10 times of pulses have accumulated (10000 pulses).

From the diffusion reflectance FTIR spectra of PET surfaces treated with high fluence laser irradiation, peaks corresponding to C-O, O-H and C=O groups of the material increase rapidly with the number of laser pulses up to around 100 shots and then drop to a lower value. For the C=O bond (1745 eV peak), there is also a shift in wavenumber at / after 200 laser shots. Polarized FTIR spectra show that absorbance of IR polarized along the fiber axis is greater than that perpendicular to the axis. The overall increase in absorbance after high fluence laser treatment is also obtained and it was believed that surface roughness enhance the absorption property. Spectra of PET surfaces treated with low fluence laser irradiation on the other hand have little change compared with those of the untreated sample. This concluded that low fluence treatment has effect only on a thin surface layer of sub-micron thickness. UV spectra of PET surface treated with a small number (less than 10) of high fluence laser pulses have a lower absorbance compared with the untreated samples for wavelength less than 300 nm. This is believed to be partly due to the removal of the contaminated surface layer. Spectra of samples treated by increased number of pulses have increased absorbance over the whole spectrum. This is due to both roughening, coloring and chemical modification of the fiber surface. UV spectra of low fluence treated surfaces have an interesting feature when compared with the untreated samples. The absorbance changes mainly occurs at the range of far UV region (240 nm to 300 nm) whereas there is no significant enhancement in the visible and near UV regions. Similar to the case of high

fluence laser treatment, the absorption has a great drop in value from untreated sample up to 200 pulses and then increases gradually.

Subsequent study on textile properties as a result of surface modification indicates changes to various extents in surface luster, wettability and dyeability. The treated fabrics are relative stable after exposure to chemicals and high temperature enironment common to textile processing. Glossiness for surfaces undergone high fluence irradiation can be reduced by 50 % with increasing dosage. Whiteness index, however, decreases at the same time. Low fluence laser treatment is not as effective in reducing glossiness but can retain the surface whiteness. Hence low fluence treatment has a better application potential in this respect. The most significant change is in wettability property. After high fluence laser treatment, the contact angle increases as the number of pulses increases. Compared with untreated fabrics, the value of MR % decreased by 14.59 % and 9.03 % for 248 nm and 193 nm laser irradiation (both 100 mJ cm^{-2} and 5 pulses) respectively. On the other hand, low fluence laser treatment induces an increase in MR % (by 7.53 %) and a decrease in contact angle on the samples. Surface modification also enhances dyeability especially in the dyeing rate. Greater slopes have been obtained in exhaustion curves and deeper color results in color difference measurement.

Publications

Wong Mendel, Lau K. S. and Chan K. "Characteristics of submicrometer periodic surface structure produced on PET fibers with low-fluence ultraviolet excimer laser radiation". *Physical Society of Hong Kong, Fourth Annual Conference*, Hong Kong, 12 June 1999, pp. 20 (1999)

Wong Mendel, Lau K. S. and Chan K. "Surface structuring of synthetic fibers by 193 nm and 248 nm uv laser irradiation" .. *The 5th Asian Textile Conference,* Kyoto, Japan, 30th September-2nd October, 1999, Proceeding 2, pp. 815-818.

Wong Mendel, Lau K. S. and Chan K. "Sub-micrometer periodic surface structure produced on PET fibres with low-fluence ultraviolet excimer laser" (submitted to Research Journal of Textile and Apparel (RJTA))

References

Anni, B.S., "Color measurement system; measurement of fluorescent samples and whiteness". Joseph W. Goodman, *Practical Color Measurement*, A Wiley-Interscience Publication, New York, pp. 97 (1994)

Bahners, T. and Schollmeyer, E. "Morphological changes of the surface structure of polymers due to excimer laser radiation: A synergetic effect?". *Journal of Applied Physics*, Vol. 66, pp. 1884-1886 (1989)

Bahners, T., Kesting, W. and Schollmeyer, E. "Designing surface properties of textile fibers by UV-Laser irradiation". *Applied Surface Science*, Vol. 69, pp. 12-15 (1993)

Bahners, T., Knittel, D., Hillenkamp, F., Bahr, U., Benndorf, C. and Schollmeyer, E. "Chemical and physical properties of laser-treated poly(ethyleneterephthalate)". *Journal of Applied Physics*, Vol. 68, pp. 1854-1858 (1990)

Birnbaum, M. "Semiconductor surface damage produced by ruby laser". *Journal of Applied Physics*, Vol. 28, pp. 3688-3689 (1965)

Bolle, M. and Lazare, S. "Characterization of submicrometer periodic structure produced on polymer surfaces with low-fluence ultraviolet laser radiation". *Journal of Applied Physics*, Vol. 73, pp. 3516-3524 (1993a)

Bolle, M. and Lazare, S. "Submicron periodic structures produced on polymer surfaces with polarized laser ultraviolet radiation". *Applied Surface Science*, Vol. 65/66, pp. 349-354 (1993b)

Bolle, M. and Lazare, S. "Large scale excimer laser production of submicron periodic structures on polymer surface". *Applied Surface Science*, Vol. 69, pp.31-37 (1993c)

Chan, C. M., Ko, T. M. and Hiraoka, H. "Polymer surface modification by plasmas and photons". *Surface Science Reports*, Vol. 24, pp. 1-54 (1996)

Csete, M. and Bor, Zs. "Laser-induced periodic surface structure formation on Polyethylene-terephthalate". *Applied Surface Science*, Vol. 133, pp. 5-16 (1998)

Dauscher, A., Feregotto, V., Cordier, P. and Thomy, A. "Laser induced periodic surface structures on iron". *Applied Surface Science*, Vol. 96-98, pp. 410-414 (1996)

Dyer, P. E. "Excimer laser ablation of low and high absorption index polymers". *Applied Surface Science*, Vol. 96, pp. 596-600 (1996a)

Dyer, P. E. and Farley R. J. "Periodic surface structures in the excimer laser ablative etching of polymers". *Applied Physics Letters*, Vol. 57, pp. 765-767 (1990)

Dyer, P. E. and Sidhu, J. "Development and origin of conical structures on XeCl laser ablated polyimide". *Applied Physics Letters*, Vol. 49, pp. 453-455 (1986)

Dyer, P. E. and Sidhu, J. "Excimer laser ablation and thermal coupling efficiency to polymer films". *Journal of Applied Physics*, Vol. 57, pp. 1420-1422 (1985)

Dyer, P. E. and Sidhu, J. "Novel method for measuring excimer laser ablation thresholds of polymers". *Applied Physics Letters*, Vol. 52, pp. 1880-1882 (1988)

Dyer, P. E., Farley, R. J., Giedl, R. and Karnakis, D. M. "Excimer laser ablation of polymers and glasses for grating fabrication". *Applied Surface Science*, Vol. 96-98, pp. 537-549 (1996b)

Emmony, D. C., Howson, R. P., Howson, L. P. and Willis, L. J. "Laser mirror damage in germanium at 10.6 μm". *Applied Physics Letters*, Vol. 23, pp. 598-600 (1973)

Isenor, N. R. "CO_2 laser produced ripple patterns on Ni_xP_{1-x} surfaces". *Applied Physics Letters*, Vol. 31, pp. 148-150 (1977)

Brandrup, J., Immergut, E. H. (Eds.), *Polymer Handbook*, Wiley, New York (1975)

Keilmann, F. "Laser-driven corrugation instability of liquid metal surfaces". *Physical Review Letters*, Vol. 51, pp. 2097-2100 (1983)

Kesting, W., Bahners, T. and Schollmeyer, E. "The effect of vacuum-ultraviolet laser wavelengths on the surface treatment of polyolefinic polymer". *Journal of Polymer Science B*, Vol. 31, pp. 887-890 (1993)

Knittel, D. and Schollmeyer, E. "Surface structuring of synthetic fibers by UV laser irradiation. Part III. Surface functionality changes resulting from excimer-laser irradiation". *Polymer International*, Vol. 45, pp. 103-109 (1998a)

Knittel, D. and Schollmeyer, E. "Surface structuring of synthetic polymers by UV-laser irradiation. Part IV. Applications of excimer laser induced surface modification of textile materials". *Polymer International*, Vol. 45, pp. 110-117 (1998b)

Knittel, D., Kesting, W. and Schollmeyer, E. "Surface structuring of synthetic fibers by UV laser irradiation, Part I: Phenomenological report". *Polymer International*, Vol. 43, pp. 231-239 (1997a)

Knittel, D., Kesting, W. and Schollmeyer, E. "Surface structuring of synthetic fibers by UV laser irradiation, Part II: Mechanism and models". *Polymer International*, Vol. 43, pp. 240-250 (1997b)

Lau, K. S., Chan, K. and Gong, W. Z. "Release of materials from fiber encapsulated matrices". *Physical Society of Hong Kong, Fourth Annual Conference*, supplementary paper S-1, (1999)

Lau, K. S., Chan, P. W., Wong, K. H., Yeung, K. W., Chan, K. and Gong, W. Z. "Surface properties of polyester fabrics induced by excimer laser processing". unpublished data. (1995a)

Lau, K. S., Chan, P. W., Wong, K. H., Yeung, K. W., Chan, K. and Gong, W. Z. " Laser-induced modification of surface luster of polyester fabric". *Proceedings of The 3rd Asian Textile Conference*, Vol. I, pp. 50-56 (1995b)

Laurens, P., Sadras, B., Decobert, F., Arefi, F. and Amouroux, J. "Modifications of polyether-etherketon surface after 193 nm and 248 nm excimer laser radiation". *Applied Surface Science*, Vol. 138-139, pp. 93-96 (1999)

Lazare, S. and Banet, P. "Surface amorphization of Mylar films with the excimer laser radiation above and below ablation threshold: Ellipsometric measurements". *Journal Applied Physics*, Vol. 74, pp. 4953-4957 (1993)

Lazare, S. and Granier, V. "Ultraviolet laser photoablation of polymers: A review and recent results". *Laser Chemistry*, Vol. 10, pp. 25-40 (1989)

Lazare, S. and Srinivasan, R. "Surface properties of Poly(ethykeneterephthalate) films modified by far-ultraviolet radiation at 193 nm (laser) and 185 nm (low Intensity)". *Journal of Physical Chemistry*, Vol. 90, pp. 2124-2131 (1986)

Leamy, H. J., Rozgonyi, G. A., Sheng, T. T. and Celler, G. K. "Periodic regrowth phenomena produced by laser annealing of ion-implanted silicon". *Applied Physics Letters*, Vol. 32, pp. 535-537 (1978)

Lippert, T., Nakamura, T., Niino, H. and Yabe, A. "Laser induced chemical and physical modifications of polymer films: dependence on the irradiation wavelength". *Applied Surface Science*, Vol. 109, pp. 227-231 (1997)

Lu, Y. F., Choi, W. K., Aoyagi, Y., Kinomura, A. and Fujii, K. "Controllable laser-induced periodic structures at silicon-dioxide / silicon interface by excimer laser irradiation". *Journal of Applied Physics*, Vol. 80, pp. 7052-7056 (1996)

Maracas, G. N., Harris, G. L., Lee, C. A. and McFarlane, R. A. "On the origin of periodic surface structure of laser annealed semiconductors". *Applied Physics Letters*, Vol. 33, pp. 453-455 (1978)

Niino, H. and Yabe, A. "Chemical surface modification of fluorocarbon polymers by excimer laser processing". *Applied Surface Science*, Vol. 96-98, pp. 550-557 (1996)

Niino, H. and Yabe, A. "Formation of conjugated polyene and Polyyne structure by KrF excimer laser-induced dehydrochlorination on Polyvinylidenechloride film". *Journal of Polymer Science : Part A: Polymer Chemistry*, Vol. 36, pp. 2483-2487 (1998)

Niino, H., Shimoyama, M. and Yabe, A. "XeCl excimer laser ablation of a polyethersulfone film: Dependence of periodic microstructures on a polarized beam". *Applied Physics Letters*, Vol. 57, pp. 2368-2370 (1990)

Niino, H., Yabe, A., Nagano, S. and Miki, T. "Surface morphological microstructures of poly(ethylene 2,6-naphthalate) modified by excimer laser ablation". *Applied Physics Letters*, Vol. 54, pp. 2159-2161 (1989)

Praschak, D., Bahners, T. and Schollmeyer, E. "PET surface modifications by treatment with monochromatic excimer UV lamps". *Applied Physics A*, Vol. 66, pp. 69-75 (1998)

Sendora, M. and Hiraoka, H. "Laser induced periodic structures on polymer surfaces". *Materials and Manufacturing Process*, Vol. 9, No. 3, pp. 467-473 (1994)

Siegmen, E. Anthony and Fauchet, M. Philippe "Stimulated Wood's Anomalies on laser-illuminated surfaces". *IEEE Journal of Quantum Electronics*, Vol. QE-22, No. 8, pp. 1384-1403 (1986)

Silvain, J. F., Niino, H., Ono S., Nakaka, S. and Yabe, A. "Surface modification of elastomer / carbon composite by Nd^{+}:YAG laser and KrF ecimer laser ablation". *Applied Surface Science*, Vol. 141, pp. 25-34 (1999)

Simon, P. and Ihlemann, J. "Ablation of submicron structures on metals and semiconductors by femtosecond UV-laser pulses", *Applied Surface Science*, Vol. 109/110, pp. 25-29 (1997)

Sipe, J. E., Young, J. F. and Preston, J. S., Driel, H. M. "Laser induced periodic surface structure. I. Theory". *Physical Review B*, Vol. 27, pp. 1141-1154 (1982)

Srinivasan, R. and Braren, B. "Ablative photodecomposition of polymer films by pulsed far-ultraviolet (193nm) Laser radiation: dependence of etch depth on experimental conditions". *Journal of Polymer Science*, Vol. 22, pp. 2601-2609 (1984)

Srinivasan, R. and Braren, B. "ultraviolet laser ablation of organic polymers". *Chemical Reviews*, Vol. 89, pp. 1303-1316 (1989)

Srinviasan, R. "Kinetics of the ablative photodecomposition of organic polymers in the far ultraviolet (193 nm)". *Journal of Vacuum Science and Technology B1*, Vol. 4, pp. 923-926 (1983)

Tungol, W.M., Bartick, E.G. and Montaser, A. "The development of a spectra data base for the identification of fibers by infrared microscopy". *Applied Spectroscopy*, Vol. 44, pp. 543-549 (1990)

Watanabe, H. and Yamamoto, M. "Chemical Structure Change of a KrF-laser irradiated PET fiber surface". *Journal of Applied Polymer Science*, Vol. 71, pp. 2027-2031 (1999)

Watanabe, H. and Yamamoto, M., "Laser ablation of poly (ethylene terephthalate)". *Journal of Applied Polymer Science*, Vol. 64, pp. 1203-1209 (1997)

Watanabe, H., Takata, T. and Tsuge, M. "Polymer surface modification due to excimer laser radiation chemical and physical changes in the surface structure of poly (ethyleneterephthalate)". *Polymer International*, Vol. 31, pp. 247-254 (1993)

Wefers, L., Bosbach, D., Rammensee, W. and Schollmeyer, E. "Determination of UV-laser induced surface structures by atomic force microscopy". *Applied Surface Science*, Vol. 69, pp.418-423 (1993)

Wong, Wilson, Chan, K., Lau, K. S. and Yeung, K. Y. "Pulsed UV laser modification of polyester textile materials: effect on wettability". *Journal of China Textile University (Eng. Ed)*, Vol. 16, No. 3, pp. 31-36 (1997)

Wong, Wilson, Chan, K., Lau, K. S. and Yeung, K. Y. "A potential textile application of UV excimer laser irradiation on polyester fabrics". *Research Journal of Textiles and Apparel*, Vol. 3, No. 2, pp. 1-6 (1999)

Wong, W. Y. Y., Wong, T. M. and Hiraoka, H., "polymer segmental alignment in polarized pulses laser-induced periodic surface structures", *Applied Physics A: Materials Science & Processing*, Vol. 65, pp. 519-523 (1997)

Yi, X. S., Feng, Y., Pan, Y. and Shu, X. Z. "Laser etching of polymer compounds". *Journal of Applied Polymer Science*, Vol. 67, pp. 2119-2123 (1998)

Young, J. F., Preston, J. S., Driel, H. M. and Sipe, J. E. "Laser induced periodic surface structure. II. Experiments on Ge, Si, Al, and brass". *Physical Review B*, Vol. 27, pp. 1155-1172 (1983)

Young, J. F., Sipe, J. E., Preston, J. and Driel, H. M. "Laser induced periodic surface structure damage and radiation remnants". *Applied Physics Letters*, Vol. 41, pp. 261-264 (1982)

Yu, J. J. and Lu, Y. F. "Laser-induced ripple structures on Ni-P substrates". *Applied Surface Science*, Vol. 148, pp. 248-252 (1999)